Asian Journal of Pharmaceutical Sciences 19 (2024) 100980

Available online at www.sciencedirect.com

ScienceDirect

journal homepage: www.elsevier.com/locate/AJPS

Review Article

Biopharmaceutical and pharmacokinetic attributes to drive nanoformulations of small molecule tyrosine kinase inhibitors

Soumyadip Mukherjee[1], *Vedant Joshi*[1], *Kolimi Prashanth Reddy, Nidhi Singh, Priyanka Das, Pallab Datta*[*]

Department of Pharmaceutics, National Institute of Pharmaceutical Education and Research Kolkata, 168, Maniktala Main Road, Kolkata 700054, West Bengal, India

ARTICLE INFO

Article history:
Received 16 October 2023
Revised 13 June 2024
Accepted 29 June 2024
Available online 26 October 2024

Keywords:
Pharmacokinetics
Tyrosine kinase inhibitors
Nanoparticles
Liposomes
Peak plasma concentration

ABSTRACT

Buoyed by the discovery of small-molecule tyrosine kinase inhibitors (smTKIs), significant impact has been made in cancer chemotherapeutics. However, some of these agents still encounter off-target toxicities and suboptimal efficacies due to their inferior biopharmaceutical and/or pharmacokinetic properties. Almost all of these molecules exhibit significant inter- and intra-patient variations in plasma concentration-time profiles. Thus, therapeutic drug monitoring, dose adjustments and precision medicine are being contemplated by clinicians. Complex formulations or nanoformulation-based drug delivery systems offer promising approaches to provide drug encapsulation or spatiotemporal control over the release, overcoming the biopharmaceutical and pharmacokinetic limitations and improving the therapeutic outcomes. In this context, the present review comprehensively tabulates and critically analyzes all the relevant properties ($T_{1/2}$, solubility, pK_a, therapeutic index, IC_{50}, metabolism etc.) of the approved smTKIs. A detailed appraisal is conducted on the advancements made in complex formulations of smTKIs, with a focus on strategies to enhance their pharmacokinetic profile, tumor targeting ability, and therapeutic efficacy. Various nanocarrier platforms, have been discussed, highlighting their unique features and potential applications in cancer therapy. Nanoformulations have been shown to improve area under the curve and peak plasma concentration, and reduce dosing frequency for several smTKIs in animal models. It is inferred that extensive efforts will be made in developing complex formulations of smTKIs in near future. There, the review concludes with key recommendations for the developing of smTKIs to facilitate early clinical translation.

[*] Corresponding author.
E-mail address: pd@niperkolkata.edu.in (P. Datta).
[1] These authors contributed equally.
Peer review under responsibility of Shenyang Pharmaceutical University.

https://doi.org/10.1016/j.ajps.2024.100980

1. Introduction

Cancer persists as the leading contributor to global healthcare burden, with nearly 2 million new patients and 600,000 fatalities predicted in 2023 in the USA alone. Chemotherapy, radiation therapy, surgery, hormone therapy, immunotherapy and targeted therapies are the common treatment options. Among them, chemotherapy is most widely applied due to its ease of administration. However, most conventional chemotherapeutic agents still cannot effectively distinguish between rapidly dividing non-pathological (bone marrow) cells and malignant cells, causing significant toxic effects.

In 2001, the United States Food and Drug Administration (FDA) approved imatinib (IM) to be used in chronic myelogenous leukemia (CML) with Philadelphia chromosome [1], introducing a new category of chemotherapeutic drugs with higher targetability to cancer cells called small-molecule tyrosine kinase inhibitors (smTKIs) that minimizes damage to healthy tissues, reducing adverse effects. These smTKIs specifically target the family of tyrosine kinase receptors like epidermal growth factor receptor (EGFR) and human epidermal growth factor receptor 2 (HER2) and disrupt intracellular signaling cascades involved in tumor progression. These receptors are overexpressed in several cancer types [2]. Thus, smTKIs confer a targeted approach compared to conventional chemotherapeutic agents, which primarily work by disrupting DNA and cell division, leading to non-specific cytotoxicity. For instance, IM is a competitive pyridine-based inhibitor binds to the ATP-binding site of tyrosine kinase enzymes, like platelet-derived growth factor receptors (PDGFR), BCR-ABL fusion protein, and stem-cell factor receptor (c-Kit). These kinases play a crucial role in transduction of signaling pathways that are necessary for cell division, proliferation and death. The targeted approach leads to apoptosis in CML, where IM significantly prolongs survival rates, setting a precedent for targeted therapies in oncology. The overall survival percentage with first-line IM therapy was 83.3%. This number is comparable to the CML-IV research, which found that 84% overall survival of patients received IM-based regimens [3]. This brought a remarkable advancement in cancer chemotherapeutics as long-term follow-up studies reinforced its clinical significance [3,4]. To date, about 50 smTKIs have been approved by FDA (Fig. 1A) for clinical use in cancer, while some of these molecules are indicated against multiple target diseases. Certain smTKIs like ruxolitinib are utilized in non-malignant diseases such as polycythemia vera and myelofibrosis. The latest molecule in this class to obtain approval is neratinib, indicated for lung malignancies [5]. More number of smTKIs and their combinations continue to be investigated against varied clinical conditions [6,7] even as the identification of receptor mutations that can surmount specific resistances against these drugs also gains interest [8]. It is evident that these molecules represent a rapidly expanding class of anticancer drugs that have high potential in the treatment of various malignancies.

Conversely, many of smTKIs exhibit high protein binding and metabolism, limiting their effectiveness, which results in dose-dependent adverse effects [10]. High protein binding can reduce free concentration of the drug in the bloodstream, potentially lowering its efficacy. IM is recognized for its significant binding to plasma proteins, notably albumin and alpha-1-acid glycoprotein. This high protein binding characteristic of IM can restrict the amount of free drug available to produce therapeutic effects, potentially requiring higher doses to achieve the desired clinical outcomes [11]. Studies have shown that variations in protein binding among patients can lead to differences in drug efficacy and side effects. High protein binding can limit the availability of free drug, impacting efficacy, necessitating careful dose management and monitoring to ensure therapeutic benefits [12]. In case of metabolism, erlotinib (ETB) is metabolized predominantly by the CYP3A4 enzyme. Co-administration of ETB with strong CYP3A4 inhibitors, such as ketoconazole, can significantly increase its plasma levels, leading to enhanced toxicity, therefore, should be avoided, as it can lead to increased ETB concentrations and a higher risk of adverse effects. Conversely, the co-administration of ETB with CYP3A4 inducers can decrease ETB exposure and potentially reduce its therapeutic efficacy [13].

Most of these agents are quinazoline derivatives, possessing pH-dependent solubility profiles and suffer from solubility-limiting bioavailability. Nilotinib exhibits poor aqueous solubility, resulting in variable absorption and bioavailability. Its solubility decreases as the pH increases, as it is more soluble in the acidic environment of stomach (pH 1–2) compared to the higher pH of the gastrointestinal tract (pH 5–7). This solubility issue is further complicated by the need to take nilotinib on an empty stomach to avoid unpredictable food-drug interactions that can increase its bioavailability. If nilotinib is taken with food, it may precipitate rapidly in the gastrointestinal tract, leading to poor bioavailability. Various approaches have been explored to improve the solubility and bioavailability of nilotinib, such as formulating it as salts with inorganic counterions or maintaining it in a highly energetic amorphous state. However, these methods may not always provide sufficient solubility enhancement to achieve optimal bioavailability. Managing these patients often requires alternative dosing strategies, such as amorphous solid dispersion, to enhance drug absorption [14].

High inter- and intra-patient variability, with marked food effects, is also observed in the drugs of this class. These high fluctuations in the blood levels of smTKIs have often been attributed to both toxicity and sub-optimal efficacy [15]. Additionally, smTKIs are prescribed over extended period of time, raising concerns about patient compliance. The variability in blood levels of smTKIs is a significant challenge in their clinical use, which can result from

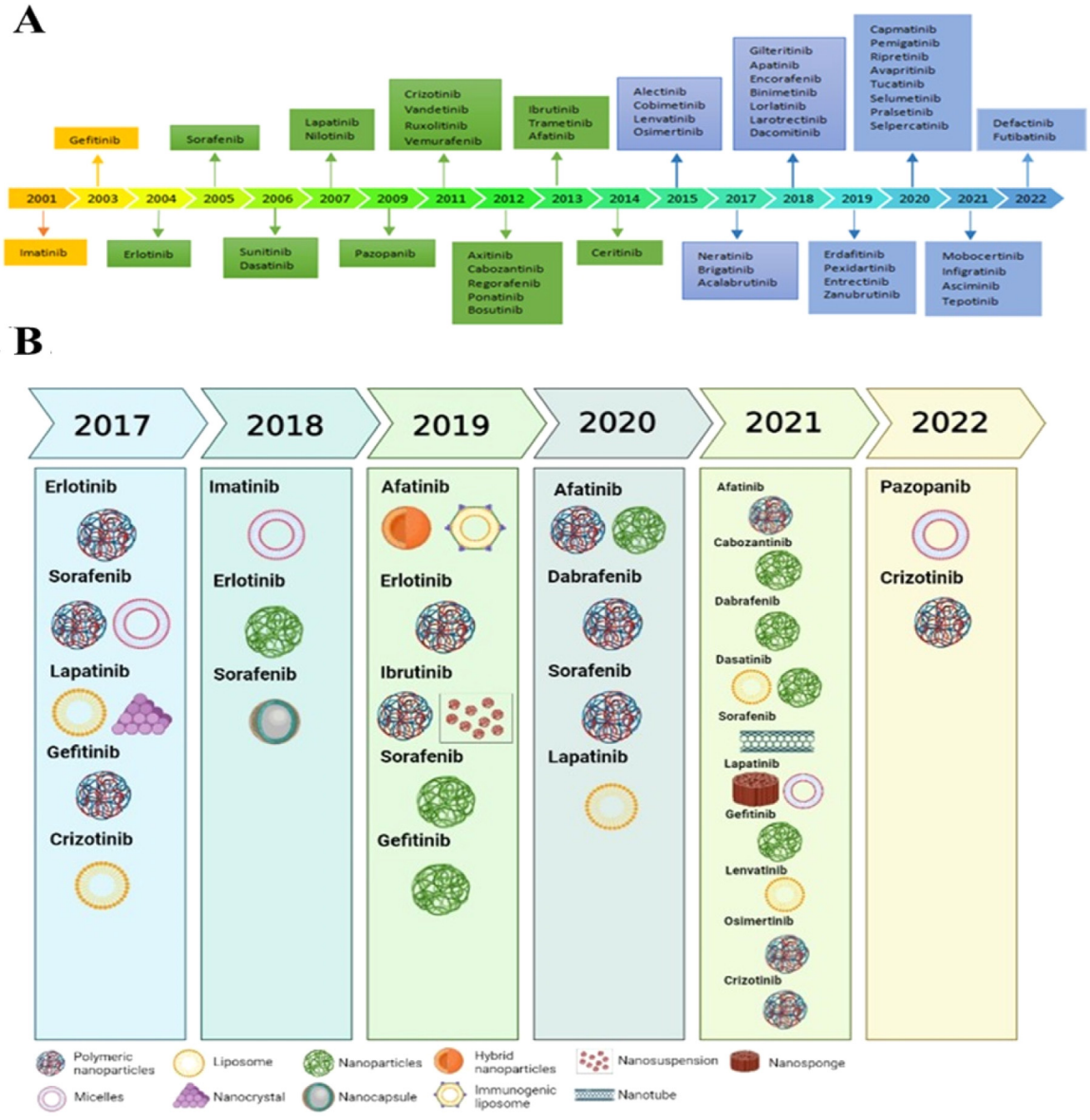

Fig. 1 – (A) Timeline of smTKIs approved by the FDA for clinical use in different forms of cancer and (B) a year-wise depiction of *in vivo* studies reported in literature on complex formulations of smTKIs (data collected from FDA website) [9].

a complex interplay of factors, including poor aqueous solubility, issues with permeability, membrane transport, and enzymatic metabolism. Additionally, food and drug-drug interactions can play a significant role in affecting the bioavailability of smTKIs. The impact of these factors on the bioavailability of smTKIs can lead to significant variations in plasma levels and exposure, which can affect treatment outcomes [16,17]. Clinicians often recommend an intermittent cessation of therapy or dose reduction to manage the complications and improve quality of patients' life [18–21]. It is thus noteworthy that even after development of such a large pool of "targeted" small molecules, application of therapeutic drug monitoring (TDM)and precision medicine practices involving genetic screening are being contemplated to achieve the desired clinical efficacy of these compounds [22–25]. Some of these challenges are addressed by TDM and precision medicine in treating CML with IM. TDM has been effectively used to adjust doses based on plasma levels, improving clinical outcomes. Personalized dosing considers patient-specific factors like age, weight, liver function and genetic polymorphisms affecting drug metabolism. However, TDM and precision medicine practices can be costly due to the need for specialized testing, frequent monitoring, and advanced technologies and equipment. Access to TDM and genetic testing facilities may be limited, particularly in rural or underserved areas. Regular monitoring and dose adjustments require coordination between patients and healthcare providers, which can be challenging to maintain consistently [26]. Simplifying treatment regimens, such as using sustained-release formulations, can also enhance patient adherence and improve therapeutic results. These strategies help to manage the variability in drug levels

and ensure that patients benefit most from their treatment [27]. Thus, there exist critical needs to develop delivery systems that modify the pharmacokinetics of smTKIs, reduce dependence of pharmacokinetics on host factors, and ultimately improve therapeutic outcomes.

Complex formulations, especially nanomedicines, have evolved greatly in last decade [28,29]. Fundamentally, these formulations allow for encapsulation of drugs, improving their solubility and stability. They can also provide a mechanism for temporal and spatial control over drug release, causing a reduction of off-target distribution, while a controlled release rate minimizes fluctuations in plasma concentration and modifies the metabolism kinetics of the drugs. In addition, nanoformulations are increasingly proving their applicability in precision medicine because of their ability to overcome systemic, tissue and cell-level barriers to drug delivery [30], all of which show high heterogeneity across patients [31–33]. These nanoparticles (NPs) target diseased cells or tissues specifically based on their physical and chemical properties or by specific stimuli at pathological sites, minimizing unwanted effects [34,35]. A case study on NP delivery of gefitinib (GFT), an EGFR inhibitor used in non-small cell lung cancer (NSCLC), demonstrated that NPs could enhance drug delivery to tumor cells while reducing systemic toxicity. This innovative approach allows for better control over the drug release and distribution, potentially overcoming solubility and metabolism challenges. This method not only improves drug delivery efficiency but also enhances drug cytotoxicity and impedes the advancement of prostate cancer, showcasing its potential for targeted and effective cancer therapy [36]. Antibody-drug conjugates (ADCs) have also been explored to deliver tyrosine kinase inhibitors (TKIs). For instance, a conjugate of dasatinib (DAS) with a HER2-targeting antibody showed improved delivery and efficacy in HER2-positive breast cancer models, highlighting the potential for targeted therapies to improve treatment outcomes [37]. Polymeric micelles for the delivery of ETB have been shown to significantly improve pharmacokinetics of the drug, leading to better tumor accumulation and reduced systemic toxicity. This approach helps address solubility issues and allows for more controlled drug release [38]. Thus, there is a huge interest in development of complex formulations for various difficult-to-deliver drugs [39–41]. Several such formulations have already been established in market to provide superior therapeutic outcomes over conventional formulations. A popular nanomedicine called Doxil®, a liposomal doxorubicin (DOX), is used to treat many different cancers, including ovarian cancer and multiple myeloma. The liposomal formulation alleviates the toxicity of anti-cancer drug to healthy tissues and increases drug exposure. Abraxane™, albumin-bound paclitaxel (PTX)-based NPs, modifies drug pharmacokinetics and enhances drug concentration at target site compared to traditional PTX formulation. Emerging delivery systems, such as NPs, ADCs and polymeric micelles, offer promising solutions to improve the delivery and efficacy of smTKIs while reducing systemic toxicity. These innovative approaches have the potential to address the solubility issues, enhance tumor accumulation, and allow for more controlled drug release. However, there is an urgent need for further research and development of these novel delivery systems to optimize their performance and clinical applicability. The past commercial experience of complex nanoformulations of cytotoxic drugs provides a strong rationale for pursuing these innovations in order to enhance the clinical applicability of smTKIs.

Since a large number of smTKIs are being approved for clinical use and it is imminent that their complex formulations will be extensively investigated. The objective of this review is to provide a critical analysis of the biopharmaceutical and pharmacokinetic properties of smTKIs approved for clinical use, followed by examination of complex formulations of them developed in the past few years (2017 onwards). Investigations that have reported *in vivo* evaluation of pharmacokinetic and pharmacodynamic performance of complex formulations have been considered in the analysis (Fig. 1B). Furthermore, it offers a comprehensive review of the current state of research on innovative delivery systems for smTKIs, highlighting their potential benefits, limitations and future directions for the field.

2. Structure of the receptor tyrosine kinase (RTK)

RTKs are located on cellular surfaces and structurally do not vary much from receptor to receptor. Their primary components are a single transmembrane helix, an extracellular region with a ligand-binding area, a tyrosine kinase domain in cytoplasm, and regulatory domains with carboxy (C-) terminal at juxta membrane [42]. Tyrosine kinases are found in monomer form on the plasma membrane. Ligand binding, mediated by receptor crosslinking, results in conformational alterations that activate and phosphorylate the receptor. In phosphorylated form, RTK act as a docking site for adaptor proteins or directly phosphorylate signaling molecules which bind to phosphorylated receptors or phosphotyrosine-binding (PTB) domains. Docked adaptor proteins phosphorylate additional downstream molecules to continue signal transduction.

Different RTK members contain distinctive binding structures determining varying drug recognition. RTK complex formation and ligand recognition can both take distinct forms. For example, the VEGF subfamily possesses seven exterior motifs that recognize ligands, resulting in receptor dimerization. Fig. 2A shows the monomer structure of EGFR and dimer structure of VEGFR (vascular endothelial growth factor receptor). Given that the VEGF ligand is dimeric in this case, a tetrameric complex containing two monomeric polypeptides that resemble VEGFR is recruited. The contact between a single EGFR polypeptide and an epidermal growth factor (EGF) molecule leads to the dimerization of EGFR and the formation of a receptor-ligand tetramer complex. In many higher eukaryotes, the insulin receptor (INSR) is a conserved gene family that belongs to the insulin-like growth factor receptor (IGFR) subfamily. A single polypeptide that underwent post-translational cleavage to generate a soluble extracellular domain, which is connected to the membrane-spanning polypeptide by a disulfide bond, is the source of the $\alpha 2\beta 2$ complex, that permits the binding of ligands,

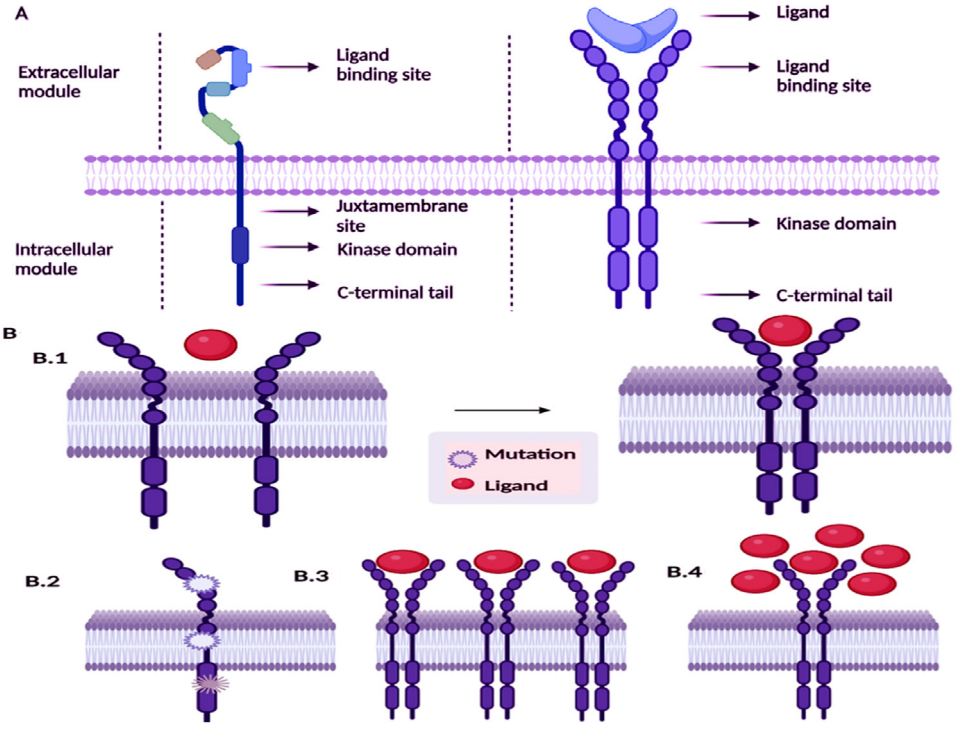

Fig. 2 – (A) Structure of EGFR monomer and VEGFR Dimer. (B) Activation of RTK in normal conditions (B1), gain-of-function mutation (B2), overexpression (B3), and autocrine activation (B4).

activation, and subsequent initial phase of intracellular signaling pathways, resulting in cellular responses like growth, differentiation and survival. The RTK is presented as a pre-assembled, disulfide-linked heterotetramer, which makes this subfamily unique. Cells that produce both the INSR and IGFR gene products can express mixed or hybrid tetramers. Fibroblast growth factor receptors (FGFR) based signal transduction is maximized by the presence of heparan sulfate proteoglycans (HSPGs) as essential co-factors [43].

2.1. *Activation of RTK*

Tyrosine kinases have different pathways of activation in normal physiological conditions compared to an oncogenic conditions.

2.1.1. *Activation in normal physiological conditions*

When ligands bind to RTKs' extracellular regions, resulting induction of dimerization or oligomerization of the receptor, leading to conformational changes that enable the receptor to release trans-autophosphorylation and cis-autoinhibition of the kinase domains. This structural rearrangement allows the kinase domains to assume an active configuration, leading to downstream signaling and cellular responses specific to the ligand-receptor interaction. The autophosphorylation of these receptors triggers downstream signaling with Src homology 2 or PTB domains. By binding to particular residues, these domains collaborate with subsequent mediators to propagate important cellular signaling pathways [43].

2.1.2. *Oncogenic activation of RTK*

The oncogenic state can arise through three primary mechanisms of activation: overexpression or amplification of the gene, gain-of-function mutations, and autocrine activation. These pathways cause abnormal cellular reactions and signaling, which may aid in the onset and spread of cancer. Gain-of-function mutations in RTKs result in aberrant downstream signal transduction that cannot be accounted for by the regular "checks and balances" that occur in case of physiological signaling. It is particularly interesting to identify and characterize "driver mutations," which are described as modifications that might provide cells a selective growth advantage [44]. RTKs have been suspected of being overexpressed in several human cancers, which include EGFR in lung, glioblastoma multiforme (GBM), oesophageal and thyroid cancers, HER2/ErbB2 in breast and bladder cancer, and MET in gastric and lung cancer. Overexpression causes a local rise in receptor concentration, which elevates RTK signaling and overpowers the opposing regulatory effects. In addition to transcriptional and translational increase, oncogenic viruses and disruption of normal regulatory mechanismscan also induce RTK overexpression. Gene amplification is primarily responsible for the occurrence of RTK overexpression [43].

In order to communicate amongst cells, secretory cells produce "messengers" in the form of growth factors and cytokines, which are transported to distant target cells.

Constitutive autocrine activation may cause clonal growth and tumor development, and autocrine activation of several RTKs, including TGF-EGFR, HGF-MET and SCF-KIT autocrine loops, has been well-studied in different types of malignancies. The RTK autocrine loop may promote tumor growth by collaborating with other autocrine growth pathways [45]. Fig. 2B illustrates the activation of RTK in normal condition (B.1), gain-of-function mutation (B.2), overexpression (B.3) and autocrine activation (B.4).

2.2. *Types of RTK*

2.2.1. *EGFR*

EGFR has received extensive research, particularly in regard to lung cancer, and it is appropriately broad to include many RTK oncogenic changes. The alterations that activate EGFR in NSCLC have received the greatest attention in studies. The tyrosine kinase domain gene's exons 18, 19, 20 and 21 are the most often affected by these mutations [43,46]. These modifications disrupt the active-inactive balance of the receptor by independently activating EGFR without ligand binding and promoting increased kinase activity. Mutations in the extracellular domain (ECD) of EGFR are found in lung, brain, and colon tumors. Amplification of EGFR is a frequent consequence of mutation and occurs in breast, lung, ovarian and prostate cancers. Overexpression of EGFR leads to an increase in surface abundance which promotes receptor dimerization and subsequent kinase activation [47,48]. For epithelial cells to develop and proliferate, they require the EGFR, ErbB2, ErbB3, and ErbB4 members of the EGFR-related (ErbB) family. Examples are cetuximab (CTX), GFT, ETB, afatinib (AFA), osimertinib (OSI) and dacomitinib [49–51].

2.2.2. *Vascular endothelial growth factor receptor (VEGFR)*

VEGF ligands, such as VEGF-A, VEGF-B, VEGF-C, VEGF-D, and placenta growth factor, have structural similarities to the three different types of VEGFRs, namely VEGFR1, VEGFR2 and VEGFR3 (also known as PIGF). Neuropilins are co-receptors that engage in ligand binding. Normal VEGFR activation results in biological activities such as angiogenesis, lymph angiogenesis, endothelial cell migration, fatty acid absorption, and so on. It has been found that lung, breast, colorectal, prostate and stomach cancer express VEGFRs and their ligands. The most frequent cause of abnormal VEGFR activation is overexpression. The MAPK pathway was activated as a result of increased expression of VEGFR1 and VEGF as exhibited in pancreatic cancer cells, hastening their growth. The presence of seven extracellular immunoglobulin-like domains that can recognize ligands and promote VEGFR dimerization is what makes the VEGF system unique. In this scenario, the dimeric version of the VEGF ligand promotes the recruitment of two monomeric polypeptides that resemble VEGFR to create a tetrameric complex. Examples are axitinib (AXT), pazopanib, sunitinib, sorafenib (SFN), vandetanib and cabozantinib [52].

2.2.3. *Fibroblast growth factor receptor (FGFR)*

Four distinct genes—FGFR1, FGFR2, FGFR3, and FGFR4—encode seven different types of FGFRs. Each gene has two different isoforms produced by alternative splicing, with the exception of FGFR4. However, there are more than twenty FGFs that may be divided into seven families. FGFR1 (49%) is the most often found genetically altered FGFR in malignancies, others are FGFR3, FGFR2 and FGFR4. Breast, brain, lung, head and squamous cell carcinomas all have mutations in all four FGFR receptors [42,43]. It has frequently been demonstrated that the formation of cancer-causing gene fusions involves FGFR2 and FGFR3. Examples of smTKIs targeting these subfamilies are erdafitinib and rogaratinib [46,47].

2.2.4. *Platelet-derived growth factor receptor (PDGFR)*

A pair of receptors called PDGFR-α and PDGFR-β respond to platelet-derived growth factors (PDGFs). Five distinct PDGFs, including PDGF-AA, PDGF-AB, PDGF-BB, PDGF-CC and PDGF-DD, stimulate these receptors. However, PDGFR-α mutations, particularly in exon 18, are often observed in gastrointestinal stromal tumors (GISTs). PDGFR gene fusions are frequent in myeloproliferative neoplasms, including acute myeloid leukemia, lymphoblastic leukemia, and hematological tumors. PDGFR-α only fuses with 5 intracellular proteins and 1 RTK, compared to 29 additional intracellular proteins of PDGFR-β. Examples of FDA-approved PDGFR are IM mesylate, sunitinib malate and regorafenib [46,47,53].

2.2.5. *Insulin receptor*

Insulin receptor (IR) is a conserved group of genes that belongs to the subfamily of the IGFR receptor, which can be found in many higher eukaryotes. This subfamily is distinctive in that the TK is displayed as a pre-assembled disulfide-linked heterotetramer. Mixed or hybrid tetramers can be expressed by cells that express both the INSR and IGF-1R gene products. The IGF-1R, IRA, IRB, IGF-1R/IR (hybrid), and IGF-2R molecules are all members of the IR family. Among these, ligands like IGF-1 and IGF-2 specifically activate IGF-1R. IGF-2R is a nonsignaling receptor that removes IGF2 from the surface of the cell. In cancers including colon, pancreatic, lung, and breast cancer, IGF-1R is reported to be overexpressed [53]. In animal studies with transgenic mice, activation of Akt, Erk1/Erk2 and STAT3, IGF-1R overexpression promotes the formation of breast tumors. In addition, it improves the migratory capability of mammary tumors with an increment in the proliferative genetic signature and decreases the latency period of tumors, and also protects cells from stressors in the tumor microenvironment and cell death [47].

2.2.6. *Hepatocyte growth factor receptor*

The MET gene encodes hepatocyte growth factor (HGF), a ligand of the hepatocyte growth factor receptor (HGFR). Malignancies of breast, lung, ovaries, colon, cervix, kidney, and blood have been shown to overexpress C-Met. HGF overexpression was found in NSCLC, and resulted in lymph node invasion by RhoA overexpression. According to a meta-analysis, breast cancer with high levels of c-Met overexpression had a larger tumor, distant metastases, and a higher histologic grade. Lung cancer is where MET-ATXN7L1 gene fusions have primarily been found, for example, savolitinib and crizotinib (CZT) [47]. Fig. 3 depicts the overview of several pathways followed by RTK along with their downstream signaling pathway.

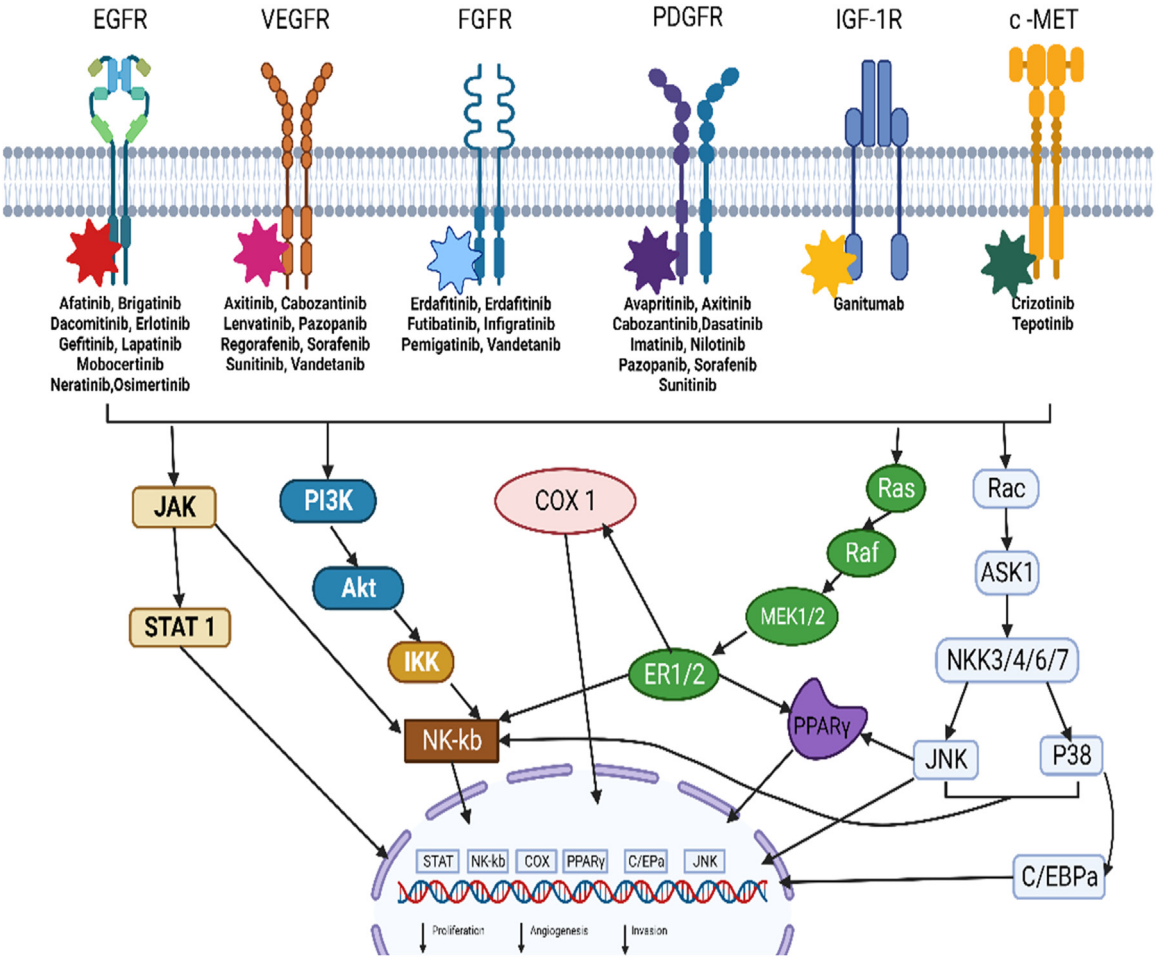

Fig. 3 – Overview of RTK and their downstream pathway components.
Abbreviations: Akt, Ak strain transforming; PI3K, Phosphoinositide 3-kinase; IKK, Inhibitor of nuclear factor kappa B kinase; NF-κB, nuclear factor kappa-light-chain-enhancer of activated B cells; PPARγ, Peroxisome proliferator-activated receptor γ; Ras, Rat sarcoma virus protein; ASK1, Apoptosis signal-regulating kinase 1; MEK, Mitogen-activated protein kinase; Raf, Rapidly accelerated fibrosarcoma protein; c-MET, Mesenchymal epithelial transition factor/receptor; STAT1, Signal transducer and activator of transcription 1; COX2, Cyclooxygenase-2; ERK, Extracellular signal-regulated kinase; Rac, Ras-related C3 botulinum toxin substrate.

3. Important biopharmaceutical and pharmacokinetic properties for complex formulation development

3.1. *Molecular weight, permeability and solubility*

As per the Lipinski Rule, drugs with a molecular weight (MW)< 500 daltons (D), lipophilicity not >5, and no >10 hydrogen bond acceptors or 5 donors have acceptable oral bioavailability. These guidelines are widely accepted in the pharmaceutical industry as a useful tool for predicting a drug's potential for oral bioavailability. The average MW of the 54 FDA-approved smTKIs is 540 D, ranging from 42 D for alectinib to 1221 D for gilteritinib (see supplementary Table S1). The drugs having MW of >500 D as found to be capmatinib, tofacitinib, DAS, selpercatinib, bosutinib, ponatinib, pralsetinib, sunitinib, encorafenib, tepotinib, selumetinib (SEL), ceritinib, entrectinib, nilotinib, brigatinib, dabrafenib (DAB), cabozantinib, SFN, infigratinib, neratinib, trametinib, mobocertinib, AFA, lapatinib (LPT), cobimetinib, and gilteritinib. Thus, out of the 54 smTKIs 32 violated Lipinski's rule with MW over 500 D, indicating the need for formulation intervention. The majority of the smTKIs approvaled by FDA have log P values under 5, except for vandetanib, entrectinib, ceritinib, cobimetinib, brigatinib, nilotinib, sunitinib, tofacitinib and alectinib (Table S1). It has also been recognized over the years that molecules with high log P are candidates for high metabolism (first-pass metabolism) at the liver when their orally administered. The median value of log P is 3.7.

The variable bioavailability of smTKIs can lead to plasma drug concentrations that are either ineffectively low or toxically high. Since smTKIs are prepared using combinatorial chemistry, they possess structures with low intrinsic solubility. Many biopharmaceutical concerns with smTKIs

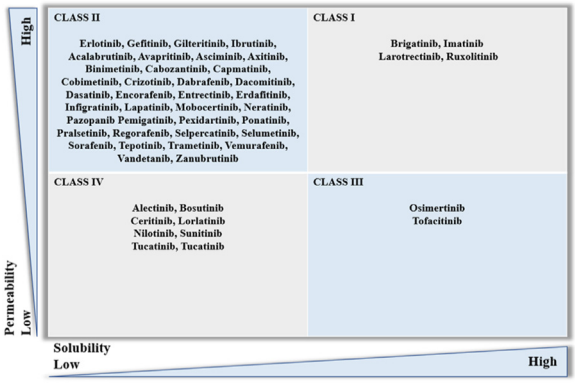

Fig. 4 – Classification of the FDA-approved smTKI till 2022 in BCS.

are related to their structure and function, and it has been noticed that their high specificity and poor absorption into the systemic circulation are related [54,55].The advancement in molecular modeling enables structural activity relationship studies of inhibitory molecules with their target proteins. Highly lipophilic groups such as aromatic amines, heterocyclic aromatics, (substituted) phenyl and biaryl constructs are important for receptor binding. Drug development may also involve adding a hydrophilic group to the structure to enhance the drug's overall aqueous solubility. But this strategy may not be useful as hydrophobicity of the structure is necessary for its inhibitory action. This is the reason why the aqueous solubility of smTKIs remains low (Fig. 4). The majority of smTKIs structure consists of a nitrogen-containing core combined with secondary amines, which causes their aqueous solubility to be pH-dependent. The few exceptions are vemurafenib, regorafenib and trametinib, which have a nearly pH-independent solubility. Most smTKIs contain an ionizable group, which facilitates their conversion into a salt form. Thus, most of the commercially available stable polymorphs of smTKIs are in the form of salt, which helps to enhance their solubility. However, for many drugs, the salt form alone is insufficient to significantly increase their solubility to meet the requirements for classification as BCS I. The solubility of smTKIs also depends on the solvate, hydrate and solventless crystalline form of the drug, but all these solid-state modifications have mostly been used to obtain stability via GIT. Moreover, solid state modification cannot overcome the metabolism (first pass) concerns. The drug's limited therapeutic window reflects severe side effects and decreased activity [54,55]. However, certain inherent limitations in considering additional factors that impact the disposition of drugs, including metabolism, distribution, and elimination, were later identified. To address the BCS limitation, Benet and his colleagues developed the Biopharmaceutics Drug Disposition Classification System (BDDCS), specifically designed to overcome the limitations of the BCS classification by incorporating essential aspects such as metabolism, distribution, elimination, and to predict metabolizing enzymes and drug-drug interactions into its framework [56,57]. Since most smTKIs are taken orally, it is necessary to classify them into BDDCS, which can provide valuable insights into their oral absorption, metabolism and potential drug-drug interactions. BDDCS primarily focuses on rate and not on the extent of permeability (as stated in BCS), the extent of metabolism and solubility. High permeability drugs exhibit extensive metabolism as it is reabsorbed from the kidney tubules, leading to higher exposure to metabolizing enzymes in the liver and other tissues, affecting the pharmacokinetics of drugs [57]. Oral smTKIs classified under BDDCS classes 1 and 2 can undergo extensive metabolism (Table 2). Complex oral formulation strategies need to be developed to overcome the drug metabolism for BDDCS class 1, as well as solubility and drug metabolism for BDDCS class 2 smTKIs. Combining metabolic enzyme inhibitory agents with smTKIs can enhance oral bioavailability [58]. Thus, it is evident that >18% of present smTKIs can be benefited

3.2. *Absorption pharmacokinetics*

All the FDA-approved smTKIs, as of 2022, are administered orally as tablets or capsule dosage forms. Their larger molecular counterparts, such as monoclonal antibodies, are administered intravenously. The dose of smTKIs vary from 2 mg/d for trametinib on the lowest side to the highest dose recommended for vemurafenib (1,920 mg/d). The median dose of smTKIs is 160 mg/d (Table 1). Some smTKIs needs repeated dosing in a single day like zanubrutinib, tucatinib, vemurafenib, SFN, SEL, pexidartinib, acalabrutinib, alectinib, AXT, binimetinib, CZT, DAB, erdafitinib and nilotinib need to be administered two times a day while neratinib needs to be administered thrice a day. Thus, from dose point of view, several smTKIs are good candidates for complex formulations.

Absorption of smTKIs from their dosage form depends on various factors such as physicochemical properties (solubility, polymorphism, pKa, pH, lipophilicity), dosage form characteristics and patient-related factors. Table S1 demonstrates that most of the smTKIs show pH-dependent solubility. The solubility of smTKIs is reduced by using drugs that alter the stomach pH [60]. LPT significantly increases exposure when administered in the fed state compared to the fasting state. Studies have shown that LPT exposure is ~4 times higher when taken with food [61]. On the other hand, the bioavailability of SFN decreases with food [62]. Systemic clearance (metabolism in the GI tract and liver, as well as excretion), solubility, stability, permeability, efflux/uptake transporters and small bowel dissolution rate all play a significant role in overall oral exposures. To determine whether the clearance is fast, moderate or slow, as compared to liver blood flow. Clearance values are typically classified as rapid if they go over 70% of liver blood flow [63]. In preclinical species (rats), about 26% of these drugs were quickly eliminated. Acalabrutinib, the smTKIs with the lowest T_{max} value, is prescribed at a higher dose because of its quick metabolism. A smTKIs with the highest T_{max} value is sunitinib.

3.3. *Distribution properties of smTKIs*

Distribution involves the movement of a drug from the bloodstream to various tissues and organs, allowing it to reach

Table 1 – Fundamental biopharmaceutical and clinical pharmacokinetic properties of smTKIs.

Drug/Proprietary name	Indication and approved year	Form, Dose and inhibitor	Biopharmaceutical and clinical pharmacokinetic properties
Acalabrutinib CALQUENCE®	MCL, CLL and SLL; 2017	Capsules; 100 mg b.i.d; BTK Inhibitor	IC_{50}: 5.10 nM; AUC $_{24\ h}$:1,843 ng·h/ml C_{max}: 563 ng/ml, oral bioavailability 25% PPB: 98% V_d (steady state): 101 l T_{max}: 0.9 h; $T_{1/2}$: 1.0 h Cl (steady state): 71 l/h
Afatinib/ GILOTRIF®	Metastatic NSCLC with EGFR mutation and squamous NSCLC after prior chemotherapy; 2013	Tablet; 40 mg q.d.; EGFR Inhibitor	IC_{50}: 0.70-50.00 nM C_{max}: Fat meal decrease C_{max} by 50% and AUC by 39% PPB: 95% T_{max}: 2.0–5.0 h; $T_{1/2}$ 37.0 h after repeated dosing in cancer patient
Avapritinib/ AYVAKIT™	GIST, AdvSM and ISM;2020	Tablet; 300 mg; Mutants KIT (stem cell factor receptor) and PDGFR Inhibitor	IC_{50}: 0.50 nM AUC $_{24\ h}$: 15,400 ng·h/ml C_{max}: 813 ng/ml PPB: 98% V_d (steady state):1,200 l T_{max}: 2.0 to 4.0 h; $T_{1/2}$: 32- 57 h Cl (steady state): 21.8 l/h
Alectinib/ ALECENSA®	ALK+ NSCLC; 2015	Capsules; 600 mg b.i.d.; ALK protein Inhibitor;	IC_{50}: 1.90 nM Steady-state $AUC_{0–12h}$: 7,430 ng·h/ml $C_{max,\ ss}$: 665 ng/ml (Reaches by 7 d) PPB: 99% V_d Apparent: 4,016 l T_{max}: 4.0 h; $T_{1/2}$: 33.0 h Cl (steady state): 82 l/h
Asciminib SCEMBLIX®	pH+ CML with at least one TKI prior treatment; 2021	Tablet; 80 mg q.d.; BCR gene and the ABL gene Inhibitor	IC_{50}: 5.80 nM C_{max}: 5,642 ng/ml PPB: 97% Vd Apparent:151 l T_{max}: 2.5 h; $T_{1/2}$: 5.5 h Cl (steady state): 4.1 l/h
Axitinib INLYTA®	ARCC; 2012	Tablet; 5 mg b.i.d.; Inhibits VEGFR, PDGFR, KIT RET, CSF1R and FLT3	IC_{50}: 0.10 nM AUC $_{24\ h}$: 265 ng·h/ml Moderate fat meal causes 10% low AUC & High-fat meals resulted in 19% higher AUC. C_{max}: 27.8 ng/ml PPB:> 99% Apparent V_d: 160 l T_{max}: 2.5–4.1 h; $T_{1/2}$: 2.5–6.1 Cl (steady state): 38 l/h
Binimetinib MEKTOVI®	Metastatic melanoma in combination with encorafenib with BRAF V600E or V600 K mutation; 2018	Tablets; 45 mg b.i.d combine with encorafenib; Inhibits MEK/Raf	IC_{50}: 12.0 nM < 40 % at steady state PPB: 97% Blood-to-plasma ratio-0.72. Apparent V_d: 92 l T_{max}: 1.6 h; $T_{1/2}$:3.5 h Cl (steady state): 20 l/h
Bosutinib BOSULIF®	pH+ CML; 2017	Tablet; 500 mg q.d.; ABL Inhibitor	IC_{50}: 1.20nM AUC $_{24\ h}$: 3,650 ng·h/ml in high-fat meal, AUC of bosutinib increases 1.7-fold. C_{max}: 200 ng/ml in high-fat meals, C_{max} increased 1.8-fold PPB: 94% Mean apparent Vd ± Sd: 6,080 ± 1,230 l T_{max}: 4–6 h; $T_{1/2}$:2.5 h Cl (steady state):189 l/h

(*continued on next page*)

Table 1 (*continued*)

Drug/Proprietary name	Indication and approved year	Form, Dose and inhibitor	Biopharmaceutical and clinical pharmacokinetic properties
Brigatinib ALUNBRIG®	ALK+ NSCLC; 2017	Tablet; 90 mg q.d (First 7 d) after 180 mg q.d.; Inhibits ALK, T790MF EGFR	IC_{50}: 1.50–2.10 nM AUC $_{24\,h}$:90 mg: 8,165 ng·h/ml; 180 mg: 20,276 ng·h/ml C_{max} 90 mg: 552 ng/ml; 180 mg: 1452 ng/ml PPB: 91% Steady-state apparent Vd: 307 l T_{max}: 1–4 h; $T_{1/2}$:25.0 h Cl (steady state): 8 l/h
Cabozantinib CABOMETYX®	ARCC and HCC; 2012	Tablet; 60 mg q.d.; Inhibits VEGFR2, PDGFR, KIT FLT3	IC_{50}: 0.04nM PPB: 99% V_d (steady state): 319 l T_{max}: 3–4 h; $T_{1/2}$: 99.0 h Cl (steady state): 2 l/h
Capmatinib TABRECTA™	Metastatic NSCLC with MET mutation; 2020	Tablet; 400 mg b.i.d.; Mutant MET	IC_{50}: 0.9 nM Vd (steady state): 164 l T_{max}: 1–2 h; $T_{1/2}$: 7 h PPB: 96% Cl (steady state): 24 l/h
Ceritinib ZYKADIA®	Metastatic ALK+ NSCLC; 2014	Capsule; 750 mg q.d.; ALK Inhibitor	IC_{50}: 8.0 nM AUC $_{0\text{-}\infty}$:10,600 ng·h/ml C_{max}: 219 ng/ml Vd (steady state): 4,230 l T_{max}: 4–6 h; $T_{1/2}$: 41.0 h PPB:97% Cl (steady state): 33 l/h
Cobimetinib fumarate COTELLIC®	Metastatic melanoma with BRAF V600E or V600 K mutation; 2015	Tablet; 60 mg q.d (First 21 d of each 28-d); MEK1/2 Inhibitor	IC_{50}: 1.9 nM AUC $_{24\,h}$: 4,340 ng·h/ml C_{max}: 273 ng/ml Vd (steady state): 806 l T_{max}: 2.4 h; $T_{1/2}$: 44.0 h PPB: 95% Cl (steady state): 13 l/h
CZT XALKORI®	ALK/ROS1 positive NSCLC in adults and ALK+ ALCL in pediatric patients; 2011	Capsule; 250 mg b.i.d for metastatic NSCLC and 80 mg/mm^2 orally b.i.d for systemic ALCL; Inhibits ALK, MET	IC_{50}: 6.0 nM Vd (steady state): 1,772 l T_{max}: 4–6 h; $T_{1/2}$: 42.0 h for single dose PPB: 91% Cl (steady state): 100 l/h for single oral dose – 250 mg
DAB mesylate TAFINLAR®	NSCLC and metastatic melanoma; 2013	Capsule;150 mg b.i.d.; BRAF Inhibitor	IC_{50}: 2.80 Nm Vd (steady state): 70.3 l T_{max}: 2 h; $T_{1/2}$: 8.0 h PPB: 99% Cl (steady state): Single dose17 l/h; Twice dose 34 l/h
Dacomitinib VIZIMPRO®	NSCLC; 2018	Tablet 45 mg q.d.; Inhibits Mutant EGFR	IC_{50}: 0.4 nM AUC $_{24\,h}$: 2,213 ng·h/ml C_{max}: 108 ng/ml Vd (steady state): 1,889 l T_{max}: 6.0 h; $T_{1/2}$:70.0 h PPB: 98% Cl (steady state): 24 l/h
DAS SPRYCEL®	pH+ CML and pH+ ALL; 2006	Tablet 100 mg q.d.; Inhibits ABL, PDGFR, KIT, SRC	IC_{50}: > 5 nM T_{max}: 0.5–6 h Vd (steady state):2,505 l PPB: 96%
Encorafenib BRAFTOVI®	Combination treatment for metastatic melanoma and CRC; 2018	Capsule; 450 mg q.d.; Inhibits MEK/RAF	IC_{50}1.2–5.7 nM T_{max}: 2 h; $T_{1/2}$: 3.5 h Vd (steady state):164 l PPB: 86% Cl (steady state): 14 l/h

(*continued on next page*)

Table 1 (*continued*)

Drug/Proprietary name	Indication and approved year	Form, Dose and inhibitor	Biopharmaceutical and clinical pharmacokinetic properties
Entrectinib ROZLYTREK®	ROS1-positive NSCLC and solid tumors; 2019	Capsule; 600 mg q.d. for NSCLC; Inhibits NTRK1/2/3 ROS1, ALK	IC_{50}: 30 nM T_{max}: 4–6 h; $T_{1/2}$: 20.0 h Vd (steady state): 551 l PPB: 99% Cl (steady state): 19 l/h
Erdafitinib BALVERSA	Urothelial carcinoma; 2019	Tablet; 8 mg b.i.d.; FGFR inhibitor	IC_{50}: 4 nM AUC $_{24\,h}$: 29,268 ng·h/ml C_{max}: 1,399 ng/ml Mean apparent Vd: 29 l $T_{1/2}$: 59.0 h PPB: 99% Cl (steady state):0.36 l/h
Erlotinib TARCEVA®	Metastatic NSCLC and pancreatic cancer; 2004	Tablet; 150 mg q.d.; EGFR Inhibitor	IC_{50}: 220 nM Vd (steady state): 232 l $T_{1/2}$: 36.0 h PPB: 93%
Futibatinib LYTGOBI®	Metastatic intrahepatic cholangiocarcinoma with FGFR2 gene fusion; 2022	Tablet;20 mg q.d.; Inhibits FGFR2	IC_{50}: 0.7 nM AUC $_{24\,h}$: 790 ng·h/ml C_{max}: 144 ng/ml Vd (steady state): 66 l T_{max}: 2 h; $T_{1/2}$: 2.9 h PPB: 95% Cl (steady state):20 l/h
Gefitinib IRESSA®	First-line treatment of metastatic NSCLC with EGFR mutation; 2015	Tablet; 250 mg q.d.; EGFR Inhibitor	Vd (steady state): 1,400 l PPB: 90%
Gilteritinib XOSPATA®	AML with FLT3 mutation; 2018	Tablet; 120 mg q.d.; Inhibits FLT3, RTKs	IC_{50}: 100 to 600 nM AUC $_{24\,h}$: 6,943 ng·h/ml C_{max}: 374 ng/ml T_{max}: 4–6 h; $T_{1/2}$:113.0 h Vd (steady state): 1,092 l PPB: 94% Cl (steady state):14 l/h
Ibrutinib IMBRUVICA®	MCL, CLL, and MZL; 2013	Capsule and tablet; 560 mg q.d.; BTK Inhibitor	IC_{50}: 0.9 nM AUC $_{24\,h}$: 420 mg: 708 ng·h/ml; 560 mg: 865 ng·h/ml T_{max}: 1–2 h; $T_{1/2}$: 4.0–6.0 h Vd (steady state): ~ 10,000 l PPB: 97% Cl (steady state): 76 l/h
Imatinib GLEEVEC®	pH+ CML; 2001	Tablet; 400 to 600 mg q.d.; Inhibits Bcr-Abl, c-KIT PDGFR	IC_{50}: 5.0 to 11.0 nM AUC $_{24\,h}$: 42,600 ng·h/ml C_{max}: 2,900 ng/ml T_{max}: 2–4 h; $T_{1/2}$: 18.0 h PPB: 95% Cl (steady state):8–14 l/h depending on weight
Infigratinib TRUSELTIQ®	Locally advanced or metastatic cholangiocarcinoma; 2020	Capsule;125 mg q.d.; FGFR1–3 Inhibitor	IC_{50}: 9.20 and 10.80 nM AUC $_{24\,h}$:3,780 ng·h/ml C_{max}: 282 ng/ml T_{max}: 6 h; $T_{1/2}$: 34 h Vd (steady state): 1,600 l PPB: 97% Cl (steady state): 33 l/h
Larotrectinib VITRAKVI®	Solid tumors;2018	Capsules 25 mg/100 mg; And solution 20 mg/ml; Inhibits TRKs	IC_{50}: 4.0–39.00 nM AUC $_{24\,h}$: 4,351 ng·h/ml C_{max}: 788 ng/ml T_{max}: 1 h; $T_{1/2}$: 2.0 h Vd (steady state): 48 l PPB: 70% Cl (steady state): 98 l/h

(*continued on next page*)

Table 1 (*continued*)

Drug/Proprietary name	Indication and approved year	Form, Dose and inhibitor	Biopharmaceutical and clinical pharmacokinetic properties
Lapatinib TYKERB®	Metastatic breast cancer; 2007	Tablet; 1250 mg q.d.; Inhibits EGFR, ERBB2	IC_{50}: 0.07–6.0 nM AUC $_{24\,h}$: 362 ng·h/ml C_{max}: 243 ng/ml T_{max}: 4 h; $T_{1/2}$: 14.0 h Vd (steady state): 2,200 l PPB: > 99%
Lenvatinib LENVIMA®	Differentiated TC, ARCC and HCC; 2015	Capsules; 24 mg q.d.; VEGFRs Inhibitor	IC_{50}: 1.3–4.0nM AUC $_{24\,h}$:3,710 ng·h/ml C_{max}: Increased proportionally with dose T_{max}: 1–4 h post-dose; $T_{1/2}$: 28.0 h Vd (steady state): 50–163 l PPB: 99% Cl (steady state): 4–7 l/h
Lorlatinib LORBRENA®	ALK+ NSCLC;2018	Tablet; 100 mg q.d.; Inhibits ALK /ROS	IC_{50}: 59–92 nM AUC $_{24\,h}$: 5,650 ng·h/ml C_{max}: 577 ng/ml T_{max}: 0.5–4 h; $T_{1/2}$: 24.0 h Vd (steady state): 305 l PPB: 66% Cl (steady state): 11 l/h
Mobocertinib EXKIVITY™	Advanced and metastatic NSCLC; 2021	Capsule; 160 mg q.d.; Inhibits EGFR	IC_{50}: 2.5–250.0 nM T_{max}: 4 h; $T_{1/2}$: 18 h Vd (steady state): 3,509 l Cl (steady state): 138 l/h
Neratinib NERLYNX®	early-stage HER2-overexpressed breast cancer; 2017	Tablet; 4 mg t.i.d. (Day 1–14); Inhibits EGFR	IC_{50}: 1.70–40.70 nM Vd (steady state): 6,433 l $T_{1/2}$: 7–17 h PPB: 99% Cl: First dose 216 l/h; steady state 281 l/h
Nilotinib TASIGNA®	pH+ CML in patients resistant to prior therapy including IM; 2007	Capsule; 300 to 400 mg b.i.d.; Inhibits ABL, PDGFR KIT	IC_{50}: 10–146 nM AUC $_{24\,h}$: 300 mg: 11,865 ng·h/ml; 400 mg: 13,656 ng·h/ml T_{max}: 3 h after oral administration $T_{1/2}$: 17.0 h PPB: 98% Cl (steady state): 300 mg:25 l/h; 400 mg: 29 l/h
OSI TAGRISSO®	First-line treatment of metastatic NSCLC with EGFR exon 19 deletion or exon 21 mutation; 2015	Tablet; 80 mg q.d.; EGFR Inhibitor	IC_{50}: 1.4 nM C_{max} and AUC $_{24\,h}$: Increased dose proportionally T_{max}: 6 h; $T_{1/2}$: 48.0 h Vd (steady state): 918 l PPB: 95% Oral clearance (Cl/F): 14 l/h
Pazopanib VOTRIENT®	ARCC and ASTS individuals with prior treatment; 2009	Tablet; 200 mg q.d.; Inhibits VEGFR2, PDGFR, c-KIT	IC_{50}: 20 nM AUC $_{24\,h}$: 1,037 ng·h/ml C_{max}: 58,100 ng/ml T_{max}: 2–4 h; $T_{1/2}$: 30.0 h Vd (steady state): 22.3 l PPB: > 99% Cl (steady state): 0.46 l/h
Pemigatinib PEMAZYRE®	Relapsed or refractory MLNs and in unresectable metastatic cholangiocarcinoma with FGFR2; 2020	Tablet 13.5 mg q.d.; FGFR Inhibitor	IC_{50}: 0.37 - 5.4 nM AUC $_{24\,h}$:1.21 ng·h/ml C_{max}: 2.88 ng/ml T_{max}: 1 h; $T_{1/2}$: 15.4 h Vd (steady state): 235 l PPB: 91% Cl (steady state): 10.6 l/h

(*continued on next page*)

Table 1 (*continued*)

Drug/Proprietary name	Indication and approved year	Form, Dose and inhibitor	Biopharmaceutical and clinical pharmacokinetic properties
Pexidartinib TURALIO™	TGCT; 2019	Capsule; 400 mg b.i.d.; Inhibits CSF1R, c-KIT FLT3	IC_{50}: 0.4 nM AUC $_{24\ h}$: 77,465 ng·h/ml C_{max}: 8,625 ng/ml T_{max}:2.5 h; $T_{1/2}$: 26.6 h Vd (steady state): 187 l PPB: 99% Cl (steady state): 5.1 l/h
Ponatinib ICLUSIG®	pH+ ALL and chronic, blast, accelerated CML; 2012	Tablet; 45 mg q.d.; Inhibits ABL	IC_{50}: 3.0 nM AUC $_{24\ h}$: 1,253 ng·h/ml C_{max}:73 ng/ml T_{max}: 6 h; $T_{1/2}$: ~ 24.0 (12–66) h Vd (steady state): 1,223 l PPB: 99%
Pralsetinib GAVRETO™	Metastatic RET fusion-positive NSCLC and TC;2020	Capsule; 400 mg q.d.; Inhibits RET	11–28 nM AUC $_{24\ h}$:284,089 ng·h/ml C_{max}: 2,830 ng/ml T_{max}: 2–4 h; $T_{1/2}$: 14.7 h Vd (steady state): 228 l PPB: 97% Cl (steady state): 9.1 l/h
Regorafenib STIVARGA®	Metastatic GIST and previously treated CRC; 2012	Tablet; 160 mg q.d. (First 21 d of 28-d cycle); Inhibits VEGFR2 Tie_2	IC_{50}: 3.3 ± 1.2/ 2.8 ± 1.2 nM (JAK 1/JAK 2) AUC $_{24\ h}$: 35,070,000 ng·h/ml C_{max}: 2,500 ng/ml T_{max}: 4 h; $T_{1/2}$: 28.0 (14−58) h PPB: 99%
Ripretinib QINLOCK™	Advanced GIST with prior treatment of three or more kinase inhibitors, including IM; 2020	Tablet; 150 mg q.d.; Inhibit KIT, PDGFR-α mutants	IC_{50}: 1–2 nM AUC $_{24\ h}$: 5,678 ng·h/ml C_{max}: 761 ng/ml T_{max}: 4 h; $T_{1/2}$: 15 h Vd (steady state): 307 l PPB: 99% Cl (steady state): 15 l/h
Ruxolitinib JAKAFI®	myelofibrosis and polycythemia vera; 2011	Tablet; 5–25 mg; Inhibits KIT, PDGFR-α include mutants	IC_{50}: 14 nM T_{max}: 1–2 h post-dose; $T_{1/2}$: 3.0 h Vd (steady state): 72 l (patients with MF) & 75 l (patients with PV) PPB: 97%Cl :17 l/h (women)& 22 l/h (men)
Selpercatinib RETEVMO®	RET fusion-positive NSCLC, solid tumor and in TC for pediatric patients; 2020	Capsule; Based on body weight <50 kg: 120 mg; 50 kg or greater: 160 mg; Inhibits RET fusions	IC_{50}: 2,000−6,000 nM AUC $_{24\ h}$: 51,600 ng·h/ml C_{max}: 2,980 ng/ml T_{max}: 2 h; $T_{1/2}$: 32 h Vd (steady state): 191 l PPB: 96% Cl (steady state): 6 l/h
SEL KOSELUGO®	pediatric Patients (2 years or above) with neurofibromatosis type 1; 2020	Capsule 25 mg/m^2 b.i.d.; Inhibits MEK1/2	IC_{50}: 2–80 nM AUC $_{24\ h}$: 2,009 ng·h/ml C_{max}: 731 ng/ml T_{max}: 1–1.5 h; $T_{1/2}$: 6.2 h Vd (steady state): 78–171 l Cl (steady state): 8.8 l/h
SFN NEXAVAR®	Unresectable HCC, ARCC; 2005	Tablet; 400 mg b.i.d.; Inhibits VEGFR2, PDGFR, KIT, FLT3,BRAF	IC_{50}: 4 nM T_{max}: ~3 h PPB: 99% Cl (steady state) (Cl/F): 8 l/h

(*continued on next page*)

Table 1 (*continued*)

Drug/Proprietary name	Indication and approved year	Form, Dose and inhibitor	Biopharmaceutical and clinical pharmacokinetic properties
Sunitinib malate SUTENT®	GIST and ARCC; 2006	Capsule; 12.5–50 mg; Inhibits VEGFR, KIT, PDGFR, RET, CSF1R, FLT3	IC_{50}: 56–1377 nM T_{max}: 6–12 h; $T_{1/2}$: 40.0–60.0 h Vd (steady state): 2,230 l PPB: 95% Cl (steady state): 34–62 l/h
Tepotinib TEPMETKO®	metastatic NSCLC with MET exon 14 alteration; 2020	Tablet; 450 mg q.d.; Inhibits MET ex 14 alterations	IC_{50}: 0.70–0.90 nM AUC $_{24\,h}$: 27,438 ng·h/ml C_{max}: 1,291 ng/ml T_{max}: 8 h; $T_{1/2}$: 32 h Vd (steady state):1,038 l PPB: 98% Cl (steady state): 24 l/h
Tofacitinib XELJANZ®/XELJANZ XR	Rheumatoid and psoriatic arthritis, ulcerative colitis, repurposed for cancer	IR Tablet 5 mg and ER Tablet11 mg q.d.; Inhibits JAK3	IC_{50}: 40 nM (IR) & 31 nM (ER) T_{max}: 0.5–1 h(IR) &4 h (ER) $T_{1/2}$: 3.0 h (IR) & 6.0 h (ER) Vd (steady state): 87 l PPB: 40%
Trametinib MEKINIST®	metastatic melanoma with BRAF V600E or V600 K mutations; 2013	Tablets; 2 mg q.d.; MEK Inhibitor	IC_{50}: 450 nM AUC: increases proportionally with dose C_{max}: Dose-dependent T_{max}: 1.5 h post-dose; $T_{1/2}$: 93.0–115.0 h Vd (steady state): 214 l PPB: 97%
Vandetanib CAPRELSA®	Metastatic TC; 2011	Tablet; 300 mg q.d; Inhibits RET, VEGFR, FGFR, EGFR	IC_{50}: 0.5–5.1 nM AUC $_{24\,h}$: 15,438 ng·h/ml C_{max}: 739 ng/ml T_{max}: 6 h; $T_{1/2}$: 456.0 h Vd (steady state):7,450 l PPB: 90% Cl (steady state): 13 l/h
Vemurafenib ZELBORAF®	Metastatic melanoma and Erdheim Chester Disease with BRAF V600E and V600 mutation; 2011	Tablet;960 mg b.i.d; BRAF Inhibitor	IC_{50}: 0.9 nM AUC $_{24\,h}$: 601,000 ng·h/ml C_{max}: 62,000 ng/ml T_{max}: 3 h; $T_{1/2}$: 57 h Vd (steady state):106 l PPB: 99% Cl (steady state): 1.3 l/h
Tucatinib TUKYSA®	HER2-positive BC; 2020	Tablet; 300 mg b.i.d; ErbB2 Inhibitor	IC_{50}: 8.0 nM AUC $_{24\,h}$: 5,620 ng·h/ml C_{max}: 747 ng/ml T_{max}: 1–4 h; $T_{1/2}$: 12 h Vd (steady state):903 l PPB: 97% Cl (steady state): 53 l/h
Zanubrutinib BRUKINSA®	MCL with prior therapy, Waldenström's macroglobulinemia and MZL; 2019	Capsules; 160 mg b.i.d; BTK Inhibitor	IC_{50}: 1.9 nM AUC $_{24\,h}$: 2,099 ng·h/ml C_{max}: 295 ng/ml T_{max}: 2 h; $T_{1/2}$: 2–4 h Vd (steady state): 537 l PPB: 94% Cl (steady state): 128 l/h

Data collection from FDA website.

Abbreviations: BCR, breakpoint cluster region; ALK, Anaplastic lymphoma kinase; b.i.d, bis in die; q.d., quaque die; ABL, Abelson; CSF1R, colony-stimulating factor 1 receptor; FLT3, Fms-like tyrosine kinase 3; AdvS, Advanced systemic mastocytosis; BRAF, v-raf murine sarcoma viral oncogene homolog B1; TRKs, tropomyosin receptor kinases; IR, Immediate-release; ER, Extended-release; SLL, Small lymphocytic lymphoma; ISM, Indolent systemic mastocytosis; ARCC, Advanced renal cell carcinoma; HCC, Hepatocellular carcinoma; ALCL, Anaplastic large cell lymphoma; ALL, Acute lymphoblastic leukemia; CRC, Colorectal cancer; NTRK, Neurotrophic tyrosine receptor kinase; MZL, Marginal zone lymphoma; TC, Thyroid cancer; ASTS, Advanced soft tissue sarcoma; MLN, myeloid lymphoid neoplasms; TGCT, Tenosynovial giant cell tumor.

Table 2 – BDDCS classification of smTKIs [57,59].

smTKIs	BDDCS	smTKIs	BDDCS
Acalabrutinib	II	Lapatinib ditosylate	II
Afatinib	III	Larotrectinib sulfate	I
Alectinib	II	Lenvatinib	NA
Amivantamab	NA	Lorlatinib	II
Asciminib	NA	Mobocertinib	NA
Avapritinib	II	Neratinib maleate	II
Axitinib	II	Nilotinib	II
Binimetinib	I	OSI	NA
Bosutinib	NA	Pazopanib	II
Brigatinib	II	Pemigatinib	II
Cabozantinib	NA	Ponatinib	NA
Capmatinib hydrochloride	II	Pralsetinib	II
Ceritinib	NA	Regorafenib	NA
Cobimetinib fumarate	I	Ripretinib	NA
CZT	II	Ruxolitinib	NA
DAB	II	Selpercatinib	I
Dacomitinib	II	SEL sulfate	I
DAS	II	SFN	NA
Encorafenib	NA	Sunitinib malate	I
Entrectinib	II	Tepotinib	NA

its target sites of action. Factors influencing drug distribution include blood flow to different organs, drug properties (lipophilicity and molecular size), and drug transporters. Log P (pH independent) and log D (pH dependent) are used to measure the lipophilicity of drugs. Since smTKIs are pH dependent and contain an ionizable moiety at a particular pH, log D is considered a more comprehensive and accurate lipophilicity descriptor than Log P, providing a more realistic representation of how an ionizable compound behaves in biological systems [64,65]. Drug protein binding is another factor that affects the distribution. From Table 1, most of the smTKIs exhibit high protein binding results in low volume of distribution (V_d) and longer half-life ($T_{½}$). V_{ss} is a theoretical parameter used to represent how extensively a drug is distributed throughout the body. While it lacks physiological significance, it provides a general understanding of drug distribution. In a study involving 54 smTKIs, these drugs were found in various tissues, such as the liver, kidney, lung, gastrointestinal tract, and glandular tissues. However, most of them had limited penetration into the central nervous system. The apparent volume of distribution at steady state ($V_{d,ss}/F$) values ranged from 48 to 10,000 l. Reviewing the plasma protein binding (PPB) levels across rats in all 54 smTKIs (Table 1) revealed that about 29% of these drugs had ~99% protein binding, and only ~8% of them exhibited < 70% binding. PPB was as low as 40% for a drug such as tofacitinib.

3.4. *Metabolism*

Bioavailability measures the fraction of an administered drug dose that reaches system circulation in an unchanged form. Extensive research on the clinical pharmacokinetics of AFA shows that it has 95% bioavailability and is minimally metabolized in the human body, primarily eliminated

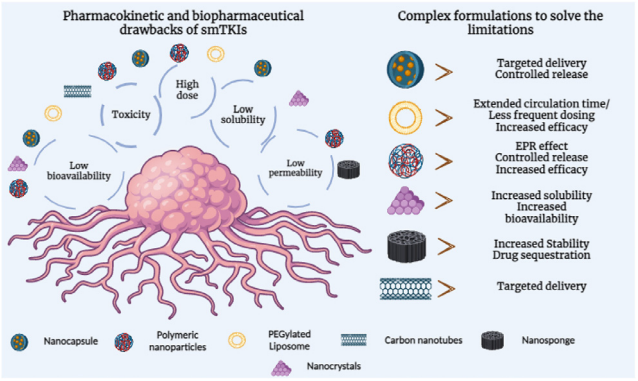

Fig. 5 – Schematic diagram of biopharmaceutical and pharmacokinetic properties of various smTKIs with respect to complex drug delivery system.

unchanged through feces. Only a small portion of the drug is eliminated through urine. The low metabolism of AFA may be due to the formation of covalent bonds with the plasma proteins via a chemical reaction called Michael addition, which bypasses enzymatic catalysis [66]. However, the metabolism of smTKIs can be influenced by various factors such as liver function, age and disease conditions (cirrhosis). Adjustment of smTKIs dosage is necessary for these individuals. After exploring the metabolic pathways and enzymes involved in the clearance of these smTKIs, around CYP3A4 cleared 76% of kinase inhibitors. In addition, CYP2D6, CYP1A1, CYP2C8, UGT1A19, CYP2C9, UGT, SULT1A1 CYP1A2, CYP2C19, CYP2C8, CYP3A5, and UGT1A3, CYP3A4, and UGT1A4, as well as hydrolytic enzymes, play a role in metabolizing 24 % of these drugs. Though not much data, first-pass metabolism (FPM) is a serious concern, and changing route of administration may be the only effective way.

4. Complex formulations for improving the therapeutic efficacy of smTKIs

Various complex formulations have been approved in the last decades for drugs such as DOX, IM, DAS and others. This complex formulation can be one among micelles, NPs, liposomes, nanosponges, nanocrystals, nanocapsules and CNTs. These systems provide benefits, such as targeted drug delivery, improved drug stability, prolonged circulation, and improved therapeutic outcomes, as shown schematically in Fig. 5. Examples include polymeric micelles with drug-loaded cores, NPs with enhanced permeability and retention (EPR), liposomes with extended circulation times, nanosponges for drug sequestration and delivery, nanocrystals for solubility enhancement, polymeric nanocapsules with liquid/solid cores, and functionalized CNTs for targeted therapy. The section briefly describes the various complex nanoformulations close to realizing clinical translation and their properties in correlation with various smTKIs and their route of administration, as shown in Fig. 6.

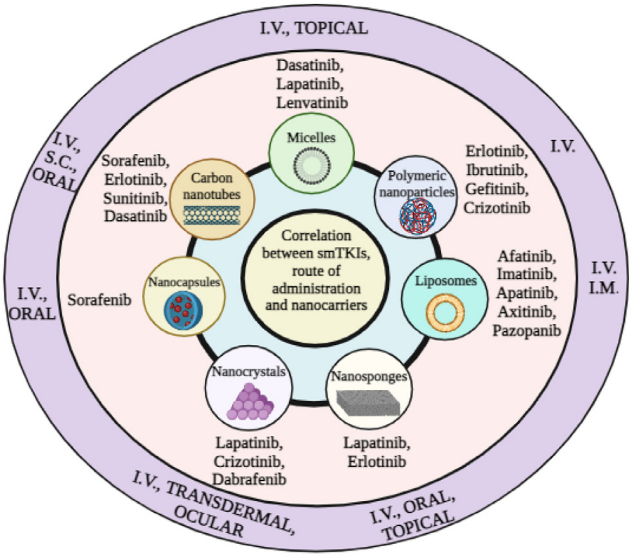

Fig. 6 – Schematic representation of correlation between smTKIs, route of administration and nanocarriers.

4.1. *Micelles*

These are systems of amphiphilic nature with a hydrophobic core and hydrophilic outer layer in a spherical shape. The hydrophobic core carries drugs of the same nature while the hydrophilic surface makes it easy to deliver the payload. Such amphiphilic carriers are formed by using di- or tri-block, graft and ionic copolymers. Due to their nano-size (<100 nm), polymeric micelles can successfully enter tissue without being detected by the mononuclear phagocyte system (MPS), giving them enough time to accumulate at the target region. Moreover, the presence of polymers in polymeric micelles has been demonstrated to make them biodegradable. Further to these benefits, polymeric micelles exhibit a regulated drug release profile, an improved drug loading capacity, and environmental protection for the encapsulated pharmaceuticals. Although there are drawbacks to polymeric micelles, such as low stability in the gastrointestinal environment, numerous methods have been documented to increase the stability of the polymeric micelle. In order for the polymer to maintain the drug in the gastrointestinal environment, crystallized polycaprolactone is primarily utilised to improve the stability of polymeric micelles [67]. The physical stability of the drug-loaded polymeric micelles can also be increased by increasing the intensity of the cohesive force that persists between the drugs and the polymeric core [68]. Multiple parameters, including pH, enzymes, and bile salts, need to be taken into account when determining the stability of polymeric micelles in the GI environment. Therefore, to address the stability issues with polymeric micelles, a mix of various solutions may be used. USFDA has approved estrogen-based polymeric micelles formulations for marketed use, namely Estrasorb® [69]. Genexol-PM is another PEG-based di-block copolymer-based micelles of PTX approved for the treatment of metastatic breast cancer in South Korea.

4.2. *NPs (polymeric or lipidic)*

These are nanoparticulate systems made of various polymers (PLGA, PLA, chitosan, alginate etc.) or inorganic material between the range of 10–1,000 nm [69]. In pharmaceutical research, particularly in the area of oncology, NPs have drawn a lot of interest. The extensive focus on NPs in cancer therapies has been greatly influenced by the EPR effect; because of this effect, NPs can gather preferentially in tumor masses, as well as inflammatory and infectious locations. It occurs because tumors have aberrant and leaky vasculature, which enables NPs to extravasate and build up in the tumor microenvironment. According to reports, the majority of peripheral human tumors have effective blood vessel endothelial pore size in the range of 200 to 600 nm in diameter. Passive targeting of NPs to tumors may be achievable, depending on the size of the leaky vasculature. For administration of cancer drugs, the EPR effect has various benefits, including enhanced accumulation, prolonged retention and selective targeting [70]. By attaching certain ligands or antibodies to their surface, NPs can be generated to actively target tumor cells. More precise delivery of drugs to tumor cells is made possible while minimizing systemic side effects thanks to this active targeting and the passive accumulation caused by the EPR effect [71–73]. In 2005, FDA approved Abraxane®, a nanoparticle-bound albumin formulation of PTX, to diagnose breast cancer, pancreatic cancer and NSCLC. Ontak® is another inorganic NP approved by FDA.

4.3. *Liposomes*

The fundamental composition of liposome is consists of an aqueous core encircled by one or more lipid bilayers. Amphiphilic molecules, which have both hydrophilic and hydrophobic areas, join together to form lipid bilayers. Multiple types of liposomes can be identified depending on the size, content and structure of the individual particles. Liposomes can be classified into unilamellar, multilamellar, as well as small unilamellar (SUVs) and large unilamellar vesicles (LUVs). Main drawback of liposomes is their low $T_{1/2}$ due to the activation of the MPS. Several strategies have been used to improve the liposomes' circulation half-lives. One method is to add a negatively charged lipid called phosphatidylinositol to the liposomal formulation, which stabilizes the liposomes *in vivo*. This changes the surface charge composition of liposomes. Stealth liposomes are another approach to counter the high blood clearance of liposomes [74]. A biocompatible polymer that could elude immune detection was grafted onto liposomes. A biocompatible polymer is one like that, such as polyethylene glycol (PEG). When PEG-lipid conjugates are present, a hydrophilic, sterically stabilized aqueous shell forms, making the liposomes immune system elusive. An example of such a stealth liposome is Doxil® [75], it is a FDA-approved marketed product containing DOX in its core and coated with PEG. Another marketed liposomal formulation includes a liposomal formulation of daunorubicin and cytarabine called vyxeos®. Thermodox, a heat-sensitive liposomal construct of DOX, received USFDA fast track designation.

4.4. *Nanosponges*

Nanosponges are extremely small, sponge-like particles that are often made of biocompatible polymers such as cyclodextrins, PEG and polyvinyl alcohol (PVA). These particles can absorb and sequester a variety of compounds, including poisons and therapeutic substances, due to their porosity shape. Anticancer drugs can be added to nanosponges either physically encapsulated within the porous structure or chemically conjugated to the surface. Nanosponges are appealing for cancer treatment due to their special characteristics, such as great stability, extended blood circulation times, and immune system evasion. Additionally, targeting ligands or antibodies can be functionalized on nanosponges to enable targeted therapy and precise drug administration by allowing them to recognize and bind to cancer cells. Preclinical studies have shown that nanosponges have the potential to limit tumor growth, reduce drug resistance and enhance therapeutic outcomes, even if the concept of using them to treat cancer is still in its infancy. To completely comprehend their safety, effectiveness and potential for inclusion in cancer therapy regimens, however, more investigation and clinical trials are required. Cyclodextrin, DNAzyme and ethycellulose-based nanosponges have extensively been used in cancer research for delivering drugs like ETB, PTX, camptothecin, DOX and withaferin A [76].

4.5. *Nanocrystals*

High manufacturing cost, platform instability, loading issues and hurdles in scale-up are some of the common problems related to NPs, liposomes or solid lipid NPs (SLNs). Contrarily, drug nanocrystals can be injected intravenously without the use of any carrier materials for encapsulation and/or solubilization, albeit most of the time surfactants or polymers are required for stabilizing pure drug crystals in order to minimize aggregations. Drug crystals with a particle size of a few hundred nanometers are known as nanocrystals. These nanocarriers are preferred for drugs with poor solubility, and most of the smTKIs are BCS class II drugs. It can increase pharmacokinetics properties and decrease fed-fasted variability of drug substances. Panzem® [77] is an example of 2-methoxyestradiol drug nanocrystal which completed its phase II study for safety and effectiveness in relapsed multiple myeloma and phase I study for advanced solid tumor indication. Paxceed^{TM} [78] is another example of PTX drug nanocrystal under investigation.

4.6. *Nanocapsules*

Polymeric nanocapsule consisting of a liquid/solid core coated with a polymeric shell. Due to their core-shell microstructure, polymeric nanocapsules have gained increased attention in recent years for use in drug delivery applications. The solid/oil core of nanocapsules can significantly improve drug-loading efficiency as compared to polymeric nanospheres. Moreover, smart compounds that may interact with certain proteins can functionalize the polymeric shell, providing targeted drug delivery. Since an amount of anti-cancer drugs have hydrophobic qualities, different nanocapsule delivery techniques have been developed to get around this restriction and boost the effectiveness of anti-cancer therapy. The choice of polymers and formulation techniques is primarily determined by the properties of the pharmaceutical ingredient and the intended application. Polymeric nanocapsules have the potential to increase the bioavailability of medications and allow for sustained and targeted distribution when utilized as drug delivery vehicles. Additionally, they can successfully reduce the negative interactions between the drug and the tissue milieu around it. The drug is shielded against biologically-induced efficacy loss or degradation by being enclosed in polymeric nanocapsules. Additionally, this strategy can lessen the negative effects the drug has on healthy tissues. The majority of studies have concentrated on creating and describing polymeric nanocapsules filled with bioactive materials. The storage and sterilization procedures for these drug-loaded polymeric nanocapsules, however, must also be taken into consideration and call for additional study and development [79]. DOX, 5-fluorouracil, camptothecin and gemcitabine are some anti-cancer drugs that have been investigated as nanocapsule formulations.

4.7. *Carbon nanotubes (CNTs)*

The cylindrical group of carbon allotropes known as fullerenes includes CNTs with special physicochemical characteristics that make surface modification simple. The development of polyvalent CNTs as cancer therapeutic tools is moving very quickly. The most promising strategy is the targeted administration of medications, which is intended to aim the therapeutic treatment specifically for tumors. Based on their capacity to penetrate biological barriers, functionalized CNTs have demonstrated considerable potential as innovative delivery systems. Various *in vitro* and *in vivo* studies demonstrated that a wide variety of chemically functionalized CNTs are compatible with the biological environment, highlighting how the degree and type of functionalization, both crucial factors that need to be precisely controlled, could modulate the material's behavior when used in living organisms. DOX, PTX, gemcitabine and camptothecin have been investigated as CNT formulations and have shown better profiles than the conventional therapies of the same drugs [80,81].

5. Recent advances in complex formulation of smTKIs

The following section describes and analyses the recent advancements in complex formulations of the smTKIs, especially appraising and discussing in detail the *in vivo* improvements in pharmacokinetics of the smTKIs from complex formulations. The key components and results of these systems are summarized in Table 3.

Table 3 – Advances in complex formulations of smTKIs.

Drug	Complex formulation: Ingredients /Technique	Pharmacokinetic Studies/Findings	Ref
Imatinib (IM)	Liposome: DOX and IM in a combination. And FA-PEG3350-CHEMS and mPEG2000-Hz-VES modified the pH sensitivity of the liposomes.	Compared to the free DOX groups, FPL-DOX/IM liposomes enhanced IM concentrations by 1–8 folds and DOX concentrations by 2–8 times at the tumor site.	[82]
	NPs: IM loaded in the hydrophobic domain of BSA to develop a realgar (As_4S_4) nanocrystal co-delivery system. FA was used as a stabilizer.	Free IMA showed a $T_{1/2}$ of 8.8 h, whereas the As/IMA+FA NP extended $T_{1/2}$ of IMA to 11.9 h, AUC and efficacy increased.	[83]
Afatinib (AFA)	Redox-sensitive lipid-polymer hybrid NPs: Self-assembled Tf-modified redox-sensitive AFA-loaded LPNs were synthesized using the nanoprecipitation method.	C_{max} was 26 l/kg/h, and the estimated AUC was 867 mg/l/h. Terminal $T_{1/2}$ was around 43.25 h	[84]
	Polymeric NPs (P-NPs): A combination therapy of AFA and CPT was formulated as LPHNPs. PLGA is used as a polymer.	Concentration above IC_{50} values (5 g/ml) were obtained.	[85]
	Liposomes: Transmembrane ammonium sulfate gradients were used to create AFA LPs. Immuno-LPs were created by reacting thiolated antibodies with sulfhydryl-containing LPs.	Approximately 68.97 g/ml of liposomes (LPs) were present in the plasma, whereas 55.06 g/ml of LPs loaded with CTX were present.	[86]
Apatinib (APA)	NPs: APA loaded in Poloxamer 407 and PLGA NPs	Tumor volume reduction by more than two-fold was achieved.	[87]
	Liposome: Lecithin, cholesterol and PEG-DSPE polymer were used to develop an APA-containing PEG-modified liposome.	The quantity of tumor nodules and tumor weight were both considerably decreased.	[88]
	Liposome: cRGD and PEG-modified liposomes (cRGD-Lipo-PEG) loaded with APA.	82.1% reduction in tumor mass three times higher tha than free APA.	[89]
Axitinib (AXT)	Liposomes AXT-loaded NPs were prepared by using DDAB and DPPC in an appropriate amount along with cholesterol: DPPC in ration 2:7. This optimized DDAB contributes to the LPs having sufficient charge density to allow electrostatic interactions. Following that, the LPs were electrostatically coated using PEG-b-PAsp.	Efficacy shown by tumor volume, angiogenesis and apoptosis	[90]
	P-NPs: AXT was loaded in MSNPs containing CST, which was further coated with PEG, forming a lipid bilayer.	Decreased expression of HIF-1αin hypoxic environments.	[91]
Cabozantinib	NPs: Cabozantinib-loaded NPs were prepared by using poly [DL-lactic-co-glycolic]-COOH and DiR dye at a ratio of 50:50, which was further coated with BSA.	BSA coating of the NPs improved the intratumoral distribution of cabotezumab.	[92]
Dabrafenib (DAB)	NPs: DAB was mixed with HSA and formulated into an emulsion. An acid-labile linker CA was conjugated with D-HSA which been further conjugated with CD47.	Enhanced deposition of the formulation in the tumor, efficient tumor suppression, and little off-target retention.	[93]
	NPs: Formed by incorporating the drug in PCL-PEI, a cationic and amphiphilic block copolymer. It delivered the Dab and miR-200c.	At low dose, the development of tumors was reduced.	[94]
Dasatinib (DAS)	Micelles: DAS was encapsulated in micelles. The polymer used was SMA.	Nanoformulations were seven times more efficient in reducing the development of tumors.	[95]
	NPs: A self-delivery system was developed by modifying DAS with succinic anhydride followed by connecting with hydrophilic CPT to produce an amphiphilic drug-drug conjugation with a DAS: CPT ratio of 2:1.	Survival of the animals treated with CPT-DAS NPs approached 90% within 30 d	[96]
Erlotinib (ETB)	P-NPs: PAA-ss-OA used to encapsulate ETB by emulsification and solvent evaporation method to formulate redox responsive and pH sensitive NPs.	After 21 d, PAA-ETB-NP inhibited tumor growth by 84.5% than ETB solution (38.1%).	[97]
	P-NPs: In this study, ERT-HSA-HA NP was prepared by precipitation method.	ERT-HSA NPs and ERT-HSA-HA NPs identical $T_{1/2}$ of approximately 91.2 and 96.4 min.	[98]
	P-NPs: ETB was used to prepare a PLA-based nanoplatform for tumor drug delivery (NP-EB). GSI-DAPT was entrapped within the NPs (NP-EB/DART). CF peptide was decorated on the surface (CF-NP-EB/DART).	Mice injected with CF-NP were found to have large deposition at the tumor site.	[99]

(*continued on next page*)

Table 3 (*continued*)

Drug	Complex formulation: Ingredients /Technique	Pharmacokinetic Studies/Findings	Ref
Ibrutinib (IBR)	P-NPs: PLGA NPs loaded with IBR, nanoprecipitation technique been employed in the preparation of polymeric NPs.	Bioavailability of reported NPs almost 4.2-fold higher than pure IBR. C_{max} and AUC were also 4 times higher as compared to IBR suspensions.	[100]
	Nanosuspension: BBD was applied and solvent-antisolvent precipitation method was used with pluronic F127.	Better bioavailability and less variation between the fed and fasting stages.	[101]
Pazopanib	Liposome: Colon-targeted liposomal drug delivery system of pazopanib by utilising a high-pressure homogenization process.	Considerably lower tumor volume and weight.	[102]
Sorafenib (SFN)	Nanotubes: SFN loaded CNTs using an alginate-based technique.	AUC found to be 680.60 μg·h/ml, $T_{1/2}$ was 18.43 h which are many folds higher than the conventional therapies with SFN.	[103]
	Nanocapsule: Prepared by the phase-inversion temperature technique, using Transcutol HP, Labrafil, Peceol, Labrafac, and Captexand oleic acid.	Nanocapsule-treated mice had an improved blood flow in the tumor's centre.	[104]
	Liposomes: Three liposome were developed: uncoated, a HA-coated and a PEGylated HA-coated	Increased AUC value, ~3 times higher than the SFN solution, and also extended $T_{1/2}$ by ~2.4 times.	[105]
	NPs: Known as NPTPGS-SFB, was made up of the aryl-containing segment PBLG, the dendritic molecule PAMAM-G3, and a TPGS polymer.	NP-TPGS-SFB therapy can stop tumor development up to 87 mm^3 in size.	[106]
	NPs: Ring-opening polymerization was used to synthesize the mPEGPDLLA block copolymer for using it as a carrier system.	Rate of clearance was significantly lower.	[107]
	NPs: Using NUFS technique, SFN was made into NPs.	AUC $_{0-48\ h}$ (ng·h/ml) was 35,560 ± 10,549; C_{max} (ng/ml) was 4,316 ± 1,798; T_{max} (h) 3.71 ± 1.46.	[108]
Lapatinib (LPT)	Nanosponges (NS) Eudragit RS100-based NS with LPT were formulated.	C_{max} of LPT NSs increased three times more than that of the LPT pure drug group.	[109]
	Micelles Thin-film hydration method was used. After that the formulation was lyophilized using mannitol as a cryoprotectant.	Better encapsulation and solubility of LP are connected to the increased cytotoxicity of LP-PMs against SKBr3 breast cancer at considerably lower doses.	[110]
	Micelles: Pluronic F127 micelles loaded with PTX-LPT.	The investigated formulation is more concentrated in the liver.	[111]
	Nanocrystals: For tumor targeting, HA-coated LPT-NCs were created utilizing high-pressure homogenization.	LPT-HA-NCs produced higher tumor suppression and improved survival rates in animals.	[112]
	Liposome: Film hydration method was used in the formulation of liposome.	Enhance the drug's accumulation in organs, anticancer activity and survival time are improved.	[113]
	Liposome: Liposomal LPT combined with photodynamic therapy.	Survival time for U87 tumors clocked at 16 d with LPT alone, 22 d with only PDT, and almost 30 d with a combination of PDT and LPT.	[114]
Gefitinib (GFT)	NPs: GFT SLNs use Lipoid S PC-3.	SLN significantly decreased the nephrotoxicity. To increase the bioavailability and effectiveness of the delivery of SLN to treat breast cancer at all stage	[115]
	NPs: PCEC was used in the preparation of NPs using solid dispersion method.	Increased survival time.	[116]
	NPs: GFT and curcumin-loaded NPs.	The overall tumor size was significantly decreased by the reported formulation.	[117]
Lenvatinib (LFT)	Micelles: Soy PC and SGC were the main component; By classical coprecipitation under the optimal conditions.	C_{max} of LFT MM was 1,497.14 ng/ml. Showed a noticeable 500-fold increase in LFT solubility.	[118]
Osimertinib (OSI)	NPs: PEG-S- SEL and a film-dispersion technique been employed to make OSI+SEL NPs.	The weight of the tumor in the reported nanoparticle's treatment group was less than that in the OSI NP or SEL NP treatment groups.	[119]

(*continued on next page*)

Table 3 (*continued*)

Drug	Complex formulation: Ingredients /Technique	Pharmacokinetic Studies/Findings	Ref
Crizotinib (CZT)	P-NPs: SFN and CZT were combined to form P-NPs in biodegradable triblock PEG-PCL-PEG, PECE. Using PCEC as a promising nanocarrier, the drug's water solubility was increased.	*In vivo* studies were conducted using the mouse model. Combined drug kills >80% of viable cells. Effectively decrease tumor development, indicating its effectiveness in treating lung cancer.	[120]
	P-NPs: Prepared by using poly(lactide), a biodegradable polymer combined with TPGS, which increases oral bioavailability of the formulation. Combined to form CZT/pD-PT NPs.	CZT NPs significantly inhibit tumor growth.	[121]
	Micelles: Synthesized using a 1:1 WT ratio of EDAC and SMA. Cricotinib and DAS were used in a combination.	Showed tumor suppression by 80%.	[122]

5.1. *Afatinib (AFA)*

AFA, an irreversible TKI, exerts its pharmacological activity by inhibiting certain tyrosine kinases, particularly in the ErbB family, including EGFR (ErbB1), HER2 (ErbB2), and HER4 (ErbB4). It is highly soluble over the physiological pH range of 1–7.5 with T_{max} of 2–5 h, minimal FPM, and covalent protein binding with $T_{1/2}$ of 37 h after repeated dosing. AFA's BCS Classification is unknown because of its high solubility and susceptibility to efflux transport by intestinal P-glycoprotein (Pgp). Based on its characteristics, it can be categorized into BCS class 1 or 3 drug [123]. The above parameters suggest that AFA is more appropriate for oral administration, with caution regarding the concomitant use of Pgp inhibitors or inducers. FDA approved AFA, an aniline-quinazoline derivative, in the year of 2013 for metastatic NSCLC treatment as a first-line drug. Jinli et al. prepared transferrin-containing, redox-sensitive ligand-polymer hybrid NPs loaded with AFA (Tf-SS-Afa-LPNs) in the year 2019. Nano-precipitation technique was employed to fabricate Tf-SS-Afa-LPNs using PLGA as a polymeric material. The optimized Tf-SS-Afa-LPNs showed an average size of 104 nm and surface charge of −21 mV with an entrapment efficiency of 90 %. The condition of tumor site was simulated by studying the *in vitro* release of the drug in presence of NSCLC (GSH), which showed an enhancement in release profile in the absence of GSH. In *in vitro* studies, the AFA -LPNs showed higher efficiency than free AFA on PC-9 cells. The *in vivo* study was conducted by intravenous administration of the formulation and free drug in Sprague-Dawley rats at a dose of 2.5 mg/kg of body weight. The obtained results demonstrated NPs site-specific release and improved pharmacokinetics than pure drug. AUC of Tf-SS-Afa-LPNs was ∼867 mg/l·h, which was larger than free AFA (404.73 mg/l·h, $P < 0.05$). Tf-SS-Afa-LPNs showed a peak plasma concentration (C_{max}) of 25 l/kg/h and a plasma $T_{1/2}$ of 43 h The final formulation exhibited appreciable anti-tumor efficacy and reduced volume of tumor cells compared to free AFA from 920 ± 1 mm^3 to 211 ± 1 mm^3 after 28 d of treatment as compared to pure drug [84].

To enhance drug loading efficiency and enable effective tracking of NSCLC cells, Ming-Hsien et al. [124] have developed near infrared-persistent luminescence nanomaterials (NIR PLNs) using a silica shell-assisted synthetic route to achieve uniform dispersion and utilized in the nano vehicle. NPs were prepared initially as mesoporous silica NPs (MSNPs) and further modified with $ZnGa2O4:Cr^{3+}$ to form PLNs for the loading of AFA. The surface of PLNs was further modified by a specific sequence of aptamer named MAGE-A3 by utilizing the Michael addition reaction. The optimized formulation showed an excitation band of PLN at around 265 nm, which revealed that doping Sn^{4+} is advantageous for increasing the efficiency and stability of PLNs. The surface-functionalized AFA-loaded PLN showed a significant tumor accumulation in lung cancer cells. The *in vitro* cell viability and cytotoxicity were carried out in CL1–5 lung cancer, Beas2B normal lung, and A549 cell lines, which showed that surface-modified AFA-loaded PLNs were effective against metastatic CL1–5 cancer cells. The drug was administered subcutaneously at a concentration of 10 μg/ml injecting orthotopically to cancer-induced left lung of mouse for *in vivo* study. The surface-modified AFA-loaded PLN could act as a highly sensitive sensor and a therapeutic agent for inhibiting lung cancer metastasis.

Dehui et al. [85] developed lipid-polymer hybrid NPs (LPH NPs) loaded with AFA and cisplatin (CPT) to treat nasopharyngeal carcinoma (NPC) using PLGA, 1,2-distearoyl-sn–glycero-3-phosphoethanolamine-N-amino(polyethylene glycol) (DSPE-PEG) and 1,2-dilauroyl-sn–glycero-3-phosphocholine (DLPC). The anti-tumor efficacy of drug-loaded NPs was tested using NPC xenograft model at a 5 mg kg^{-1} dose given intravenously. After evaluation, compared to free drug complex, particulate formulations were more effective in increasing cell apoptosis, decreasing cell viability and inhibiting cell migration and cell cycle. In CPT monotherapy, cell viability was 85.1 %, reduced to 39.5 % in CPT+AFA (1:1 w/w) combination therapy. The AFA+CPT-loaded NPs showed a significant delay in tumor growth with no cytotoxicity as compared to AFA/CPT-loaded LPH NPs and thus displayed a higher potential to treat NPC.

In another study, Xiaoyan et al. [86] prepared AFA-loaded immuno-liposomes (immuno-LPs) by incorporating CTX to enhance the circulation time and selectivity. CTX was conjugated with drug-loaded LPs to prepare "immune LPs" and provide selectivity towards tumor cells. Transmembrane ammonium sulfate gradients were used to develop AFA-LPs using hydrogenated soybean phospholipids (HSPCs), cholesterol and $DSPE\text{-}PEG_{2000}$ at a ratio of 60:36:4, with

(DSPE-PEG_{2000}_Maleimide) and solution of ammonium sulfate. Further, these sulfhydryl-containing LPs reacted with thiolated antibodies to form immuno-LPs and mAb. After evaluation, the internalization rate into A549 and H1975 cells of immuno-LPs was greater than normal liposomes and free drug. The *in vivo* study was carried out by intravenous administration at a dose of 4 mg/kg body weight in male Sprague–Dawley rats, which resulted in an increased AUC (92 h·μg/ml) with prolonged $T_{1/2}$ (9.5 h). The results showed that compared to free AFA and liposomes, immuno-LPs enhanced the tumor efficacy selectivity and reduced side effects in NSCLC xenograft model.

To enhance the efficacy of AFA in treating NSCLC, researchers have explored combination therapy and site-specific targeted delivery approaches. One such approach involves the use of liposomes and lipid polymer hybrid NPs (LPHNPs). These NPs can be tailored to improve drug stability, drug uptake by cancer cells, and prolong drug release at the tumor site. By utilizing these delivery systems, the researchers aim to achieve a more efficient and targeted delivery of AFA to the tumor cells in NSCLC.

However, despite the success of these delivery systems, the issue of patient compliance may arise. Taking AFA through intravenous administration can be inconvenient and may have certain drawbacks. An alternative approach to address this issue is to develop a dry powder inhalation formulation of AFA, which is cost-effective and allows direct deposition of the drug particles in the respiratory tract, enabling efficient drug absorption by the target cells in the lungs while minimizing systemic exposure. This approach bypasses the need for intravenous administration and offers a more patient-friendly and convenient option for administering AFA. Vanza et al. prepared AFA dimaleate loaded liposomes, later lyophilized with trehalose to form dry powder inhalation. A cellular uptake study showed that liposomes were internalized and exhibited lower IC_{50} value than plain drug.

5.2. *Apatinib (APA)*

APA is a smTKIs used to treat advanced or metastatic gastric cancer that specifically targets and inhibits VEGFR-2. APA shows a non-linear dose proportionality in relative bioavailability model using a sigmoidal E_{max} curve. Dosing of APA in certain patient groups requires adjustments [125], indicating that precision nanomedicines can improve therapeutic outcomes.

APA was encapsulated in PLGA and Poloxamer 407 NPs (APA/p NPs) by Zhang et al. [87] to enhance the effectiveness in treating melanoma. B16 cells were employed to investigate *in vitro* efficacy. On tumor B16 cells, APA/p NPs had a greater level of cytotoxicity than the free drug solution. The cytotoxic impact was stronger on B16 cells as the drug concentration had been increased. The viability of B16 cells significantly decreased when exposed to APA/p NPs containing 40 mg APA, resulting in a minimal number of surviving cells after 48 h Furthermore, ~0.1 ml B16 cell solution was injected into male C57BL/6 mice to develop a melanoma mouse model for testing *in vivo* effectiveness of the NPs. The investigation was accomplished by comparing with normal saline, blank NPs, APA (2, 4 and 6 mg/kg) and APA/p NPs (6 mg/kg^{-1}). The drug was administered over a 10-s period after the tumor was pierced. The saline-injected blank control group witnessed the quickest tumor development, on Day12, the tumor volume had increased up to 4,690 $mm^{3,}$ and the weight of tumor get doubled in control and PLGA groups than the APA group. The tumor weight and development in the APA/p NPs group were the lowest. The inhibition of tumor growth in melanoma mice treated with APA/p NPs was considerably greater than the other treatment groups, APA/p NPs were capable of efficiently eradicating tumor cells *in vivo*. As seen from Fig. 7, APA/p NPs were prepared for the effective treatment of melanoma.

Lecithin, cholesterol and PEG-DSPE polymer were used to develop an APA-containing PEG-modified liposome (APA-Lipo/PEG) by Hu et al. [88]. To improve aqueous solubility, hydrophilic PEG was extended out at the liposomal surface, while the water-insoluble APA was enclosed in the hydrophobic domains. APA-Lipo/PEG therapy for 48 h caused 4.6%, 8.3%, 6.7%, 15.9%, 40.6% and 44.9% of Annexin V+ cells in the CT26 cell line, according to cell apoptosis assay, rendering APA-Lipo/PEG therapy effective *in vitro*. CT26 cells-injected female BALB/c mice were investigated to confirm the *in vivo* efficacy of the liposomal formulation. A subcutaneous and peritoneal model was developed, and three distinct treatment groups, normal saline (NS), PEG-modified liposome (Lipo/PEG), and APA-Lipo/PEG were employed. The APA-Lipo/PEG group received an oral dosage of 50 mg/kg. The mice body weight of the APA-Lipo/PEG group in the peritoneal model was lower than that of the NS and Lipo/PEG group and the quantity of tumor nodules and tumor weight were both considerably decreased with APA-Lipo/PEG therapy, which demonstrated a notable decrease in tumor volume and tumor weight in the subcutaneous model. As a result, the findings showed that APA-Lipo/PEG had remarkable *in vivo* anti-tumor activity against mouse colorectal cancer.

When delivering APA to human colonic cancer, Song et al. [89] produced cRGD and PEG-modified liposomes (cRGD-Lipo-PEG) as a targeted delivery method. The results of an *in vitro* apoptosis study on HCT116 cells treated for 24 h with free APA, APA-loaded cRGD-Lipo-PEG and LipoPEG revealed significant apoptosis in the liposome-treated groups. For Lipo-PEG/APA and cRGD-Lipo-PEG/APA, early apoptotic ratios were around 7% and 14%, respectively, whereas late apoptotic ratios were 4.5% and 28%. HCT116 cells were implanted in female BALB/c nude mice for an *in vivo* study. A group of control and treated with free APA and cRGD-Lipo-PEG/APA was there, where the APA was given at a dose of 50 mg/kg. With a tumor mass of 0.18 ± 0.08 g and tumor volume of 272.5 ± 168.11 mm^3, cRGD-Lipo-PEG/APA was shown to be more effective against tumor than free APA and the PBS-treated control groups. The results show a significantly stronger impact of cRGD-Lipo-PEG/APA (82.1%) than free APA, which only had a statistically significant impact of 26.3% on the rate of reduction of tumor mass.

Although APA is approved to treat metastatic gastric cancer, ongoing research and clinical trials are exploring its potential use in other types of cancer, such as metastatic breast cancer, melanoma, metastatic colorectal cancer, and hepatocellular carcinoma (HCC). VEGFR-2 plays a crucial role in facilitating angiogenesis, a vital process for the growth and metastasis of various types of cancer. By inhibiting VEGFR-

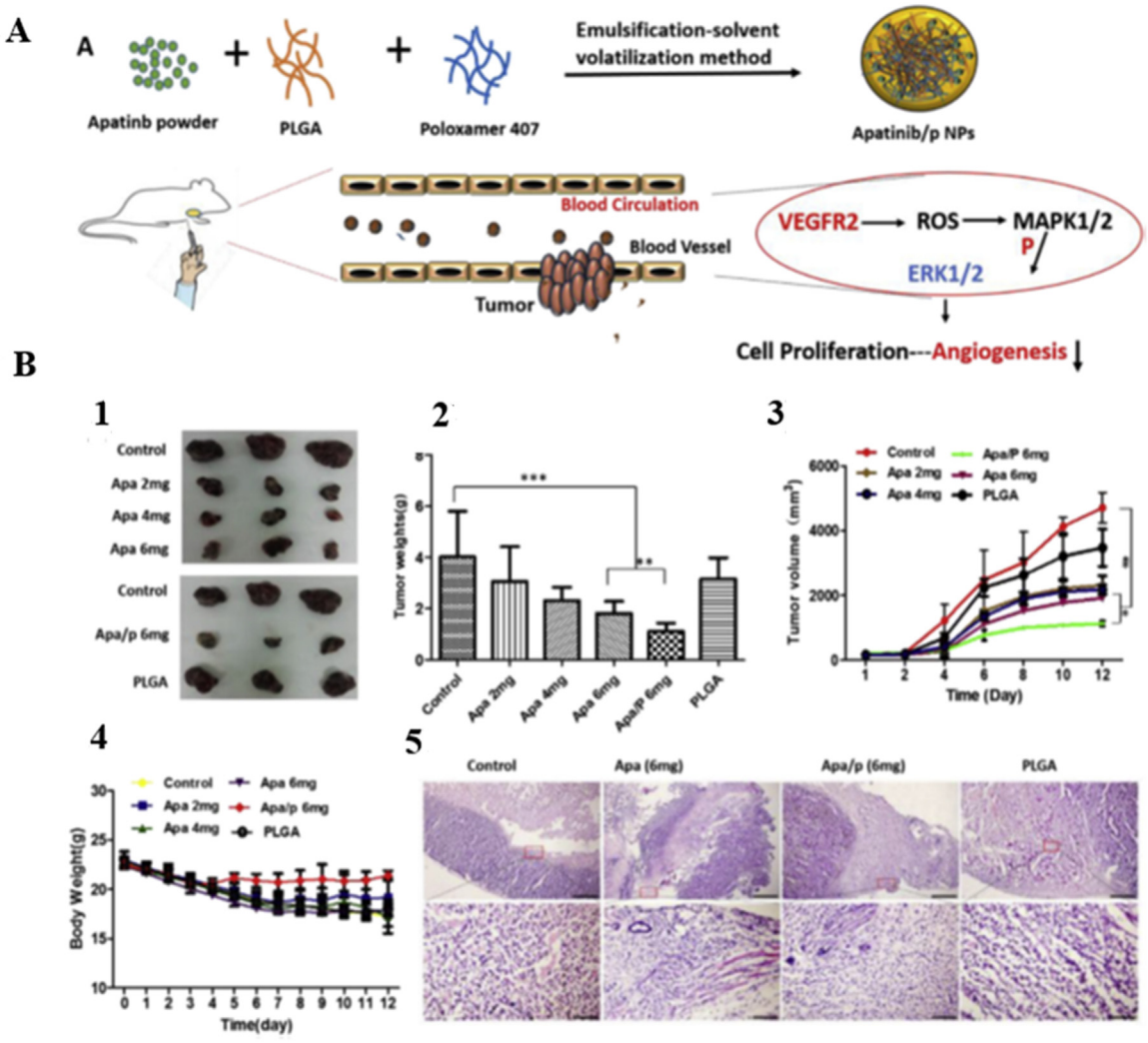

Fig. 7 – APA complex formulation and its efficacy in mice illustrated by (A) APA/p NPs preparation method and its inhibitory mechanism against melanoma. (B) *In vivo* antitumor effects in tumor-bearing C57BL/6 mice using B16 cells: (B1) Tumor photo from divergent mice group, (B2) Tumor weight, (B3) Tumor volume, (B4) Body weight, and (B5) H&E staining analysis. Reproduced with permission from [87].

2, APA can block angiogenesis in various cancers, leading to tumor regression or inhibition of further development.

5.3. *Axitinib (AXT)*

AXT, a potent VEGFR inhibitor (molecular weight 386 g mol^{-1}, log P 4.2, IC_{50} 0.10 nM), rapidly soluble with $T_{1/2}$ of 2.5 h and 58% mean absolute bioavailability. AXT's pharmacokinetic properties are ideal for preparing control release drug delivery system, which can reduce the dosing frequency (b.i.d). AXT shows substantial inter- and intra-patient variation in C_{max} was observed (0.02–11.2 ng/ml/mg), which depends upon glucuronidation activity, while another study has reported C_{max} in metastatic renal cell carcinoma (mRCC) between 12.4–40.2 ng/ml [126]. Precision nanomedicines can therefore improve the therapeutic efficacy.

AXT, used as second-line therapeutic agent for mRCC, inhibits VEGFR as reported in a clinical trial study conducted in 2016 [127]. Choi et al. [90] have developed AXT-loaded hybrid liposomal NPs coated with polypeptide (P-LNP/AXT) by utilizing a thin-film hydration technique, and the optimized formulation exhibited higher drug loading of 95% with narrow size distribution (~150 nm). Compared with free AXT and LNP/AXT, P-LNP/AXT had majorly inhibited tumor growth when the drug was injected intravenously at 1 mg/kg dose into mice. P-LNP/AXT demonstrated limited internalization by the mouse macrophage cell line RAW 264.7, implying their potential ability to evade the reticuloendothelial system. Furthermore, an upregulation in the levels of poly (ADP-ribose) polymerase and caspase-3, as well as a downregulation in the level of platelet/endothelial cell adhesion molecule 1 (PECAM1, CD31), were observed in tumor tissues, indicating the occurrence of apoptosis.

Choi et al. [91] developed MSNPs -loaded with celastrol (CST) and AXT within the PEGylated lipid bilayer. The complex formulation showed significant ($P < 0.05$) mitochondrial-

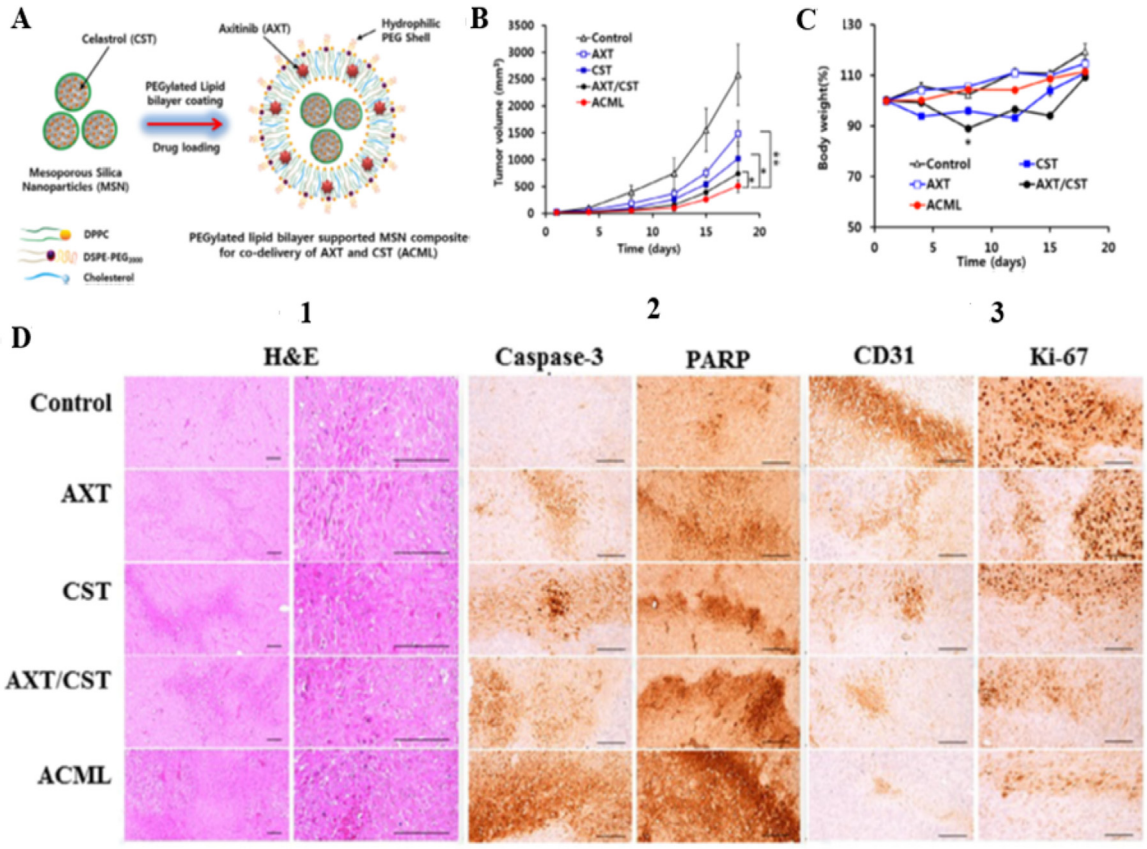

Fig. 8 – A complex formulation of AXT shown by its (A) preparation method of MSN-loaded AXT within the PEGylated lipid bilayer after intravenous administration of AXT, CST, AXT/CST and ACML to SCC7 xenografted mice its effect on (B) tumor volume and (C) body weight. (D1) Histopathological changes in nude mice antitumor activities of AXT and CST after treatment with AXT/CST-loaded combination NPs. Immunoreactivities of (D2) caspase-3 and poly (ADP-ribose) polymerase (PARP) and (D3) CD-31 and Ki-67 in tumor masses of nude mice following treatment with the indicated formulations. Reproduced from [91].

based apoptosis and cancer angiogenesis. Exposure of neuroblastoma (SH-SY5Y), squamous carcinoma (SCC7) and breast cancer (BT474) cell lines to the complex formulation resulted in a reduction in the expression of hypoxia-inducible factor (HIF)−1α, which might be a crucial factor for inhibiting tumor growth. Western blotting revealed that the NPs had a superior anticancer impact in many cancer cells. In complex formulation, both drugs synergistically controlled VEGFR. In tumor xenograft model, mice treated with the complex formulation exhibited 64% tumor inhibition. Immune-histochemistry revealed overexpression of poly (ADP-ribose) polymerase, caspase-3, and downregulation of Ki-67 and CD31 expression, indicating tumor apoptosis via mitochondrial and anti-angiogenic actions. As seen in Fig. 8A, the CST-AXT loaded PEGylated MSNs were prepared. The optimized formulation possesses reduction in tumor volume (Fig. 8B), and body weight (Fig. 8C). Histopathological changes in nude mice after treatment with AXT/CST-loaded combination NPs (D1), immunoreactivities of caspase-3 and poly (ADP-ribose) polymerase (PARP) (D2) and CD-31 and Ki-67 (D3) in tumor masses of nude mice showed tumor apoptosis via mitochondrial and anti-angiogenic activity.

5.4. *Cabozantinib*

Cabozantinib is a potent multiple TKI BCS class II drug (IC_{50}: 0.04 nM, practically insoluble in water) with an extended $T_{1/2}$ of ~99 h Due to its multiple tyrosine kinase inhibitory properties, cabozantinib can simultaneously target several signaling pathways (MET, VEGFR2, RET and AXL) involved in cancer cell growth and angiogenesis. This sustained inhibition of relevant kinases and extensive protein binding (>99%) is facilitated by its extended $T_{1/2}$, allowing for less frequent dosing schedules [128]. Furthermore, the therapeutic window for cabozantinib has been expected to be 540–620 ng/ml, which is considerably narrow, illustrating a drug with high efficacy but also high toxicity [129]. USFDA-approved cabozantinib to treat differentiated thyroid cancer, by inhibiting the tyrosine kinase activity of c-MET (mesenchymal-epithelial transition factor), VEGFR, MER (MerTK or Mer tyrosine kinase), KIT proto-oncogene, RET (rearranged during transfection) and AXL RTK.

Kiranj et al. [92] developed cabozantinib PLGA-COOH polymeric NPs coated with bovine serum albumin (BSA) for murine PTEN/p53-deficient prostate tumors. The *in vitro* study of the NPs showed that activated neutrophils internalized

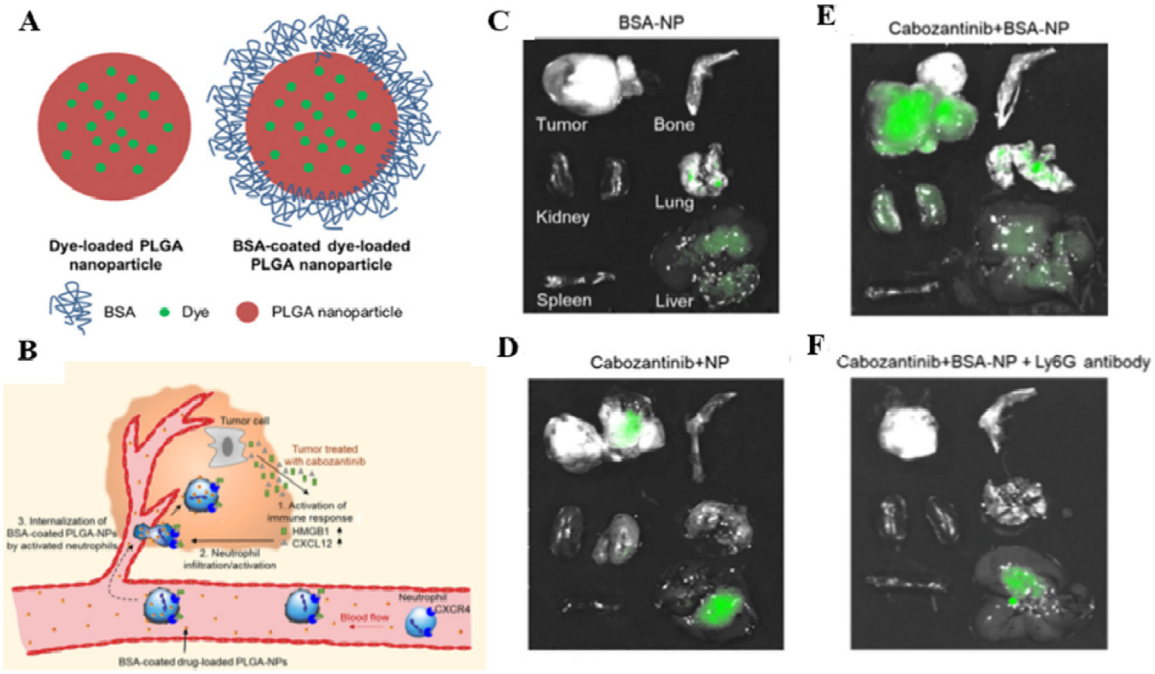

Fig. 9 – (A) Dye-loaded PLGA NPs with and without BSA coating. (B) Proposed model for cabozantinib poly (DL-lactic-co-glycolic)-COOH polymeric NPs coated with BSA for murine PTEN/p53-deficient prostate tumors. Fluorescence/bright field images of PTENflp53fl/fl mice with established prostate tumors after administration of BSA-NP (C), cabozantinib + uncoated NPs (D), cabozantinib + BSA-NP (E), and cabozantinib+BSA-NP+ Ly6 G antibody-treated groups (F). Reprinted from [92].

the BSA-coated NPs to a greater extent than the uncoated NPs. *In vivo* experiments were conducted on p53 mice using intravenous administration of BSA-coated NPs for 12 h daily, 3 d consecutivly. Study findings suggested that as compared to control group, the cabozantinib-loaded BSA-coated NPs treated group showed enhanced neutrophils up to 4-fold within tumor microenvironment. Targeted intratumoral delivery of NPs mediated by neutrophils was demonstrated by the depletion of Ly6 G and neutrophils, eliminating dye-loaded BSA-NP accumulation within tumors to normal levels. Figs. 9A and B represents the methods opted for the preparation of dye-loaded BSA-coated PLGA NPs and the mechanism of uptake of NPs. The cellular uptake of BSA-NP, cabozantinib-NPs, cabozantinib-BSA-NPs, and cabozitinib-BSA-NPs-Ly6 G antibody in various organs such as liver, kidney, spleen and lungs showed that BSA coating significantly increased NPs internalization by ~6 fold compared to uncoated NPs (Figs. 9C–9F). Due to its multiple kinase activity, it is tested in various cancers such as prostate, HCC and RCC. Additional research is required to explore the potential of cabozantinib in clinical treatment for various cancers.

5.5. *Crizotinib* (CZT)

CZT, a BCS class II drug, exhibits poor bioavailability (< 45%) and non-linear pharmacokinetics due to metabolism and is administered orally twice daily at a dose of 250 mg. It exhibits pH-dependent solubility (poor at higher pH) and a primary mode of elimination through feces with an extended $T_{1/2}$ of 42 h [130]. Bioavailability of CZT is 30%–60%, and high-fat meals reduce the AUC and C_{max} by ~14% [131]. Improving the pharmacokinetic properties of CZT is a compelling objective of formulation advances. CZT is a receptor d'origine nantais (RON) and HGFR (c-Met) inhibitor of RTK. CZT, along with alectinib, is used in the treatment of naive anaplastic lymphoma kinase-positive advanced NSCLC patient [132].

Zhong et al. [120] have formulated polymeric NPs for the effective delivery of CZT and SFN using a double-emulsion solvent evaporation method to treat lung cancer. The NPs were prepared at ratios of 2:1, 1:1 and 1:2 (SFN/CZT). Biodegradable triblock poly(ethylene glycol)-poly(ε-caprolactone)-poly(ethylene glycol) (PEG-PCL-PEG, PECE) polymeric NPs were prepared, and *in vitro* and *in vivo* studies were performed to investigate the effectiveness of NPs on lung cancer. Poly dispersive index (PDI) of the NPs (2:1, 1:1 and 1:2) was found 0.16, 0.11 and 0.21, respectively. SFN and CZT polymeric NPs exhibited sustained release with varying release rates over 72 h During this timeframe, the NPs released 63% of SFN and 50% of CZT. In A549 and 4T1 cells, the NPs exhibited significant apoptosis than free drugs. As compared to free drug, the intravenous administration of NPs at a dose of 10 mg/kg (SFN) and 5 mg/kg (CZT), a ratio of 2:1 (SFN/CZT) and concentration of 8.50 mg/ml to nude mice with 4T1 cancer cell xenograft model showed considerable reduction in tumor progression, improved survival rate with reduced liver toxicity, hypertension and visual disturbance.

Wang et al. [121] have evaluated the safety and efficacy of polydopamine-polylactide-TPGS NPs loaded with CZT (CZT-

pD-PT NPs) for the treatment of NSCLC. The optimized NPs demonstrated a sustained-release profile as compared to free CZT with enhanced cellular absorption. The optimized NPs showed approximately zeta potential of −23.7 mV, encapsulation efficiency of 84% and drug loading of 3%. *In vivo* studies finding suggest that as compared to free CZT and CZT NPs, the CZT-pD-PT NPs possess enhanced cellular apoptosis of cancer cells. Furthermore, the optimized formulation was evaluated against various markers such as ALT, ALP, DBIL and AST, and the result suggests that no significant effect was observed with CZT/pD-PT NPs. The study finding suggests that CZT/pD-PT NPs could be an effective strategy to modify and improve the chemotherapeutic property of CZT for NSCLC with minimum hepatotoxicity.

Khaled et al. [122] developed CZT and DAS-loaded micellar NPs for the treatment of glioblastoma multiforme. The CZT and DAS were encapsulated using poly (styrene-co-maleic acid) (SMA). The water solubility of SMA-CZT and SMA-DAS micelles was found to be 53.7 and 27.2 mg/ml, respectively. The average size and PDI of SMA-CZT were 121 nm and 0.251 and of SMA-DAS were 89 nm and 0.251. Cell viability assay performed on GBM cell lines showed 0.2 mM of free or micellar DAS and 4 mM of free or micellar CZT were capable of reducing the cell count by 60%. *In vivo* studies were conducted in female C57BL/6 mice, and the data revealed a decrease in tumor growth due to both free and micellar forms of drug, as well as the drug combination.

5.6. *Dabrafenib (DAB)*

DAB, commercialized as a mesylate salt, is classified as BCS class II drug (log P 2.9) and pH-dependent solubility where it is insoluble at pH 4–8. It exhibits high PPB (99%), with T_{max} of 2 h and $T_{1/2}$ of 8 h Oral immediate-release tablets are more suitable for DAB than control-release tablets as it shows pH-dependent solubility (practically insoluble above pH 4) [133]. Though the bioavailability of oral DAB is 95 %, DAB exposure (C_{max} and AUC) becomes non-linear function of dose after repeat twice daily dosing, attributed to induction of its own metabolism [134]. DAB has been used in combination with trametinib for the treatment of positive melanoma.

Pham et al. [93] developed DAB loaded human serum albumin (HSA) nanosystems conjugated with transmembrane protein CD47 for chemo-immunomodulation. CD47 was conjugated with DAB-loaded-HSA using cis-aconityl-PEG-maleimide (CA), an acid-labile linker (Fig. 10A). The resulting formulation demonstrated specificity for melanoma via targeting glycoprotein60 on cancer cell surface as well as release of drug in acidic tumor microenvironment pH compared to normal physiological pH. The optimized CD47-CA@D@HSA possesses an average size of ∼220 nm. In comparison to free DAB, CD47-conjugated nanosystems showed increased extent of internalization, accumulation, cytotoxicity and apoptosis by B16 F10 cells. The *in vivo* studies showed that CD47-CA@D@HSA treatment increased the migration of cytotoxic T cells and tumor-associated macrophages towards the tumors, including DAB, D@HSA, CD47-CA@D@HSA, PD-1, and CD47-CA@D@HSA + PD-1, where the doses of DAB, PD-1 and CD47 were 10, 5 and 2.5 mg/kg, respectively and the mice were treated with various intravenous injections except PD-1 (intraperitoneally). As seen from Fig. 10B, CD47-CA@D@HSA showed a reduction in tumor progression. Combination therapy using CD47-CA@D@HSA and PD-1 showed significantly enhanced antitumor activity compared to CD47-CA@D@HSA, D@HSA and free drug (Fig. 10C&10E) and no significant histopathological findings were observed in the major organs (Fig. 10D).

Nguyen et al. [94] have prepared NPs composed of a cationic amphiphilic block co-polymer called poly-b-caprolactone-polyethyleneimine (PCL-PEI) to deliver miR-200c and DAB simultaneously (miR-PCL-PEI/Dab NPs), in which DAB was entrapped within the hydrophobic core of PCL and the miR-200c was adsorbed on the cationic layer of PEI by means of electrostatic interactions. The miR-PCL-PEI/Dab NPs were further coated with Y2510924, a CXCR-4-targeting peptide conjugated with redox-sensitive polymer. The polymer was synthesized by cross-linking of poly-L-glutamic acid-thiol (PGA) with orthopyridyl disulfide (OPSS)-PEG-NHS to form a CXCR-4-targeted system for the simultaneous delivery of DAB and miR-200c (miR-PCL-PEI/Dab-PGA-pep). The *in vivo* results showed immunogenic cell death, and the PD-L1 expression gets suppressed due to treatment with CXCR-4 targeted NPs. To investigate *in vivo* biodistribution of the complex formulation Cy5.5-NHS was loaded onto the NPs following the same method as of Dab's loading. Mice with MC-38 tumors were intravenously injected with miR-PCL-PEI/Dab and miR-PCL-PEI/Dab-PGA-pep NPs that were labeled with Cy5.5.

5.7. *Dasatinib (DAS)*

Oral absorption of DAS occurs rapidly with T_{max} of 0.25–1.5 h and $T_{1/2}$ of 3–4 h Initially, DAS was administered twice daily, but due to tolerability issues, the approved dosage was optimized to 100 mg once daily, resulting in improved tolerability and lower discontinuation rates [135]. DAS inhibits receptors including c-KIT, BCR-ABL, SRC family, PDGFR-β and EPHA2, used for the effective treatment and management of Philadelphia chromosome-positive (pH+) CML. DAS exhibits high variation in exposure among patients, risking some toxicity while others obtain suboptimal efficacy [136]. Dose reduction has been implemented in CML patients. DAS within patient and between variation (40%–80%) has been observed for C_{max} and AUC [137–140]. The oral bioavailability also around 15%−50% [141,142], influenced by gastric pH ($pK_a = 3.1$, 6.8 and 10.8) as the drug precipitates in the small intestine [143]. These biopharmaceutical limitations can be overcome by developing complex formulations of DAS.

Bahman et al. [95] have formulated DAS encapsulated in SMA to produce SMA-DAS NPs (SMA@D NPs). The optimized NPs showed a zeta potential of 0.0035 mV, average size of 198 nm, PDI of 0.17 and loading capacity of 11.5%. Both free drug and SMA-drug exhibited significant cytotoxicity against 4T1 cells, which was higher compared to MCF-7 and MDA-MB-231 with IC50 values of approximately 0.014 µM and 0.083 µM, respectively. *In vivo* biodistribution studies showed that spleen, kidney and lung exhibited a higher accumulation of DAS after receiving SMA-DAS treatment (< 50%) to free DAS injection (> 50%). DAS showed positive outcome when used as a single agent or neoadjuvant to treat triple-negative breast cancer (TNBC) [95,144].

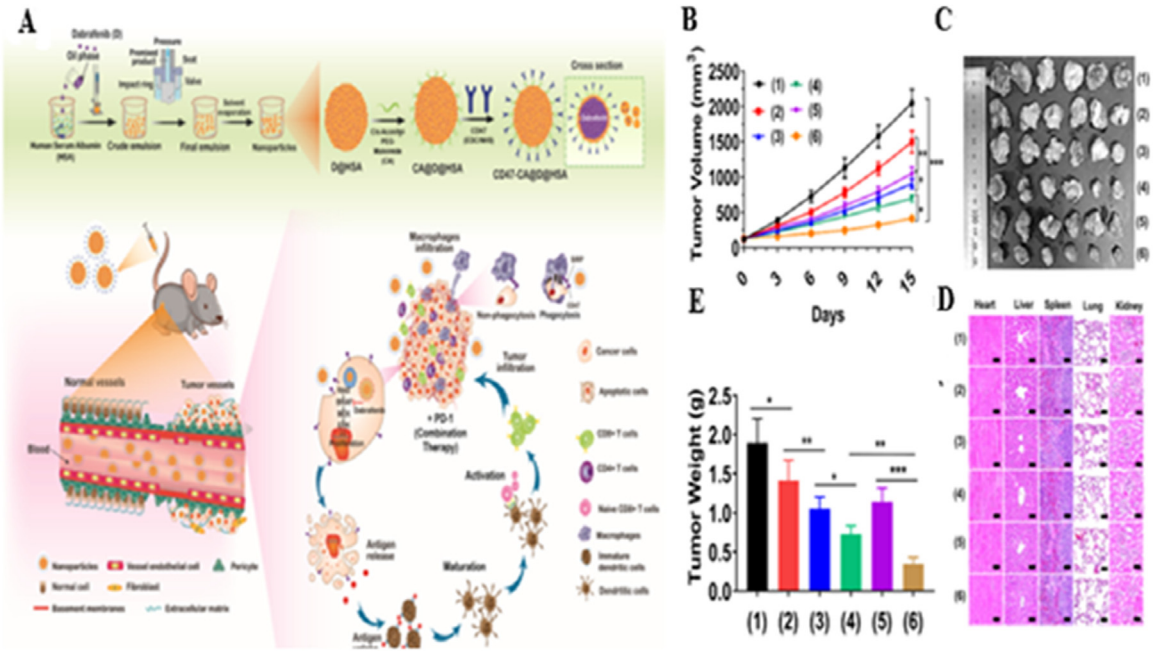

Fig. 10 – (A) Preparation and mechanism of CD-47-targeted DAB-loaded HSA NPs for anticancer chemoimmunotherapy. *In vivo* Study in B16 F10 tumor-bearing C57BL/6 mice showing (B) tumor volume examination and (C) tumor images. (D) Weight of tumor excised after 15 d and (E) histological H&E staining images of principal organs. Reprinted from [93].

Utilizing CPT and DAS derivatives, Yang et al. [96] have synthesized carrier-free amphiphilic drug-drug conjugate (ADDC), which get self-assembled and led to the formation of reduction-responsive NPs (CP-DDA NPs). DAS had been modified by succinic anhydride, and subsequently connected to CPT derivative by ester bonds. CP-DDA NPs had a size of 119 nm and PDI of 0.046. The *in vitro* release rates of CPT were 22.49% and 5.24% at pH 6.0 and 7.4, and 32.18% and 92.93% at pH 7.4+GSH and pH 6.0+GSH, respectively. The release of DAS reached 67.72 % in 24 h while being in a pH 6.0+GSH (10 mM) surroundings, and it increased to 81.97% in <50 h At pH 7.4 +GSH (2 uM), the DAS release rate was <30% in 48 h In contrast, even after 144 h, the amount of DAS released at pH 7.4 and 6.0 in the absence of GSH was below 25%. The use of CPT-DAS NPs led to a significant reduction in tumor progression, while also minimizing the toxic effects of CPT on healthy cells, particularly those located in the kidneys, nerves and the inner ear.

5.8. *Erlotinib (ETB)*

ETB belongs to BCS class II drug. It exhibits extensive FPM with T_{max} of 2–4 h and $T_{1/2}$ of 10–36 h It showed 60% bioavailability, which improved with food up to 100% [145–147]. The drug has high potency with IC_{50} values quite lower compared to other drugs in the series; however, incidences of adverse reactions are also higher (a narrow therapeutic index). Moreover, it requires 7–10 d to attain steady-state plasma concentration and is sensitive to gastrointestinal pH for effective absorption [148,149]. ETB is a well-known TKI for the treatment of advanced or metastatic pancreatic or NSCLC therapy.

Tan et al. [97] developed a pH-sensitive and redox-responsive NP containing ETB using poly (acrylic acid)-cystamine-oleic acid (PAA-ss-OA). They prepared ETB-loaded PAA-ss-OA-modified lipid NPs using an emulsification solvent evaporation technique (PAA-ETB-NPs). The particle size of the NP formulation was found to be 170 nm and zeta potential of −32 mV. The drug loading capacity and encapsulation efficiency were 2.6% and 85%, respectively. *In vitro* cytotoxicity studies revealed that ETB-NPs were more effective than ETB solution. Treatment with PAA-ETB-NPs significantly inhibited tumor growth in mice compared to ETB-NPs and ETB solution. *In vivo*, a xenograft nude mouse model with human lung cancer cells was used to evaluate the inhibition effect of ETB-NPs where PAA-ETB-NPs reduced tumor growth more than ETB-NPs ($P < 0.05$), ETB solution ($P < 0.01$) and saline control ($P < 0.001$).

Shen et al. [98] prepared ETB-albumin NPs co-modified with hyaluronic acid (HA) and HSA (ERT-HSA-HA NPs) by using precipitation method for NSCLC treatment. The drug loading and encapsulation efficiency of ERT-HSA-HA NPs were 5.65% and 81.2%, respectively. The *in vitro* release study of ETB from the NPs revealed no initial burst release effects. The optimized NPs exhibited significant anti-proliferative activity on A549 cells. *In vivo* studies showed that mice treated with ERT-HSA-HA NPs intravenously (dose = 10 mg/kg) demonstrated reduced tumor growth with no recurrence.

Wan et al. [99] prepared a PLA-based nano-platform (NP-EB) to target TNBC. Knowing EGFR inhibition resistance is due to Notch-EGFR, to counter this, a gamma-secretase inhibitor (GSI) called DAPT was incorporated into the core of the NPs to inhibit Notch signaling activation, resulting in the formation of NP-EB/DART, containing both ETB and DAPT. A new peptide

called CF was developed to achieve tumor-specific targeting by combining two distinct peptides, CREKA (a tumor-homing peptide) and F3 (a cell-penetrating peptide), linked together using a pH-sensitive hydrazone bond. Then, CF peptide was attached to the surface of NP-EB/DART, resulting in CF-NP-EB/DART, where these NPs when reached the tumor site, the unique acidic environment of the tumor triggers the breakdown of the pH-sensitive linkage exposing F3 peptide facilitating the internalization of NPs. The CF-NP-EB/DART NPs exhibited a narrow particle size distribution with a PDI of 0.179, zeta potential of 24.3 mV, entrapment efficacy of 42%, drug loading of 0.8%, and an XPS assay value of 0.56%. *In vitro* studies were conducted using human adenocarcinoma cells (MCF-7) and normal human dermal fibroblast cells (NHDF) to evaluate the cytotoxic effects of the nanoparticle formulation (5 mg/kg), demonstrated that the nanoparticle formulation exhibited higher cytotoxicity towards MCF-7 cells than NHDF cells.

5.9. *Ibrutinib (IBR)*

IBR is a Bruton's TKI (BTK) used for the treatment of mantle cell lymphoma (MCL), chronic lymphocytic leukemia (CLL) and B-cell malignancies. The drug is practically insoluble in water, rendering absolute oral bioavailability of the drug between 4%−15% depending upon food administration. IBR bioavailability is reduced because of extensive fast oxidative transformation by hepatic cytochrome P450 [150–152]. It is currently undergoing clinical investigations against patients suffering from multiple hematologic malignancies as well. In 2013, IBR approvaled by FDA under the brand Imbruvica® for mitigating MCL, CLL, Waldenstrom macroglobulinemia, lymphoma and graft-versus-host disease. IBR is considered a BCS-Class II drug as it is low soluble and highly permeable. IBR is insoluble in aqueous solvents and exhibits a maximum solubility of 13 µg/ml at pH 8.0. IBR exhibits poor bioavailability, limiting to 3.9% upon oral administration and high FPM as the solubility of drug is a pre-determined factor for drug dissolution, absorption and distribution either for onsite action or to enter into the systemic circulation. A maximum daily dose of IBR up to 420 mg is given orally for patients with CLL and up to 560 mg for MCL to exhibit better therapeutic benefits [153]. Though IBR has shown potential effects against MCL and CLL, its application in cancer has been limited because of adverse effects such as atrial fibrillation, diarrhea, bleeding and infection upon continuous use. A clinical study in patients (9%−23%), reveals that off-target effects of IBR could be the major reason for various adverse effects associated with the drug [154–156]. In a clinical study conducted on patients with CLL, IBR showed a T_{max} of 2 h and $T_{1/2}$ of 6–9 h The AUC increased gradually with the increase in dose at a range of 420–840 mg/d [157]. Investigational studies are currently underway to enhance the bioavailability and reduce its adverse effects while aiming to enhance its therapeutic efficacy in clinical setting.

Abdullah et al. [100] prepared IBR-loaded PLGA NPs using the nanoprecipitation technique to improve oral bioavailability. IBR suspensions at 10 mg kg^{-1} or an equivalent dose of IBR-loaded NPs were orally administered in a Wister albino rat. Study findings suggested enhancement of oral bioavailability of IBR-loaded NPs by around 4-fold as compared to free IBR solution. The C_{max} of the NPs and free IBR-solution was approximately 574 ng/ml and 146 ng/ml ($P < 0.01$), respectively. The results revealed that PLGA NPs could improve IBR's bioavailability and therapeutic effectiveness.

Nagarjun et al. [101] prepared IBR nanosuspension employing precipitation ultrasonication technique to enhance the oral bioavailability of IBR with reduced fast-fed state variability. Pluronic F127 was used as a stabilizer and the nanosuspension formulation exhibited mean particle sizes between 278 and 453 nm and PDIs between 0.055 to 0.198, respectively. DSC and powder XRD proved that the active ingredient transformed from a crystal to an amorphous state. The nanosuspension resulted in a 21-fold enhancement in the solubility of IBR. IBR solution possesses C_{max} of 49 ng/ml and $AUC_{(0\text{-}t)}$ 138 ng/ml ($P < 0.01$) in fasting states, whereas IBR loaded nanosuspension showed improvement in C_{max} (~3.5 folds) and $AUC_{0\text{-}t}$ (~5.8 folds) in the same states. In case of both the fed and fasted stages, no distinct variation in the pharmacokinetics of nanosuspension was found. These findings suggested that nanosuspension could be an effective method for the enhancement of solubility as well as absorption with reduced variability.

5.10. *Imatinib (IM)*

IM is a protein smTKI and blocks the Bcr-Abl tyrosine kinase, approved for the treatment of CML in 2001. It was the first ever smTKI to get approval from FDA. It is a selective inhibitor of PDGFR-α and PDGFR-β. IM marketed by Novartis under the brand Gleevec™ as. a methane sulfonate salt, which is available as a capsule equivalent to 100 mg IM-free base [158]. IM is extremely hydrophobic in nature, and conversion into the salt form enhanced its bioavailability. IM-free base in water is practically insoluble (0.001 g/100 ml), whereas its mesylate form in water shows higher solubility at a pH < 5.5 [159]. IM mesylate falls under the BCS Class-I due to its high solubility. Upon oral administration, IM mesylate exhibits a $T_{1/2}$ of 18 h and T_{max} of 2–4 h, showing around 97% bioavailability. The AUC increases with the dose range of 25–1,000 mg. The drug shows around 95% human plasma binding particularly to α1- acid glycoprotein and albumin. Similar to other smTKI-inhibitors, IM also has side effects such as diarrhea and nausea. Periorbital hypertrophy, edema and myelosuppression are the most frequently reported adverse effects associated with this drug [160,161]. IM therapy is reported to be associated with high variability in exposures, and poor compliance [162,163]. Moreover, IM concentrations > 1,000 ng/ml are needed for event-free survival, but just 1.6 times higher concentrations are correlated with diarrhea and edema [164,165]. This indicates a need for formulation interventions.

Chen et al. [82] developed DOX and IM co-loaded pH-sensitive liposomes functionalized with folate (FPL-DOX/IM) and cleavable TPGS analog where alpha tocopheryl acid succinate (VES) was chemically coupled to PEG through an acid-labile hydrazone linker. The co-loaded liposomal formulation was stable in blood circulation even after 24 h The formulation possessed a diameter of 100 nm. Co-

loaded liposomes reduced ABC transporter function and enhanced chemotherapeutic sensitivity, thus helping to overcome the chemoresistance associated with DOX. *In vivo* studies conducted for pharmacokinetics assessment in female Kunming mice via intravenous administration at a IM dose of 45 mg/kg and DOX dose of 3 mg kg^{-1} showed that after 24 h, the drug level of DOX and IM (~0.8 and ~7.2 μg/ml, respectively) was maintained. Anti-tumor efficacy study conducted in MCF-7/ADR xenografted BALB/c nude mice concluded that co-delivery of IM and DOX increased their therapeutic efficacy. Further, functionalized liposomal construct provided acid sensitivity and long circulation time with less systemic toxicity.

Wang et al. [83] developed realgar (As_4S_4) nanocrystals with a consistent size of ~40 nm by using a bottom-up method. The As_4S_4 nanocrystals were stabilized using BSA, a frequently utilized carrier for nano-drug delivery due to its affordability, compatibility with living beings, and numerous functional groups ideal for loading and modifying drugs. An As4S4 and IM co-delivery system (As_4S_4/IMA) was formed in this study due to the efficient incorporation of IM into the hydrophobic areas of BSA. Folic acid (FA) was functionalized to BSA to enable its recognition of tumor cells as a target, and FA was then used as a ligand to stabilize As_4S_4 nanocrystal (As/IMA@FA). A synergistic effect for the treatment of CML was meticulously achieved by carefully balancing the drug ratio within the co-delivery system. Healthy SD rats were used in a pharmacokinetics study, and 2 mg/kg of free IM was administered intravenously along with As/IMA@FA NPs. The outcomes showed that free IM had a $T_{1/2}$ of 8.8 h, was rapidly excreted from the body, and was almost undetectable after 10 h However, when given as As/IMA@FA NPs, which have an extended $T_{1/2}$ of 11.9 h, IM circulation was markedly prolonged. Additionally, compared to free IM, the apparent AUC of the NPs was significantly larger. Female BALB/c nude mice with K562 cell-induced tumors were injected with As/IMA NPs and As/IMA@FA NPs via the tail vein in order to examine the biodistribution and *in vivo* antitumor efficacy. The study showed that As/IMA@FA NPs improved drug uptake and extended circulation in the tumor. Additionally, the tumor-targeting effect was improved with the inclusion of FA modification, leading to greater tumor suppression for As/FA NPs. The As/IMA@FA NPs had the best results among these NPs, almost completely inhibiting tumor growth.

5.11. *Lenvatinib (LFT)*

LFT, an FDA-approved kinase inhibitor since 2015, effectively blocks the functions of various VEGF and FGF receptors, including VEGFR1 (FLT1), VEGFR2 (KDR), VEGFR3 (FLT4), FGFR1, FGFR2, FGFR3 and FGFR4. It also inhibits PDGFR, KIT and RET. LFT is a potent drug but routine follow-ups have become important due to several adverse effects [166], which indicate that complex formulations can improve therapeutic outcomes.

A conventional co-precipitation method by Zhang et al. [118] has been utilized to develop LFT-loaded sodium glycocholate and soy phospholipid mixed micelles (LFT-MMs). LFT-MMs demonstrated a significant improvement in solubility (500-fold), encapsulation efficiency (87.6%) and adequate stability (> 1 month at 4 °C). *In vitro* anti-tumor study revealed that compared to LFT and LFT mesylate, LFT-MMs demonstrated improved inhibitory action against differentiated thyroid cancer cells (BCPAP and FTC-133). Pharmacokinetic studies conducted in SD rats after oral administration showed that LFT-MMs had a relative bioavailability of 177% compared to LFT. $AUC_{0-\infty}$ of LFT-MMs was found significantly higher (~ 13,200 μg·h /l) compared to free LFT mesylate (~ 7,500 μg·h /l).

5.12. Osimertinib *(OSI)*

OSI is a kinase inhibitor of EGFR, approved by FDA in 2015. It exhibits linear pharmacokinetics but has very low solubility [167]. The $T_{1/2}$ (6 h) and dose of 80 mg make it ideal for developing a controlled release formulation (presently administered once a day).

Chen et al. [119] linked SEL with PEG to synthesize PEG-SEL prodrug using reactive oxygen species (ROS)-responsive linker (PEG-S-SEL). Due to the amphiphilic character, PEG-S-SEL self-assemble in aqueous solution to form micelle and act as a delivery vehicle for OSI. *In vivo* study conducted in female athymic mice xenografted with PC-9/AR cells revealed that OSI+SEL NPs treated group significantly showed reduction in tumor weight than OSI NP or SEL NP treated groups. Furthermore, the OSI-SEL NPs exhibited significant tumor suppression and successfully induced apoptosis by inhibiting EGFR and MEK simultaneously in OSI-resistant NSCLC cells and decreased OSI-resistant tumor.

5.13. *Pazopanib*

Pazopanib approved by FDA in 2009 for the treatment of renal cell cancer that inhibits VEGFR-1, −2 and −3, PDGFR, FGFR-1 and - 3, interleukin-2 receptor inducible T-cell kinase and cytokine receptor (Kit). Additionally, it can be utilized in the management of colorectal cancer. Pazopanib exhibits complex pharmacokinetics with a high pH-dependency of solubility. The bioavailability of the drug is low (14 % to 39%), time-dependent and non-linear, with considerable interpatient variability. Total systemic exposure, as well as pazopanib trough level (≥ 20 mg/l), correlate with observed tumor shrinkage and progression-free survival as well as toxicity. Current 800 mg daily dose fails to provide the required minimum concentration (C_{min}) in 20% of patients, exposing them to suboptimal treatment [168,169]. Therefore, several aspects of pazopanib therapy can benefit from complex formulation approaches.

Lahoti et al. [102] formulated a colon-targeted liposomal drug delivery system for colorectal cancer of pazopanib by utilizing high-pressure homogenization process. HSPC, m-PEG DSPE-2000 (phospholipid) and cholesterol were used for the preparation of drug-loaded liposomes. The optimized formulation depicted particle size of ~109 nm with PDI values of 0.998 at homogenization pressures of 1000 psi, 1500 psi and 2000 psi, and cycles of 9, 6 and 6, respectively. *In vivo* studies were conducted in wistar rats, and carcinogenesis was induced by 1,2-dimethylhydrazine. The liposomal formulation was given as an oral dose of 30 mg/kg, and the control was treated with distilled water. After 30 d pazopanib-loaded

liposomes exhibited lesser tumor weight and volume (~0.4 g and ~125 mm^3, respectively) as compared to the control group. This process was also deemed to be scalable in industrial setup, which makes it an attractive option for the treatment of colorectal cancer.

5.14. *Sorafenib (SFN)*

Numerous intracellular (cCRAF, mutant BRAF, and BRAF) and cell surface (KIT, FLT-3, RET, FLT-3, RET/PTC, VEGFR-1, 2, 3, and PDGFR-ß) kinase receptors have been demonstrated to be inhibited by SFN which is FDA-approved for hepatocellular and RCC in 2007 and 2005, respectively. SFN pharmacotherapy is limited by high variability, low therapeutic index, ~40% bioavailability and dose reduction approach has shown to benefit many clinical outcomes [170–172]. These limitations provide a driving force for developing complex formulations of SFN.

Mahmoud et al. [103] employed alginate polymer to microencapsulate SFN absorbed on the CNTs (CNTs-SFN-MC). MTT assay demonstrated that the drug-loaded CNTs were 2-fold cytotoxic to HepG2 cells compared to free SFN. Additionally, the *in vivo* experiments on male Wistar rats showed an AUC value of ~681 µg·h/ml and a $T_{1/2}$ of 18.43 h There was a considerable reduction in the circulating ratio of Lens culinaris agglutinin-reactive fraction of AFP (AFP-L3%) in N-nitrosodiethylamine (DENA) induced HCC rat model with CNTs-SFN-MCs group as compared to the DENA and SFN groups. Immunofluorescence analysis and western blot analysis of a few HCC-relevant biomarkers of control groups showed significant level of changes as compared to CNTs-SFN-MC. This research demonstrates that CNTs-SFN-MCs had higher anticancer activity both in a rat model of DENA-induced HCC and against HepG2 cells *in vitro*.

Clavreul et al. [104] prepared SFN-loaded lipid nanocapsules (LNCs) exhibiting a very high encapsulation efficiency (> 90%). SFN-loaded LNCs decreased the viability of human U87MG glioblastoma (GB) cells as well as decreased angiogenesis. *In vivo* studies conducted in female Swiss nude mice bearing an orthotopic U87MG human GB xenograft showed single dose of intratumoral injection of SFN-LNCs (3.5 µg) increased the blood perfusion to the tumor core as compared to control (HBSS) and free SFN treated group (~62 ml/100 g/min, ~50 ml/100 g/min, ~49 ml/100 g/min, respectively) ($P < 0.05$). SFN-LNCs were found to be more effective in inducing early tumor vascular normalization resulting from decreased vessel area than free SFN.

Mo et al. [105] formulated three liposomal formulations of SFN: a HA-coated liposome (HA-SFN-Lip), an uncoated liposome (SFN-Lip), and a PEGylated HA-coated SFN liposome (PEG-HA-SF-Lip). The cytotoxicity and cellular uptake of PEG-HA-SFN-Lip and HA-SFN-Lip were higher than those of SFN-Lip in MDA-MB-231 cells that overexpress CD44, but no overt changes were seen in MCF-7 cells with low CD44 expression. This shows that CD44 is involved in uptake of coated liposomes. *In vivo* study conducted in male Sprague Dawley rats exhibited that PEG-HA-SFN-Lip formulation exhibited almost higher AUC, enhanced $T_{1/2}$, and decreased clearance compared to free SFN solution and uncoated liposomal formulation. PEG-HA-SFN-Lip also recorded the highest tumor growth inhibition in the MDA-MB-231 tumor xenograft female NCr athymic nude mice model. It also displayed high plasma stability and hemocompatibility.

Li et al. [106] developed SFN-loaded TPGS-NPs by utilizing dendritic poly(amidoamine)-poly(γ-benzyl-L-Glutamate)-b-D-α-tocopheryl PEG1000 succinate (NP-TPGS-SFB) to improve the shorter $T_{1/2}$ of SFN. SFN released in response to acid was accomplished by TPGS-SFN–NPs. As compared to free SFN, PEG-conjugated NPs (NP-PEG-SFB) demonstrated noticeably greater cellular absorption in HepG2 human liver cells. The MTT assay proved that NP-PEG-SFB and free SFN both exhibited reduced cytotoxicity than NP-TPGS-SFB. Additionally, NP-TPGS-SFB considerably reduced tumor growth by ~87 mm^3 compared to 360 mm^3 of saline, 228 mm^3 of free SFB and 181 mm^3 of NP-PEG-SFB in mice receiving HepG2 xenografts.

Sheng et al. [107] developed SFN NPs by utilizing the nanoprecipitation method. SFN was combined with a copolymer composed of racemic polylactic acid and PEG monomethyl ether to prepare nanoformulation. *In vivo* study conducted in tumor-bearing mice showed that SFN–NPs possessed substantially greater SFN concentration in tumor tissues (~2,800 ng/ml) than free SFN (~870 ng/ml). *In vivo*, retention time of the formulation was considerably longer than SFN alone. SFN–NPs were found more efficient at inhibiting tumor growth (~70%) than SFN alone (~50%). Park et al. [108] developed SFN–NPs using supercritical fluid and fat. Formulation variables HPMC, PVP K30 and poloxamer were optimized. *In vivo* PK profile study performed in beagle dogs showed improvement in blood levels, greater absorption than the reference (Nexavar®), AUC_{0-48} was 35,560 ng·h /ml, C_{max} was 4,316 ng/ml, and T_{max} was 3.71 h This work demonstrated the value of systematic formulation design for determining how formulation factors affect the properties of the poorly soluble drug NPs.

Nevertheless, because certain molecules have low oral bioavailability, it becomes necessary to administer them in high doses, which can result in dose-limiting toxicity, particularly when given daily over an extended period of time. An oral complex delivery system for SFN tosylate has shown almost twice the increase in bioavailability, resulting in a better toxicity profile. The formulation contained albumin as carrier and was prepared using a scale-up-ready high-pressure homogenization process, which had a size of ~300 nm and surface charge of −55 mV. In the orthotopic murine hepatic tumor model, significantly improved tumor regression was observed at half the clinical dose of 400 mg. The complex formulation showed higher selective distribution in liver tissue [173].

5.15. *Lapatinib (LPT)*

The intracellular tyrosine kinase domains of the human epidermal receptor type 2 and the EGFR are targeted by the 4-anilinoquinazoline kinase inhibitor, named LPT which was approved by FDA in 2007 for the effective treatment of metastatic breast cancer.

Pavithra et al. [109] formulated LPT nanosponges (LPT NSs) by employe PVA as the stabilizer and Eudragit RS100 as the polymer. LPT NSs was found to be more soluble than free LPT.

In vivo pharmacokinetic investigation conducted on female Wister rats (22mg/kg dose given via oral route) recorded a significant improvement in LPT NSs compared to the free LPT with C_{max}, T_{max}, AUC_{0-t} and elimination $T_{1/2}$. Hence, it has been demonstrated that LPT NSs possesses higher bioavailability and could be helpful in reducing the oral dosage of LPT.

Dehghankelishadi et al. [111] studied the *in vitro* and *in vivo* effectiveness of PTX-LPT loaded Pluronic micelles. MTT test performed to analyze the *in vitro* cellular uptake of the drug-loaded micelles demonstrates that drug-loaded micelles are more cytotoxic than free drugs. *In vivo* studies conducted on female BALB/c mice showed that in PTX-LPT loaded micelles group, the tumor growth rate appeared to be slower. *In vivo* imaging analyses showed that in liver, the highest concentration of the micellar system was observed. The commercial Intaxel® formulation was found less effective *in vivo* than micelles loaded with PTX-LPT.

LPT, a dual TKI, absorbs poorly from the gastrointestinal system due to its limited water solubility. Sara et al. [113] formulated a highly stable, LPT-loaded liposomal formulation and tested its therapeutic effectiveness on the 4T1 and TUBO cell lines. The results demonstrated that, in comparison to control groups, liposomal LPT dramatically increases autophagy and apoptosis while inhibiting cell growth. Additionally, it demonstrated potential advantages on the life of tumor-bearing female BALB/c mice by extending the time to end in the TUBO cell line from ~24 d in the control group to 40 d and in 4T1 TNBC cell line and ~30 to ~40 d when combined with liposomal DOX. The results of biodistribution experiments exhibited that liposomal LPT tagged with I125 enhanced the drug accumulation in organs, notably in the tumor. More effectively than control group, liposomal LPT or oral Tykerb®, Caelyx® slowed the pace of tumor progression. The results revealed that more studies were necessary to completely understand the potential effects of liposomal LPT on autophagy, apoptosis and particularly immune system cells.

Bonde et al. [110] prepared LPT-loaded polymeric micelles (LP-PM), which showed greater cytotoxic properties in SKBr3 breast cancer cells and significantly inhibited the development of the tumor *in vivo* in a xenografted BALB/c mice model. After 28 d of treatment, the growth rate in the LP-PM group significantly slow down when contested against control group. The commercial oral formulation produced an inhibition in the range of 23%. There was a significant difference of around 45% between the inhibition found in animals treated with LS, marketed formulation and LP-PMs. The findings of this study suggest that LP-PMs have a larger potential for treating breast cancer effectively.

With some effectiveness, photodynamic treatment (PDT), administered by Gleolan®, has been investigated in the past to treat and prolong the life of malignant cancers. In a recent study, Fisher et al. [114] sought to ascertain anti-tumor PDT efficacy of liposomal LPT by combining it with ALA-protoporphyrin IX (PpIX). *In vivo* study was conducted in GSC30 Rag2−/ −SCID rat model at a dose of 0.125 mg/kg for 3 to 4 d following PDT. Study findings suggested that PDT with LPT treatment exhibited a mean survival time of approximately 29 d in U87 tumor cells. PDT in conjunction with LPT markedly boosted accumulation of PpIX and prominently decreased the LD50 of PpIX-initiated PDT as well as enhanced the amount of MRI-quantified glioma responses in U87 and GSC-30 cell lines.

Agarwal et al. [112] investigated the use of LPT in the form of nanocrystals coated with HA (LPT-HA-NCs) as a targeting agent for cancer cells that overexpress CD44, a cell surface receptor commonly found in TNBC. As seen from Fig. 11A, LPT-HA-NCs were prepared using pluronic F127 as a stabilizer. *In vivo* study conducted in female BALB/c mice with breast tumors caused by 4T1 cells showed significant accumulation of LPT-HA-NCs in tumors over a long period of time, and the greatest distribution observed at 24 h LPT-HA-NCs produced higher tumor suppression and improved survival rates (Fig. 11B-11E) in animals, which displayed nearly 52%, 74.65% and 83.32% reduction in tumor burden than LPT-NCs, free LPT and control groups, respectively. The study also found that compared to the control group, which had 100% lung metastasis, free LPT had only 3% lung metastasis (0.33 nodules/lung), whereas LPT-NCs and LPT-HA-NCs had 0 lung metastasis since their lungs had no nodules at all, which further confirms excellent anti-tumor and metastasis activity of LPT-HA-NCs (Fig. 11F). Histopathological analysis displays undifferentiated cells with abundant nuclei, indicating their proliferating nature (Fig. 11G).

5.16. *Gefitinib (GFT)*

GFT is a selective TKI, specifically targeting the EGFR and inhibiting cell signaling. The overexpression of EGFR was predominantly observed in numerous solid tumors present in lungs, colon, breasts, brain and ovaries [174–176]. GFT inhibits the autophosphorylation of tyrosine connected to receptors by inhibiting the kinase activity of wild-type EGFR and certain activating variants. In 2003, GFT received FDA approval to treat locally advanced or metastatic NSCLC in patients following the failure of docetaxel and platinum-based chemotherapies [177]. The solubility of GFT is very poor in aqueous phases like water and other aqueous buffers [178]. A high oral dose of GFT (250 mg/d) is necessary to achieve the desired therapeutic effects due to its low solubility in water, FPM and high Pgp efflux. In rats, C_{max}, T_{max} and AUC of GFT were measured at 248.43 ng/ml, 1.25 h and 1,342.85 ng/ml/h, respectively, after oral administration. GFT exhibits low bioavailability (60%) due to its limited aqueous solubility when administered orally [179–181]. Furthermore, oral administration of GFT results in metabolic, gastrointestinal and nutritional disturbances [182]. In recent years, efforts to enhance the bioavailability and solubility of GFT by implying novel formulation strategies have gained interest.

Nayek et al. [115] employed Lipoid S PC-3 as a novel lipid and used different concentrations of lipid and poloxamer 407 to prepared GFT SLNs by a modified hot homogenization technique. The average particle size was recorded at 178 nm with a PDI of 0.27. The SLNs showed $a > 92\%$ entrapment efficiency and negative zeta potential (−25 mV). *In vitro* study analysis revealed a steady release (> 90%) over 72 h, followed by initial burst release (25%) of SLNs. The Higuchi model was found to be best fit the release profile. The *in vitro* cytotoxicity of SLN showed greater antitumor efficacy (cell viability >

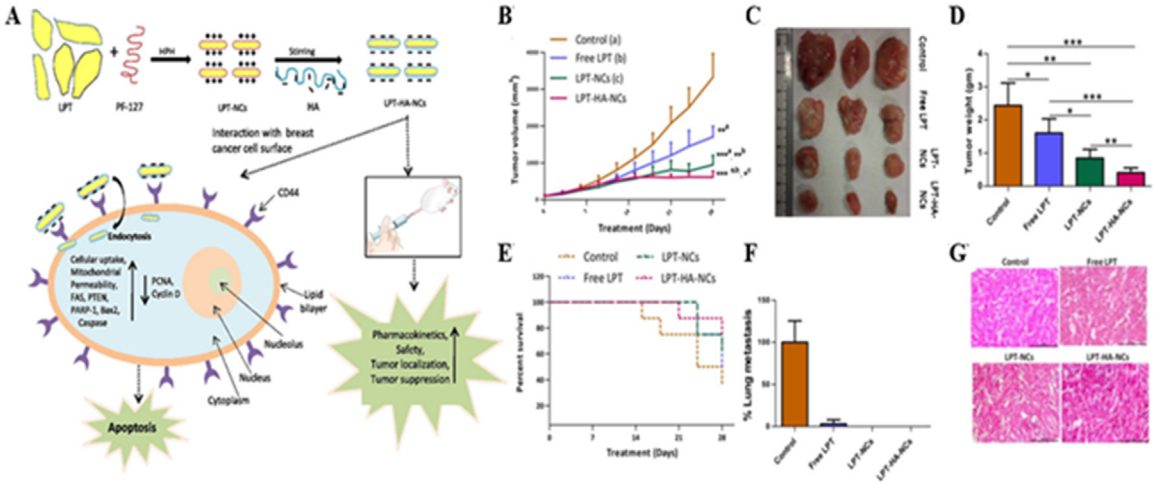

Fig. 11 – (A) LPT in the form of HA-coated nanocrystal formulation against TNBC. *In vivo* studies after IV administration of free LPT, LPT-NCs, and LPT-HA-NCs in 4T1 cells bearing female BALB/c mice showing (B) tumor volume studies, (C) tumor morphological images, (D) tumor weight studies, (E) animal survival probability, (F) lungs metastasis percentage, and (G) histopathological staining images. Reprinted with permission [112]. Copyright 2017 Elsevier Inc.

65%) than the free drug. After intravenous administration of GFT SLN (20 mg/kg) in female albino Wister rats, differential distribution showed the highest drug concentrations in liver (~29,000 ng) followed by kidneys (~22,300 ng), and brain (~7,100 ng) had the lowest drug concentrations.

GFT NP formulation using poly (e-caprolactone)-PEG-poly(e-caprolactone) polymer was formulated by solid dispersion method by Ni et al. [116]. The formulations were prepared with 9% loading and 92% entrapment efficacy while release profile showed absence of biphasic pattern. *In vivo* study conducted in A549 tumor cell bearing nude BALB/c mice, GFT NPs significantly increased antitumor efficacy (~113 d median survival time) with reduced or no side effects, in comparison with free GFT (~90 d of median survival time). Cell apoptotic rate increased in group treated with GFT NPs (~65%) than free GFT (50%) and control (~25%) due to the tumor growth without rapid angiogenesis. Also, the NPs group had significantly lower ki-67, CD31, and EGFR expression levels; thus, they can circumvent problems such as organ toxicity, treatment resistance, and illness recurrence in order to provide superior outcomes.

Lai et al. [117] have developed GFT and curcumin-loaded and polyglutamic acid (PGA) coated NPs (PGA-Gef/Cur NPs), which had a diameter of ~550 nm, a GFT loading efficacy of 89.5% and curcumin loading efficacy of 100%. The reported NPs were internalized by SAS cells, which markedly decreased their viability. *In vivo* anti-tumor study conducted in SAS cell xenografted athymic BALB/c nude mice showed that the treatments of PLGA NPs, free Gef and Cur, and PGA-Gef/Cur NPs did not significantly change the appearance or body weight of mice. But as compared to the group receiving only Gef/Cur, the PGA-Gef/Cur NPs considerably reduced tumor growth. The findings have shown that in an *in vivo* xenograft animal model obtained using SAS cells, PGA-Gef/Cur NPs exhibited better anti-cancer effects than free GFT and curcumin.

6. Conclusions and future perspectives

smTKIs target specific kinases intracellularly. Although these drugs should selectively inhibit abnormal kinase activity in cancer cells, they still have off-target effects on normal cells that express similar kinase activity leading to adverse or unwanted side effects [183,184]. Several smTKIs suffer from suboptimal biopharmaceutical and pharmacokinetic properties, limiting their therapeutic effectiveness and causing inter-patient variations. Therapeutic drug monitoring, dose adjustments and recently precision medicine are increasingly recommended by clinicians to improve therapeutic outcomes of smTKIs. On the other hand, complex formulations and nanomedicines can be employed to improve many of these shortcomings [185]. Though several nanoformulations of smTKIs have shown efficacy in animal models, their clinical translation will require careful development.

A detailed analysis of the biopharmaceutical and pharmacokinetic properties concludes that at least 10, 32 and 30 numbers of smTKIs have a narrow therapeutic index, low bioavailability and high dosing regimens, respectively. >80% of smTKIs are poorly water-soluble; however, a high number of smTKIs (around 44) have low IC_{50} values. This clearly indicates that formulation innovations through complex formulations can improve the therapeutic activity of these drugs. Currently, almost all smTKIs are delivered orally, which also leads to high inter-patient and intra-patient variations. Complex formulations through the oral route can be feasible only for drugs that do not possess pH-dependent solubility, like vemurafenib, regorafenib, and trametinib, while drugs such as acalabrutinib, binimetinib, bosutinib, ceritinib, cobimetinib, CZT, DAB, encorafenib, ETB, GFT, larotrectinib, nilotinib and pazopanib will pose significant difficulty. Controlled-release oral formulations may be an attractive

choice for delivering low $T_{1/2}$ smTKIs, such as acalabrutinib, AXT, binimetinib, bosutinib, encorafenib, ruxolitinib, and tofacitinib, which do not undergo extensive FPM. On the other hand, such formulations for larotrectinib, which undergoes extensive FPM, may not be very productive.

For many smTKIs, changing the route of administration can be a viable approach to improve therapeutic outcomes, especially for the ones with extensive FPM. For example, inhalation-targeted therapy using smTKIs will be a promising approach for treating lung cancer and can effectively target tumor cells. ETB, AFA, OSI, brigatinib, and lorlatinib may be delivered as inhalable formulations. DPI of smTKIs is an active research area, but the determination of IC_{50} values specific to inhalation delivery will need to be performed. LPT, neratinib, and pyrotinib are medications approved for treating cancer, such as breast cancer. A breakthrough approach for targeting breast cancer is the development of *in situ* tough hydrogels. These hydrogels are designed to remain at the application site, slowly releasing medication over time to deliver treatment directly to the cancerous tissue. This approach offers a promising way to deliver targeted therapy to breast cancer patients, potentially improving treatment outcomes and minimizing side effects associated with traditional chemotherapy [186]. Intramuscular and parenteral routes of administration should be considered for smTKIs as patients tend to show compliance with the parenteral route if overall quality of life is improved. Moreover, many smTKIs are recommended to be taken for 21–30 d period, and present technologies in long-acting injectables can conveniently provide drug release rates for this time duration. Since a large number of smTKIs have low IC_{50} values, this will enable their formulation as long-acting injectables.

The present studies concerning development of complex nanoformulations of smTKIs have shown an increase in pharmacokinetic parameters (AUC and C_{max}) and pharmacodynamic endpoints in terms of tumor regression volume and weight. Therefore, significant improvement in drug exposure is already established, which will overcome the suboptimal effectiveness of smTKIs. However, most of these studies have been performed at a dose of 10 mg/kg and administered intravenously. These studies have not yet emphasized the concentration fluctuation in plasma over an extended period of time that may establish their applicability in reducing plasma variation. Similarly, metabolism studies after conventional and nanoformulations should be performed and compared. Most of these studies have revealed increased bioavailability, distribution, tumor suppression and decreased off-target side effects. As several smTKIs become off-patent, it is predicted that complex formulations of these drugs will be more extensively investigated. However, such studies must take into account the physico-chemical and pharmacokinetic-pharmacodynamic properties of the drug molecule for more judicious development. As each smTKIs is approved for a specific cancer type, it should be noted that the heterogeneity of tumor microenvironment for each type of cancer will call for a specific approach to develop a targeted complex formulation of smTKIs. In addition, the manufacturing, sterilization, *in vivo-in vitro* correlation on release rate and quality control of complex formulations should be standardized within a regulatory framework to enable their clinical translation soon after *in vivo* efficacy is established.

Conflicts of interest

The authors declare that there are no conflicts of interest.

Supplementary materials

Supplementary material associated with this article can be found, in the online version, at doi:10.1016/j.ajps.2024.100980.

References

[1] de Lavallade H, Apperley JF, Khorashad JS, Milojkovic D, Reid AG, Bua M, et al. Imatinib for newly diagnosed patients with chronic myeloid leukemia: incidence of sustained responses in an intention-to-treat analysis. J Clin Oncol 2008;26(20):3358–63.
[2] Singh N, Reddy KP, Das P, Kishor BK, Datta P. Complex formulation strategies to overcome the delivery hurdles of lapatinib in metastatic breast cancer. J Drug Deliv Sci Technol 2023;82.
[3] Hochhaus A, Larson RA, Guilhot F, Radich JP, Branford S, Hughes TP, et al. Long-term outcomes of imatinib treatment for chronic myeloid leukemia. N Engl J Med 2017;376(10):917–27.
[4] Cohen P, Cross D, Jänne PA. Kinase drug discovery 20 years after imatinib: progress and future directions. Nat Rev Drug Discov 2021;20(7):551–69.
[5] Roskoski R. Properties of FDA-approved small molecule protein kinase inhibitors. Pharmacol Res 2019;144:19–50.
[6] Jin H, Shi Y, Lv Y, Yuan S, Ramirez CFA, Lieftink C, et al. EGFR activation limits the response of liver cancer to lenvatinib. Nature 2021;595(7869):730–4.
[7] Msaouel P, Goswami S, Thall PF, Wang X, Yuan Y, Jonasch E, et al. A phase 1-2 trial of sitravatinib and nivolumab in clear cell renal cell carcinoma following progression on antiangiogenic therapy. Sci Transl Med 2022;14(641).
[8] Robichaux JP, Le X, Vijayan RSK, Hicks JK, Heeke S, Elamin YY, et al. Structure-based classification predicts drug response in EGFR-mutant NSCLC. Nature 2021;597(7878):732–7.
[9] Huang L, Jiang S, Shi Y. Tyrosine kinase inhibitors for solid tumors in the past 20 years (2001-2020). J Hematol Oncol 2020;13(1):1–23.
[10] Zhao Q, Wu ZE, Li B, Li F. Recent advances in metabolism and toxicity of tyrosine kinase inhibitors. Pharmacol Ther 2022;237:108256.
[11] Kretz O, Weiss HM, Schumacher MM, Gross G. *In vitro* blood distribution and plasma protein binding of the tyrosine kinase inhibitor imatinib and its active metabolite, CGP74588, in rat, mouse, dog, monkey, healthy humans and patients with acute lymphatic leukaemia. Br J Clin Pharmacol 2004;58(2):212–16.
[12] Larson RA. Group for the I (International RI *vs* SS, Druker BJ, Group for the I (International RI *vs* SS, Guilhot F, Group for the I (International RI *vs* SS, et al. Imatinib pharmacokinetics and its correlation with response and safety in chronic-phase chronic myeloid leukemia: a subanalysis of the IRIS study. Blood 2008;111(8):4022–8.
[13] Rakhit A, Pantze MP, Fettner S, Jones HM, Charoin JE, Riek M, et al. The effects of CYP3A4 inhibition on erlotinib pharmacokinetics: computer-based simulation (SimCYP™)

predicts *in vivo* metabolic inhibition. Eur J Clin Pharmacol 2008;64(1):31–41.
[14] Herbrink M, Schellens JHM, Beijnen JH, Nuijen B. Improving the solubility of nilotinib through novel spray-dried solid dispersions. Int J Pharm 2017;529(1–2):294–302.
[15] Terada T, Noda S, Inui KI. Management of dose variability and side effects for individualized cancer pharmacotherapy with tyrosine kinase inhibitors. Pharmacol Ther 2015;152:125–34.
[16] Ma W, Zeng J, Chen S, Lyu Y, Toomey KA, Phan CT, et al. Small molecule tyrosine kinase inhibitors modulated blood immune cell counts in patients with oncogene-driven NSCLC. Biomark Res 2021;9(1):1–20.
[17] Herbrink M, Nuijen B, Schellens JHM, Beijnen JH. Variability in bioavailability of small molecular tyrosine kinase inhibitors. Cancer Treat Rev 2015;41(5):412–22.
[18] Brown JE, Royle KL, Gregory W, Ralph C, Maraveyas A, Din O, et al. Temporary treatment cessation *versus* continuation of first-line tyrosine kinase inhibitor in patients with advanced clear cell renal cell carcinoma (STAR): an open-label, non-inferiority, randomised, controlled, phase 2/3 trial. Lancet Oncol 2023;24(3):213–27.
[19] Clark RE, Polydoros F, Apperley JF, Milojkovic D, Pocock C, Smith G, et al. De-escalation of tyrosine kinase inhibitor dose in patients with chronic myeloid leukaemia with stable major molecular response (DESTINY): an interim analysis of a non-randomised, phase 2 trial. Lancet Haematol 2017;4(7):e310–16.
[20] Herviou P, Thivat E, Richard D, Roche L, Dohou J, Pouget M, et al. Therapeutic drug monitoring and tyrosine kinase inhibitors. Oncol Lett 2016;12(2):1223.
[21] Clarke WA, Chatelut E, Fotoohi AK, Larson RA, Martin JH, Mathijssen RHJ, et al. Therapeutic drug monitoring in oncology: international association of therapeutic drug monitoring and clinical toxicology consensus guidelines for imatinib therapy. Eur J Cancer 2021;157:428–440.
[22] Megyesfalvi Z, Gay CM, Popper H, Pirker R, Ostoros G, Heeke S, et al. Clinical insights into small cell lung cancer: tumor heterogeneity, diagnosis, therapy, and future directions. CA Cancer J Clin 2023:1–33.
[23] Ciardiello F, Ciardiello D, Martini G, Napolitano S, Tabernero J, Cervantes A. Clinical management of metastatic colorectal cancer in the era of precision medicine. CA Cancer J Clin 2022;72(4):372–401.
[24] Mahmood U, Lorch JH. Precision medicine in aggressive thyroid cancer: moving beyond multitargeted tyrosine kinase inhibitors. Cancer Cytopathol 2022;130(1):8–11.
[25] Hwan Kim DD. Are we ready to use precision medicine in chronic myeloid leukemia practice? Haematologica 2019;104(12):2327.
[26] Liang WS, Beaulieu-Jones B, Smalley S, Snyder M, Goetz LH, Schork NJ. Emerging therapeutic drug monitoring technologies: considerations and opportunities in precision medicine. Front Pharmacol 2024;15:1348112.
[27] Johnson-Ansah H, Maneglier B, Huguet F, Legros L, Escoffre-Barbe M, Gardembas M, et al. Imatinib optimized therapy improves major molecular response rates in patients with chronic myeloid leukemia. Pharmaceutics 2022;14(8):1676.
[28] Shi J, Kantoff PW, Wooster R, Farokhzad OC. Cancer nanomedicine: progress, challenges and opportunities. Nat Rev Canc 2016;17(1):20–37.
[29] Anchordoquy TJ, Barenholz Y, Boraschi D, Chorny M, Decuzzi P, Dobrovolskaia MA, et al. Mechanisms and barriers in cancer nanomedicine: addressing challenges, looking for solutions. ACS Nano 2017;11(1):12–18.
[30] Alhaj-Suliman SO, Wafa EI, Salem AK. Engineering nanosystems to overcome barriers to cancer diagnosis and treatment. Adv Drug Deliv Rev 2022;189:114482.
[31] Mitchell MJ, Billingsley MM, Haley RM, Wechsler ME, Peppas NA, Langer R. Engineering precision nanoparticles for drug delivery. Nat Rev Drug Discov 2020;20(2):101–24.
[32] Siemer S, Bauer TA, Scholz P, Breder C, Fenaroli F, Harms G, et al. Targeting cancer chemotherapy resistance by precision medicine-driven nanoparticle-formulated cisplatin. ACS Nano 2021;15(11):18541–56.
[33] Ahmad A, Khan F, Mishra RK, Khan R. Precision cancer nanotherapy: evolving role of multifunctional nanoparticles for cancer active targeting. J Med Chem 2019;62(23):10475–96.
[34] Wang-Bishop L, Kimmel BR, Ngwa VM, Madden MZ, Baljon JJ, Florian DC, et al. STING-activating nanoparticles normalize the vascular-immune interface to potentiate cancer immunotherapy. Sci Immunol 2023;8(83):eadd1153.
[35] Mao C, Yeh S, Fu J, Porosnicu M, Thomas A, Kucera GL, et al. Delivery of an ectonucleotidase inhibitor with ROS-responsive nanoparticles overcomes adenosine-mediated cancer immunosuppression. Sci Transl Med 2022;14(648).
[36] Xiong Z, Tong T, Xie Z, Yu S, Zhuang R, Jia Q, et al. Delivery of gefitinib loaded nanoparticles for effectively inhibiting prostate cancer progression. Biomater Sci 2024;12(3):650–9.
[37] Fuentes-Antrás J, Genta S, Vijenthira A, Siu LL. Antibody–drug conjugates: in search of partners of choice. Trends Cancer 2023;9(4):339–54.
[38] Truong DH, Le VKH, Pham TT, Dao AH, Pham TPD, Tran TH. Delivery of erlotinib for enhanced cancer treatment: an update review on particulate systems. J Drug Deliv Sci Technol 2020;55:101348.
[39] Kommineni N, Nottingham E, Bagde A, Patel N, Rishi AK, Dev SRS, et al. Role of nano-lipid formulation of CARP-1 mimetic, CFM-4.17 to improve systemic exposure and response in osimertinib resistant non-small cell lung cancer. Eur J Pharmaceut Biopharmaceut 2021;158:172–84.
[40] Schelker C, Nowak-Sliwinska P, Borchard G. HDACIs and TKIs combinations and their liposomal delivery for cancer treatment. J Controlled Rel 2023;358:59–77.
[41] Hao SJ, Zhu YX, Wu FG. Membrane fusion-mediated delivery of small-molecule HER2 tyrosine kinase inhibitor for effective tumor chemosensitization. J Control Release 2023;357:222–34.
[42] Karpov OA, Fearnley GW, Smith GA, Kankanala J, McPherson MJ, Tomlinson DC, et al. Receptor tyrosine kinase structure and function in health and disease. AIMS Biophys 2015;2(4):476–502.
[43] Du Z, Lovly CM. Mechanisms of receptor tyrosine kinase activation in cancer. Mol. Cancer 2018;17(1):1–13.
[44] Vogelstein B, Papadopoulos N, Velculescu VE, Zhou S, Diaz LA, Kinzler KW. Cancer genome landscapes. Science 2013;339(6127):1546–58.
[45] Singh AB, Harris RC. Autocrine, paracrine and juxtacrine signaling by EGFR ligands. Cell Signal 2005;17(10):1183–93.
[46] Sudhesh Dev S, Zainal Abidin SA, Farghadani R, Othman I, Naidu R. Receptor tyrosine kinases and their signaling pathways as therapeutic targets of curcumin in cancer. Front Pharmacol 2021;12:3266.
[47] Yamaoka T, Kusumoto S, Ando K, Ohba M, Ohmori T. Receptor tyrosine kinase-targeted cancer therapy. Int J Mol Sci 2018;19(11):3491.
[48] Gadgeel SM, Ruckdeschel JC, Heath EI, Heilbrun LK, Venkatramanamoorthy R, Wozniak A. Phase II study of gefitinib, an epidermal growth factor receptor tyrosine kinase inhibitor (EGFR-TKI), and celecoxib, a cyclooxygenase-2 (COX-2) inhibitor, in patients with

platinum refractory non-small cell lung cancer (NSCLC). J Thorac Oncol 2007;2(4):299–305.
[49] Arena S, Siravegna G, Mussolin B, Kearns JD, Wolf BB, Misale S, et al. MM-151 overcomes acquired resistance to cetuximab and panitumumab in colorectal cancers harboring EGFR extracellular domain mutations. Sci Transl Med 2016;8:324.
[50] Yi HG, Kim HJ, Kim YJ, Han SW, Oh DY, Lee SH, et al. Epidermal growth factor receptor (EGFR) tyrosine kinase inhibitors (TKIs) are effective for leptomeningeal metastasis from non-small cell lung cancer patients with sensitive EGFR mutation or other predictive factors of good response for EGFR TKI. Lung Cancer 2009;65(1):80–4.
[51] Hoffknecht P, Tufman A, Wehler T, Pelzer T, Wiewrodt R, Schütz M, et al. Efficacy of the irreversible ErbB family blocker afatinib in epidermal growth factor receptor (EGFR) tyrosine kinase inhibitor (TKI)–pretreated non–small-cell lung cancer patients with brain metastases or leptomeningeal Disease. J Thorac Oncol 2015;10(1):156.
[52] Bianconi M, Scartozzi M, Faloppi L, Loretelli C, Burattini L, Bittoni A, et al. Tumour vascular endothelial growth factor (VEGF) and vascular endothelial growth factor receptors (VEGFR) polymorphisms and clinical outcome in advanced renal cell carcinoma patients receiving first line sunitinib. Ann Oncol 2012;23:ix274.
[53] Zou X, Tang XY, Qu ZY, Sun ZW, Ji CF, Li YJ, et al. Targeting the PDGF/PDGFR signaling pathway for cancer therapy: a review. Int J Biol Macromol 2022;202:539–57.
[54] Herbrink M, Nuijen B, Schellens JHM, Beijnen JH. Inherent formulation issues of kinase inhibitors. J Control Rel 2016;239:118–27.
[55] Amidon GL, Lennernäs H, Shah VP, Crison JR. A theoretical basis for a biopharmaceutic drug classification: the correlation of *in vitro* drug product dissolution and *in vivo* bioavailability. Pharm Res 1995;12(3):413–20.
[56] Benet LZ. Predicting drug disposition via application of a biopharmaceutics drug disposition classification system. Basic Clin Pharmacol Toxicol 2010;106(3):162.
[57] Bocci G, Oprea TI, Benet LZ. State of the art and uses for the biopharmaceutics drug disposition classification system (BDDCS): new additions, revisions, and citation references. AAPS 2022;24(2):37.
[58] Gay C, Toulet D, Le Corre P. Pharmacokinetic drug-drug interactions of tyrosine kinase inhibitors: a focus on cytochrome P450, transporters, and acid suppression therapy. Hematol Oncol 2017;35(3):259–80.
[59] Benet LZ, Broccatelli F, Oprea TI. BDDCS applied to over 900 drugs. AAPS 2011;13(4):519–47.
[60] Herbrink M, Nuijen B, Schellens JHM, Beijnen JH. Variability in bioavailability of small molecular tyrosine kinase inhibitors. Cancer Treat Rev 2015;41(5):412–22.
[61] Devriese LA, Koch KM, Mergui-Roelvink M, Matthys GM, Ma WW, Robidoux A, et al. Effects of low-fat and high-fat meals on steady-state pharmacokinetics of lapatinib in patients with advanced solid tumours. Invest New Drugs 2014;32(3):481–8.
[62] Kane RC, Farrell AT, Saber H, Tang S, Williams G, Jee JM, et al. Sorafenib for the treatment of advanced renal cell carcinoma. Clin Cancer Res 2006;12(24):7271–8.
[63] Huang Z, Li H, Zhang Q, Tan X, Lu F, Liu H, et al. Characterization of preclinical *in vitro* and *in vivo* pharmacokinetics properties for KBP-7018, a new tyrosine kinase inhibitor candidate for treatment of idiopathic pulmonary fibrosis. Drug Des Devel Ther 2015;9:4319.
[64] van Erp NP, Gelderblom H, Guchelaar HJ. Clinical pharmacokinetics of tyrosine kinase inhibitors. Cancer Treat Rev 2009;35(8):692–706.
[65] Bhal SK, Kassam K, Peirson IG, Pearl GM. The rule of five revisited: applying log D in place of log P in drug-likeness filters. Mol Pharm 2007;4(4):556–60.
[66] Wind S, Schnell D, Ebner T, Freiwald M, Stopfer P. Clinical pharmacokinetics and pharmacodynamics of afatinib. Clin Pharmacokinet 2017;56(3):235–50.
[67] El Asmar A, Morandi G, Burel F. Synthesis of dual sensitive lipid- b-poly(dimethylaminoethyl methacrylate) copolymers, self-assemblies and modulation of cloud point temperatures through physical blends with lipid- b-poly(2-isopropyl-2-oxazoline). Macromolecules 2019;52(23):9160–7.
[68] Imran M, Shah MR. Amphiphilic block copolymers–based micelles for drug delivery. In: Grumezescu AM, editor. Design and development of new nanocarriers. Alexandru Mihai Grumezescu; 2018. p. 365–400.
[69] Varma LT, Singh N, Gorain B, Choudhury H, Tambuwala MM, Kesharwani P, et al. Recent advances in self-assembled nanoparticles for drug delivery. Curr Drug Deliv 2020;17(4):279–91.
[70] Datta P, Ray S. Nanoparticulate formulations of radiopharmaceuticals: strategy to improve targeting and biodistribution properties. J Labelled Comp Radiopharm 2020;63(7):333–55.
[71] Kingsley JD, Dou H, Morehead J, Rabinow B, Gendelman HE, Destache CJ. Nanotechnology: a focus on nanoparticles as a drug delivery system. J Neuroimmune Pharmacol 2006;1(3):340–50.
[72] Maeda H, Wu J, Sawa T, Matsumura Y, Hori K. Tumor vascular permeability and the EPR effect in macromolecular therapeutics: a review. J Controlled Rel 2000;65(1–2):271–284.
[73] Torchilin VP. Targeted pharmaceutical nanocarriers for cancer therapy and imaging. The AAPS 2007;9(2):E128–47.
[74] Immordino ML, Dosio F, Cattel L. Stealth liposomes: review of the basic science, rationale, and clinical applications, existing and potential. Int J Nanomed 2006;1(3):297.
[75] FDA. Highlights of prescribing information. 2024. Available from: https://www.accessdata.fda.gov/drugsatfda_docs/label/2015/050718s048lbl.pdf.
[76] Iravani S, Varma RS. Nanosponges for drug delivery and cancer therapy: recent advances. Nanomaterials 2022;12(14):2440.
[77] Rajkumar SV, Richardson PG, Lacy MQ, Dispenzieri A, Greipp PR, Witzig TE, et al. Novel therapy with 2-methoxyestradiol for the treatment of relapsed and plateau phase multiple myeloma. Clin Cancer Res 2007;13(20):6162–7.
[78] A study using intravenous Paxceed™ to treat patients with rheumatoid arthritis. 2018. Available from: https://ctv.veeva.com/study/a-study-using-intravenous-paxceed-to-treat-patients-with-rheumatoid-arthritis.
[79] Deng S, Gigliobianco MR, Censi R, Di Martino P. Polymeric nanocapsules as nanotechnological alternative for drug delivery system: current status, challenges and opportunities. Nanomaterials 2020;10(5):847.
[80] Fabbro C, Ali-Boucetta H, Da Ros T, Bianco A, Kostarelos K, Prato M. Targeting carbon nanotubes against cancer. Chem Commun 2012;48(33):3911–26.
[81] Thakare VS, Das M, Jain AK, Patil S, Jain S. Carbon nanotubes in cancer theragnosis. Nanomedicine 2010;5(8):1277–301.
[82] Chen Y, Cheng Y, Zhao P, Zhang S, Li M, He C, et al. Co-delivery of doxorubicin and imatinib by pH sensitive cleavable PEGylated nanoliposomes with folate-mediated targeting to overcome multidrug resistance. Int J Pharm 2018;542(1–2):266–79.
[83] Wang S, Liu X, Wang S, Ouyang L, Li H, Ding J, et al. Imatinib co-loaded targeted realgar nanocrystal for synergistic

therapy of chronic myeloid leukemia. J Control Release 2021;338:190–200.
[84] Wang J, Su G, Yin X, Luo J, Gu R, Wang S, et al. Non-small cell lung cancer-targeted, redox-sensitive lipid-polymer hybrid nanoparticles for the delivery of a second-generation irreversible epidermal growth factor inhibitor—Afatinib: *in vitro* and *in vivo* evaluation. Biomed Pharmacother 2019;120:109493.
[85] Fu D, Li C, Huang Y. Lipid–polymer hybrid nanoparticle-based combination treatment with cisplatin and EGFR/HER2 receptor-targeting afatinib to enhance the treatment of nasopharyngeal carcinoma. Onco Targets Ther 2021;14:2449.
[86] Lu X, Liu S, Han M, Yang X, Sun K, Wang H, et al. Afatinib-loaded immunoliposomes functionalized with cetuximab: a novel strategy targeting the epidermal growth factor receptor for treatment of non-small-cell lung cancer. Int J Pharm 2019;560:126–35.
[87] Zhang J, Liu P, Zhang Z, Han J, Yang X, Wang A, et al. Apatinib-loaded nanoparticles inhibit tumor growth and angiogenesis in a model of melanoma. Biochem Biophys Res Commun 2020;521(2):296–302.
[88] Hu Y, Zhou P, Lin Y, Yang D, Wang B. Anti-colorectal cancer effect via application of polyethylene glycol modified liposomal apatinib. J Biomed Nanotechnol 2019;15(6):1256–66.
[89] Song Z, Lin Y, Zhang X, Feng C, Lu Y, Gao Y, et al. Cyclic RGD peptide-modified liposomal drug delivery system for targeted oral apatinib administration: enhanced cellular uptake and improved therapeutic effects. Int J Nanomed 2017;12:1941–58.
[90] Choi JY, Ramasamy T, Tran TH, Ku SK, Shin BS, Choi HG, et al. Systemic delivery of axitinib with nanohybrid liposomal nanoparticles inhibits hypoxic tumor growth. J Mater Chem B 2014;3(3):408–16.
[91] Choi JY, Ramasamy T, Kim SY, Kim J, Ku SK, Youn YS, et al. PEGylated lipid bilayer-supported mesoporous silica nanoparticle composite for synergistic co-delivery of axitinib and celastrol in multi-targeted cancer therapy. Acta Biomater 2016;39:94–105.
[92] Chaudagar KK, Landon-Brace N, Solanki A, Hieromnimon HM, Hegermiller E, Li W, et al. Cabozantinib unlocks efficient *in vivo* targeted delivery of neutrophil-loaded nanoparticles into murine prostate tumors. Mol Cancer Ther 2021;20(2):438–49.
[93] Pham LM, Poudel K, Phung CD, Nguyen TT, Pandit M, Nguyen HT, et al. Preparation and evaluation of dabrafenib-loaded, CD47-conjugated human serum albumin-based nanoconstructs for chemoimmunomodulation. Colloids Surf B Biointerfaces 2021;208:112093.
[94] Nguyen HT, Phung CD, Tran TH, Pham TT, Pham LM, Nguyen TT, et al. Manipulating immune system using nanoparticles for an effective cancer treatment: combination of targeted therapy and checkpoint blockage miRNA. J Control Release 2021;329:524–37.
[95] Bahman F, Pittalà V, Haider M, Greish K. Enhanced anticancer activity of nanoformulation of dasatinib against triple-negative breast cancer. J Pers Med 2021;11(6):559.
[96] Yang L, Xu J, Xie Z, Song F, Wang X, Tang R. Carrier-free prodrug nanoparticles based on dasatinib and cisplatin for efficient antitumor *in vivo*. Asian J Pharm Sci 2021;16(6):762–71.
[97] Tan S, Wang G. Redox-responsive and pH-sensitive nanoparticles enhanced stability and anticancer ability of erlotinib to treat lung cancer *in vivo*. Drug Des Devel Ther 2017;11:3519.
[98] Shen Y, Li W. HA/HSA co-modified erlotinib-albumin nanoparticles for lung cancer treatment. Drug Des Devel Ther 2018;12:2285–92.
[99] Wan X, Liu C, Lin Y, Fu J, Lu G, Lu Z. pH sensitive peptide functionalized nanoparticles for co-delivery of erlotinib and DAPT to restrict the progress of triple negative breast cancer. Drug Deliv 2019;26(1):470–80.
[100] Alshetaili AS, Ansari MJ, MdK Anwer, Ganaie MA, Iqbal M, Alshahrani SM, et al. Enhanced oral bioavailability of ibrutinib encapsulated poly (lactic-co- glycolic acid) nanoparticles: pharmacokinetic evaluation in rats. Curr Pharm Anal 2019;15(6):661–8.
[101] Rangaraj N, Pailla SR, Chowta P, Sampathi S. Fabrication of ibrutinib nanosuspension by quality by design approach: intended for enhanced oral bioavailability and diminished fast fed variability. AAPS PharmSciTech 2019;20(8):1–18.
[102] Lahoti S, Kumar M, Gaikwad S. Pazopanib colon targeted liposomal drug delivery for colorectal cancer: high-pressure homogenization process optimization and *in-vivo* evaluation. Indian J Pharmaceut Educ Res 2022;56(2):387–95.
[103] Elsayed MaMA, Mostafa ME, Alaaeldin E, Sarhan HAA, Shaykoon MS, Allam S, et al. Design and characterisation of novel sorafenib-loaded carbon nanotubes with distinct tumour-suppressive activity in hepatocellular carcinoma. Int J Nanomed 2019;14:8445–67.
[104] Clavreul A, Roger E, Pourbaghi-Masouleh M, Lemaire L, Tétaud C, Menei P. Development and characterization of sorafenib-loaded lipid nanocapsules for the treatment of glioblastoma. Drug Deliv 2018;25(1):1756–65.
[105] Mo L, Song JG, Lee H, Zhao M, Kim HY, Lee YJ, et al. PEGylated hyaluronic acid-coated liposome for enhanced *in vivo* efficacy of sorafenib via active tumor cell targeting and prolonged systemic exposure. Nanomedicine 2018;14(2):557–67.
[106] Li Z, Ye L, Liu J, Lian D, Li X. Sorafenib-loaded nanoparticles based on biodegradable dendritic polymers for enhanced therapy of hepatocellular carcinoma. Int J Nanomed 2020;15:1469–80.
[107] Sheng X, Huang T, Qin J, Li Q, Wang W, Deng L, et al. Preparation, pharmacokinetics, tissue distribution and antitumor effect of sorafenib-incorporating nanoparticles *in vivo*. Oncol Lett 2017;14(5):6163–9.
[108] Park SY, Kang Z, Thapa P, Jin YS, Park JW, Lim HJ, et al. Development of sorafenib loaded nanoparticles to improve oral bioavailability using a quality by design approach. Int J Pharm 2019;566:229–38.
[109] Prabhu PP, Prathvi Gujaran T V, Mehta CH, Suresh A, Koteshwara KB, et al. Development of lapatinib nanosponges for enhancing bioavailability. J Drug Deliv Sci Technol 2021;65:102684.
[110] Bonde GV, Ajmal G, Yadav SK, Mittal P, Mishra B. Lapatinib-loaded nanocolloidal polymeric micelles for the efficient treatment of breast cancer. J Appl Pharm Sci 2020;10(9):023–9.
[111] Dehghankelishadi P, Saadat E, Ravar F, Safavi M, Pordeli M, Gholami M, et al. *In vitro* and *in vivo* evaluation of paclitaxel–lapatinib-loaded F127 pluronic micelles. Drug Dev Ind Pharm 2017;43(3):390–8.
[112] Agrawal S, Dwivedi M, Ahmad H, Chadchan SB, Arya A, Sikandar R, et al. CD44 targeting hyaluronic acid coated lapatinib nanocrystals foster the efficacy against triple-negative breast cancer. Nanomedicine 2018;14(2):327–37.
[113] Shokooh Saremi S, Nikpoor AR, Sadri K, Mehrabian A, Karimi M, Mansouri A, et al. Development of a stable and high loaded liposomal formulation of lapatinib with enhanced therapeutic effects for breast cancer in combination with Caelyx®: *in vitro* and *in vivo* evaluations. Colloids Surf B Biointerfaces 2021;207:112012.

[114] Fisher C, Obaid G, Niu C, Foltz W, Goldstein A, Hasan T, et al. Liposomal lapatinib in combination with low-dose photodynamic therapy for the treatment of glioma. J Clin Med 2019;8(12):2214.
[115] Nayek S, Raghavendra NM, Sajeev Kumar B. Development of novel S PC-3 gefitinib lipid nanoparticles for effective drug delivery in breast cancer. Tissue distribution studies and cell cytotoxicity analysis. J Drug Deliv Sci Technol 2021;61:102073.
[116] Ni XL, Chen LX, Zhang H, Yang B, Xu S, Wu M, et al. *In vitro* and *in vivo* antitumor effect of gefitinib nanoparticles on human lung cancer. Drug Deliv 2017;24(1):1501–12.
[117] Lai KC, Chueh FS, Hsiao YT, Cheng ZY, Lien JC, Liu KC, et al. Gefitinib and curcumin-loaded nanoparticles enhance cell apoptosis in human oral cancer SAS cells *in vitro* and inhibit SAS cell xenografted tumor *in vivo*. Toxicol Appl Pharmacol 2019;382:114734.
[118] Zhang S, Zhao L, Peng X, Sun Q, Liao X, Gan N, et al. Self-assembled phospholipid-based mixed micelles for improving the solubility, bioavailability and anticancer activity of lenvatinib. Colloids Surf B Biointerfaces 2021;201:111644.
[119] Chen W, Yu D, Sun SY, Li F. Nanoparticles for co-delivery of osimertinib and selumetinib to overcome osimertinib-acquired resistance in non-small cell lung cancer. Acta Biomater 2021;129:258–68.
[120] Zhong T, Liu X, Li H, Zhang J. Co-delivery of sorafenib and crizotinib encapsulated with polymeric nanoparticles for the treatment of *in vivo* lung cancer animal model. Drug Deliv 2021;28(1):2108–18.
[121] Wang H, Wu Y, Lin X. Crizotinib loaded polydopamine-polylactide-TPGS nanoparticles in chemotherapy for non-small cell lung cancer. Med Oncol 2022;40(1):26.
[122] Greish K, Jasim A, Parayath N, Abdelghany S, Alkhateeb A, Taurin S, et al. Micellar formulations of crizotinib and dasatinib in the management of glioblastoma multiforme. J Drug Target 2017;26(8):692–708.
[123] Wind S, Schnell D, Ebner T, Freiwald M, Stopfer P. Clinical pharmacokinetics and pharmacodynamics of afatinib. Clin Pharmacokinet 2017;56(3):235–50.
[124] Chan MH, Huang WT, Wang J, Liu RS, Hsiao M. Next-generation cancer-specific hybrid theranostic nanomaterials: MAGE-A3 NIR persistent luminescence nanoparticles conjugated to afatinib for *in situ* suppression of lung adenocarcinoma growth and metastasis. Adv Sci (Weinh) 2020;7(9).
[125] Yu M, Gao Z, Dai X, Gong H, Zhang L, Chen X, et al. Population pharmacokinetic and covariate analysis of apatinib, an oral tyrosine kinase inhibitor, in healthy volunteers and patients with solid tumors. Clin Pharmacokinet 2017;56(1):65–76.
[126] Fukudo M, Tamaki G, Azumi M, Kakizaki H, Matsumoto S, Tasaki Y. Absorption of the orally active multikinase inhibitor axitinib as a therapeutic index to guide dose titration in metastatic renal cell carcinoma. Invest New Drugs 2021;39(2):595–604.
[127] Axitinib (AG 013736) as second line therapy for metastatic renal cell cancer. 2022. Available from: https://clinicaltrials.gov/study/NCT00920816.
[128] Lacy SA, Miles DR, Nguyen LT. Clinical pharmacokinetics and pharmacodynamics of cabozantinib. Clin Pharmacokinet 2017;56(5):477–91.
[129] Cerbone L, Combarel D, Geraud A, Auclin E, Foulon S, Alves Costa Silva C, et al. Association of cabozantinib pharmacokinetics, progression and toxicity in metastatic renal cell carcinoma patients: results from a pharmacokinetics/pharmacodynamics study. ESMO Open 2021;6(6).
[130] Hirota T, Muraki S, Ieiri I. Clinical pharmacokinetics of anaplastic lymphoma kinase inhibitors in non-small-cell lung cancer. Clin Pharmacokinet 2019;58(4):403–20.
[131] Forde PM, Rudin CM. Crizotinib in the treatment of non-small-cell lung cancer. Expert Opin Pharmacother 2012;13(8):1195–201.
[132] A Study comparing alectinib with crizotinib in treatment-naive anaplastic lymphoma kinase-positive advanced non-small cell lung cancer participants. 2014. Available from: https://clinicaltrials.ucsf.edu/trial/NCT02075840.
[133] Puszkiel A, Noé G, Bellesoeur A, Kramkimel N, Paludetto MN, Thomas-Schoemann A, et al. Clinical pharmacokinetics and pharmacodynamics of dabrafenib. Clin Pharmacokinet 2018;58(4):451–67.
[134] Center for drug evaluation and research. Application number: 202806Orig1s000. 2013. Available from: https://www.accessdata.fda.gov/drugsatfda_docs/nda/2013/202806Orig1s000Approv.pdf.
[135] Levêque D, Becker G, Bilger K, Natarajan-Amé S. Clinical pharmacokinetics and pharmacodynamics of dasatinib. Clin Pharmacokinet 2020;59(7):849–56.
[136] Verheijen RB, Yu H, Schellens JHM, Beijnen JH, Steeghs N, Huitema ADR. Practical recommendations for therapeutic drug monitoring of kinase inhibitors in oncology. Clin Pharmacol Ther 2017;102(5):765–76.
[137] Dai G, Pfister M, Blackwood-Chirchir A, Roy A. Importance of characterizing determinants of variability in exposure: application to dasatinib in subjects with chronic myeloid leukemia. J Clin Pharmacol 2008;48(11):1254–69.
[138] Chandani R., He J., Trabelsi F. Atypical pharmacokinetic profiles observed with dasatinib reference listed drug product in bioequivalence studies. 2017. Available from: https://www.biopharmaservices.com/wp-content/uploads/2021/03/Poster-1-Dasatinib-final-AAPS-2017.pdf.
[139] Ishida Y, Murai K, Yamaguchi K, Miyagishima T, Shindo M, Ogawa K, et al. Pharmacokinetics and pharmacodynamics of dasatinib in the chronic phase of newly diagnosed chronic myeloid leukemia. Eur J Clin Pharmacol 2016;72(2):185–93.
[140] Wang X, Roy A, Hochhaus A, Kantarjian HM, Chen TT, Shah NP. Differential effects of dosing regimen on the safety and efficacy of dasatinib:retrospective exposure-response analysis of a phase III study. Clin Pharmacol 2013;5:85–97.
[141] Kamath AV, Wang J, Lee FY, Marathe PH. Preclinical pharmacokinetics and *in vitro* metabolism of dasatinib (BMS-354825): a potent oral multi-targeted kinase inhibitor against SRC and BCR-ABL. Cancer Chemother Pharmacol 2008;61(3):365–76.
[142] Luo FR, Yang Z, Camuso A, Smykla R, McGlinchey K, Fager K, et al. Dasatinib (BMS-354825) pharmacokinetics and pharmacodynamic biomarkers in animal models predict optimal clinical exposure. Clin Cancer Res 2006;12(23):7180–6.
[143] Tsume Y, Takeuchi S, Matsui K, Amidon GE, Amidon GL. *In vitro* dissolution methodology, mini-Gastrointestinal Simulator (mGIS), predicts better *in vivo* dissolution of a weak base drug, dasatinib. Eur J Pharmaceut Sci 2015;76:203–12.
[144] He S, Bian J, Shao Q, Zhang Y, Hao X, Luo X, et al. Therapeutic drug monitoring and individualized medicine of dasatinib: focus on clinical pharmacokinetics and pharmacodynamics. Front Pharmacol 2021;12.
[145] Christiansen SR, Broniscer A, Panetta JC, Stewart CF. Pharmacokinetics of erlotinib for the treatment of high-grade glioma in a pediatric patient with cystic fibrosis: case report and review of the literature. Pharmacotherapy 2009;29(7):858–66.

[146] Frohna P, Lu J, Eppler S, Hamilton M, Wolf J, Rakhit A, et al. Evaluation of the absolute oral bioavailability and bioequivalence of erlotinib, an inhibitor of the epidermal growth factor receptor tyrosine kinase, in a randomized, crossover study in healthy subjects. J Clin Pharmacol 2006;46(3):282–90.
[147] Scheffler M, Di Gion P, Doroshyenko O, Wolf J, Fuhr U. Clinical pharmacokinetics of tyrosine kinase inhibitors: focus on 4-anilinoquinazolines. Clin Pharmacokinet 2011;50(6):371–403.
[148] Ni J, Zhang L. Evaluation of three small molecular drugs for targeted therapy to treat nonsmall cell lung cancer. Chin Med J (Engl) 2016;129(3):332.
[149] Kucharczuk CR, Ganetsky A, Vozniak JM. Drug-drug interactions, safety, and pharmacokinetics of EGFR tyrosine kinase inhibitors for the treatment of non–small cell lung cancer. J Adv Pract Oncol 2018;9(2):189.
[150] De Vries R, Smit JW, Hellemans P, Jiao J, Murphy J, Skee D, et al. Stable isotope-labelled intravenous microdose for absolute bioavailability and effect of grapefruit juice on ibrutinib in healthy adults. Br J Clin Pharmacol 2016;81(2):235.
[151] Shakeel F, Iqbal M, Ezzeldin E. Bioavailability enhancement and pharmacokinetic profile of an anticancer drug ibrutinib by self-nanoemulsifying drug delivery system. J Pharm Pharmacol 2016;68(6):772–80.
[152] Eisenmann ED, Fu Q, Garrison D, Weber B, Hu S, Woyach J, et al. Modulation of CYP3A activity to increase the oral bioavailability of ibrutinib. FASEB J 2020;34(S1):1.
[153] Sodeifian G, Nasri L, Razmimanesh F, Nooshabadi MA. Solubility of ibrutinib in supercritical carbon dioxide (Sc-CO_2): data correlation and thermodynamic analysis. J Chem Thermodyn 2023;182:107050.
[154] Byrd JC, Furman RR, Coutre SE, Burger JA, Blum KA, Coleman M, et al. Three-year follow-up of treatment-naïve and previously treated patients with CLL and SLL receiving single-agent ibrutinib. Blood 2015;125(16):2497–506.
[155] Jain P, Thompson PA, Keating M, Estrov Z, Ferrajoli A, Jain N, et al. Long-term outcomes for patients with chronic lymphocytic leukemia who discontinue ibrutinib. Cancer 2017;123(12):2268–73.
[156] Estey EH. Acute myeloid leukemia: 2019 update on risk-stratification and management. Am J Hematol 2018;93(10):1267–91.
[157] Sukbuntherng J, Jejurkar P, Chan S, Tran AL, Moussa D, James DF, et al. Pharmacokinetics (PK) of ibrutinib in patients with chronic lymphocytic leukemia (CLL). J Clin Oncol 2013;31(15_suppl):7056.
[158] Yang Z, Shao D, Zhou G. Solubility profile of imatinib in pure and mixed solvents and calculation of thermodynamic properties. J Chem Thermodyn 2020;144:106031.
[159] Buckingham R. Martindale : the complete drug reference.:4852.
[160] Al-Hadiya BMH, Bakheit AHH, Abd-Elgalil AA. Imatinib mesylate. Profiles Drug Subst Excip Relat Methodol 2014;39:265–97.
[161] Sneed TB, Kantarjian HM, Talpaz M, O'Brien S, Rios MB, Bekele BN, et al. The significance of myelosuppression during therapy with imatinib mesylate in patients with chronic myelogenous leukemia in chronic phase. Cancer 2004;100(1):116–21.
[162] Arora B, Gota V, Menon H, Sengar M, Nair R, Patial P, et al. Therapeutic drug monitoring for imatinib: current status and Indian experience. Indian J Med Paediatr Oncol 2013;34(3):224.
[163] IJzerman NS, Groenland SL, Koenen AM, Kerst M, van der Graaf WTA, Rosing H, et al. Therapeutic drug monitoring of imatinib in patients with gastrointestinal stromal tumours – results from daily clinical practice. Eur J Cancer 2020;136:140–8.
[164] Cheng F, Zeng F, Li Q, Cui Z, Chen Y, Li W, et al. Imatinib dose optimization based on therapeutic drug monitoring in Chinese patients with chronic-phase chronic myeloid leukemia. Cancer 2022;128(22):3951–8.
[165] Arora B, Gota V, Menon H, Sengar M, Nair R, Patial P, et al. Therapeutic drug monitoring for imatinib: current status and indian experience. Indian J Med Paediatr Oncol 2013;34(3):224.
[166] Brown K, Comisar C, Witjes H, Maringwa J, de Greef R, Vishwanathan K, et al. Population pharmacokinetics and exposure-response of osimertinib in patients with non-small cell lung cancer. Br J Clin Pharmacol 2017;83(6):1216.
[167] Brown K, Comisar C, Witjes H, Maringwa J, de Greef R, Vishwanathan K, et al. Population pharmacokinetics and exposure-response of osimertinib in patients with non-small cell lung cancer. Br J Clin Pharmacol 2017;83(6):1216.
[168] Verheijen RB, Beijnen JH, Schellens JHM, Huitema ADR, Steeghs N. Clinical pharmacokinetics and pharmacodynamics of pazopanib: towards optimized dosing. Clin Pharmacokinet 2017;56(9):987.
[169] Deng Y, Sychterz C, Suttle AB, Dar MM, Bershas D, Negash K, et al. Bioavailability, metabolism and disposition of oral pazopanib in patients with advanced cancer. Xenobiotica 2013;43(5):443–53.
[170] Liu C, Chen Z, Chen Y, Lu J, Li Y, Wang S, et al. Improving oral bioavailability of sorafenib by optimizing the "spring" and "parachute" Based on Molecular Interaction Mechanisms. Mol Pharm 2016;13(2):599–608.
[171] Eresen A, Zhang Z, Yaghmai V. Strategies to improve sorafenib efficacy during image-guided treatment of hepatocellular carcinoma. Ann Transl Med 2021;9(23):1745.
[172] Guchelaar NAD, van Eerden RAG, Groenland SL, van Doorn L, Desar IME, Eskens FALM, et al. Feasibility of therapeutic drug monitoring of sorafenib in patients with liver or thyroid cancer. Biomed Pharmacother 2022;153:113393.
[173] Gopakumar L, Sreeranganathan M, Chappan S, James S, Gowd GS, Manohar M, et al. Enhanced oral bioavailability and antitumor therapeutic efficacy of sorafenib administered in core-shell protein nanoparticle. Drug Deliv Transl Res 2022;12(11):2824–37.
[174] Zhang G, Xie X, Liu T, Yang J, Jiao S. Effects of pemetrexed, gefitinib, and their combination on human colorectal cancer cells. Cancer Chemother Pharmacol 2013;72(4):767–775.
[175] Van Schaeybroeck S, Karaiskou-McCaul A, Kelly D, Longley D, Galligan L, Van Cutsem E, et al. Epidermal growth factor receptor activity determines response of colorectal cancer cells to gefitinib alone and in combination with chemotherapy. Clin Cancer Res 2005;11(20):7480–9.
[176] Arora A, Scholar EM. Role of tyrosine kinase inhibitors in cancer therapy. J Pharmacol Exp Ther 2005;315(3):971–9.
[177] Li X, Wang J, Li S, Liu Z, Zheng Z, Zhang Y. Development and evaluation of multifunctional poly(lactic-co-glycolic acid) nanoparticles embedded in carboxymethyl β-glucan porous microcapsules as a novel drug delivery system for gefitinib. Pharmaceutics 2019;11(9).
[178] Engelman JA, Jänne PA, Mermel C, Pearlberg J, Mukohara T, Fleet C, et al. ErbB-3 mediates phosphoinositide 3-kinase activity in gefitinib-sensitive non-small cell lung cancer cell lines. Proc Natl Acad Sci USA 2005;102(10):3788.
[179] Alanazi A, Alshehri S, Altamimi M, Shakeel F. Solubility determination and three dimensional Hansen solubility parameters of gefitinib in different organic solvents:

experimental and computational approaches. J Mol Liq 2020;299:112211.
[180] Godugu C, Doddapaneni R, Patel AR, Singh R, Mercer R, Singh M. Novel gefitinib formulation with improved oral bioavailability in treatment of A431 skin carcinoma. Pharm Res 2016;33(1):137–54.
[181] Shah NT, Kris MG, Pao W, Tyson LB, Pizzo BM, Heinemann MH, et al. Practical management of patients with non-small-cell lung cancer treated with gefitinib. J Clin Oncol 2005;23(1):165–74.
[182] Inoue A, Saijo Y, Maemondo M, Gomi K, Tokue Y, Kimura Y, et al. Severe acute interstitial pneumonia and gefitinib. The Lancet 2003;361(9352):137–9.
[183] Højer Wang L, Wehland M, Wise PM, Infanger M, Grimm D, Kreissl MC. Cabozantinib, vandetanib, pralsetinib and selpercatinib as treatment for progressed medullary thyroid cancer with a main focus on hypertension as adverse effect. Int J Mol Sci 2023;24(3):2312.
[184] Yan M, Li W, Li WB, Huang Q, Li J, Cai HL, et al. Metabolic activation of tyrosine kinase inhibitors: recent advance and further clinical practice. Drug Metab Rev 2023;55(1–2):94–106.
[185] Tian H, Zhang T, Qin S, Huang Z, Zhou L, Shi J, et al. Enhancing the therapeutic efficacy of nanoparticles for cancer treatment using versatile targeted strategies. J Hematol Oncol 2022;15(1):1–40.
[186] Xin H, Naficy S. Drug delivery based on stimuli-responsive injectable hydrogels for breast cancer therapy: a Review. Gels 2022;8(1):45.